PHYSICAL REVIEW D **93,** 075014 (2016)

Pushing Higgs effective theory to its limits

Johann Brehmer,[1] Ayres Freitas,[2] David López-Val,[3] and Tilman Plehn[1]
[1]*Institut für Theoretische Physik, Universität Heidelberg, Heidelberg 69120, Germany*
[2]*PITT-PACC, Department of Physics and Astronomy, University of Pittsburgh, Pittsburgh, Pennsylvania 15260, USA*
[3]*Centre for Cosmology, Particle Physics and Phenomenology CP3, Université catholique de Louvain, Louvain 1348, Belgium*
(Received 22 October 2015; published 6 April 2016)

At the LHC, an effective theory of the Higgs sector allows us to analyze kinematic distributions in addition to inclusive rates, although there is no clear hierarchy of scales. We systematically analyze how well dimension-6 operators describe LHC observables in comparison to the full theory, and in a range where the LHC will be sensitive. The key question is how the breakdown of the dimension-6 description affects Higgs measurements during the upcoming LHC run for weakly interacting models. We cover modified Higgs sectors with a singlet and doublet extension, new top partners, and a vector triplet. First, weakly interacting models only generate small relevant subsets of dimension-6 operators. Second, the dimension-6 description tends to be justified at the LHC. Scanning over model parameters, significant discrepancies can nevertheless arise; their main source is the matching procedure in the absence of a well-defined hierarchy of scales. While these issues require vigilance, they should not present a major problem for future LHC analyses.

DOI: 10.1103/PhysRevD.93.075014

I. INTRODUCTION

The Higgs boson [1] discovery announced on July 4, 2012 [2], is a historical milestone in the physics of the 21st century. The thorough scrutiny of the LHC run I data has so far confirmed that the narrow resonance observed at a mass around 125 GeV is compatible with the minimal Standard Model (SM) agent of electroweak symmetry breaking [3]. To date, this agreement is limited to around 20% precision in the Higgs couplings [4–7], which is not sensitive to the deviations that one would expect from typical perturbatively extended Higgs sectors. This accuracy, based on a large set of on-shell and most recently off-shell Higgs measurements [7], will soon improve with data from run II. Odds are high that the upcoming runs will shed light on a possible UV completion of the Standard Model [8,9].

Based on everything we know, such an underlying theory should be described by a gauge field theory. While the measurement of Higgs couplings from inclusive rates has been extremely successful at run I, it needs to be extended, for example to include kinematic distributions. For this purpose, Higgs effective field theories (EFTs) [10–12] have become the *koiné* for discussing the phenomenology of extended Higgs sectors. In the effective field theory language, beyond the Standard Model (BSM) effects are described in terms of a Lagrangian with local operators of increasing mass dimension $d > 4$. Each of them includes a suppression by inverse powers of a new physics scale, which should be well separated from the experimentally accessible scale, in our case the electroweak scale, $\Lambda \gg v$.

Despite its generality, the EFT approach is known to suffer from its limited applicability when the hierarchy of scales is not guaranteed. This has fueled intense investigation in the context of dark matter searches [13]. While in that field EFT-based predictions are usually robust for early-Universe and late-time annihilation rates as well as for dark matter-nucleon scattering, the required hierarchy of scales can break down for dark matter signals at colliders. Because hadron colliders do not have a well-defined partonic energy, strategies relying on boosted objects and large recoils are the most critical. While it is not clear that a marginal separation of scales invalidates the EFT approach, such observables clearly pose a challenge.

There exists a first set of studies of the applicability of EFTs to Higgs physics at the LHC [14–16]. These questions first arose in studies of tagging jet kinematics in weak boson fusion, which are sensitive to the UV structure of the theory [17–20]. Similar issues appear in Higgs-strahlung [14] and in the production of off-shell Higgs bosons in gluon fusion [21,22]. A key problem is that Higgs production at hadron colliders does not probe a single energy scale over the full relevant phase space.

On the other hand, in Ref. [7] it has been shown that a fit of dimension-6 operators to the Higgs data at run I is a sensible and practicable extension of the usual Higgs couplings fit. Dimension-6 operators including derivatives complement the Higgs coupling modifications and allow us to extract information from kinematic distributions. Because the LHC constraints do not induce a hierarchy of scales, the EFT approach is not formally well defined.

However, there appears to be no problem in describing the LHC Higgs data in terms of a truncated dimension-6 Lagrangian. This description induces theory uncertainties if we want to interpret the LHC results in terms of an effective field theory [23]. On the other hand, these and other theory uncertainties can and should be separated from the experimental uncertainties [24,25].

Related to the topic of the validity of the effective theory is the question if, given the experimental performance, the analysis of a UV-complete model offers an advantage compared to the effective theory [26]. The two approaches are only equivalent if we account for the full correlations between the effective operators in all analysis steps, and if the effective theory is applicable over the full relevant phase space. Unless the experimental collaborations provide their fully correlated results beyond a Gaussian approximation [7], a direct analysis of full models will be superior.

Given these arguments, the applicability of the dimension-6 description of the Higgs sector has to be tested on a process-to-process as well as model-to-model basis. In this paper we present a comprehensive comparison of full models and their truncated EFT description during the LHC run II. We select extensions of the Higgs sector of the Standard Model by (i) a scalar singlet, (ii) a scalar doublet, (iii) a colored top-partner scalar, and (iv) a massive vector triplet. Each of these models is mapped onto an EFT, which we obtain by integrating out the heavy fields and expanding the operators to dimension 6. We then derive predictions for selected Higgs observables in the full model and compare them to the EFT results. The key questions we aim to address are as follows:

(1) Given the LHC sensitivity, how large do relevant new physics effects have to be?
(2) Does the corresponding new physics scale respect a self-consistency condition $\Lambda \gg v$?
(3) Which observables are correctly described by the truncated EFT?
(4) What are the reasons for the potential failure of this EFT?
(5) Do they pose a problem for LHC analyses?

For weakly interacting models, visible effects at the LHC lead us to scenarios in which the heavy scale is not sufficiently separated from the electroweak scale, and the EFT description is not obviously justified. We will analyze what problems the lack of a clear hierarchy of scales leads to in practice and discuss how these might affect global LHC-Higgs fits including kinematic distributions [7].

It will turn out that two limitations of the EFT description will guide us through the different models. First, we need to ensure that the new physics scale and with it all new particles are properly decoupled, in particular when we go beyond total cross sections. Second, when we define our effective field theory in terms of a Higgs-Goldstone doublet, it is crucial that the electroweak vacuum expectation value (VEV) does not have a destabilizing effect on the hierarchy of scales.

The remainder of the paper is organized as follows: in Sec. II we review our theoretical framework. We discuss how new physics effects in the Higgs sector are accounted for in the full model and EFT languages, and we identify the reasons why the two methods can deviate from each other. In Sec. III we show these ideas at work by explicitly confronting full model versus EFT predictions for a variety of UV completions and Higgs observables. We give our conclusions in Sec. IV. We hope that Appendix A 1–A 5 with exhaustive details on the different models and their EFT parametrizations will be particularly useful to practitioners.

II. EFFECTIVE THEORY BASICS

Extensions of the SM Higgs sector involve new degrees of freedom with electroweak charges and/or color charges, coupled to or mixing with the SM-like Higgs boson. Hidden sectors coupled to the Higgs potential without any SM charge lead to nonstandard Higgs decays. Since the Higgs potential is closely linked to the electroweak sector, any model that affects the SM gauge bosons will also affect Higgs physics. This way, a wide range of new physics models can be probed in Higgs signatures at the LHC, both in total rates and kinematic distributions. The simplest effect are shifted couplings of the observed Higgs boson at 125 GeV [4]:

$$g_{xxH} = g_{xxH}^{\mathrm{SM}}(1 + \Delta_x). \tag{1}$$

In this notation Δ can reflect both a truncated EFT or a full new physics model. These coupling deviations have been used to test an effective light Higgs model with either free or model-specific couplings [4–7].

A. Higgs effective theory

Effective field theories provide a systematic method to link Higgs measurements to a large class of high-scale UV completions. Their ingredients are (i) the dynamic degrees of freedom and (ii) the symmetries at low energies. The Higgs EFT framework keeps the SM fields and requires an invariance under the SM gauge group $SU(3)\times SU(2)\times U(1)$:

$$\mathcal{L}_{\mathrm{eff}} = \mathcal{L}_{\mathrm{SM}} + \sum_{d=5}^{\infty} \sum_{a_d} \frac{C_{a_d}^{(d)}}{\Lambda^{d-4}} \mathcal{O}_{a_d}^{(d)}. \tag{2}$$

We assume a linear realization of electroweak symmetry breaking. This implies that the Higgs scalar and the Goldstones of the Standard Model form an $SU(2)$ doublet ϕ with the vacuum expectation value $v = 246$ GeV. This is justified by the level of agreement of the Standard Model with all available data on the electroweak sector. A nonlinear

formulation in terms of a general scalar field h is also possible [27]. The higher-dimensional terms denote a linear combination of local operators with mass dimension d, weighted by Wilson coefficients C_a and suppressed by inverse powers of the new physics scale Λ.

Higher-dimensional operators can be classified depending on whether they include derivatives to compensate for the mass dimension in $1/\Lambda^2$. This leads to momentum-dependent couplings, scattering amplitudes growing with energy, and eventually the violation of perturbative unitarity. It reflects the onset of new on-shell contributions, which are integrated out in the EFT.

When we link full models to an EFT description it is useful to categorize the higher-dimensional operators according to whether they arise from the tree-level exchange of heavy mediators or through loop effects mediated by the heavy fields [28,29]. This categorization is only meaningful for weakly interacting complete models.

For the linear realization there exists a set of 59 dimension-6 operators. Popular bases are the Warsaw [30], Hagiwara-Ishihara-Szalapski-Zeppenfeld (HISZ) [31], and strongly interacting light Higgs (SILH) bases [32]. All three maximize the use of bosonic operators to describe Higgs and electroweak observables. They can be mapped onto each other using equations of motion, integration by parts, field redefinitions, and Fierz transformations [33]. We use the SILH basis and retain only those operators relevant for Higgs physics at the LHC [32]. The effective Lagrangian truncated to dimension 6 reads

$$\begin{aligned}\mathcal{L}_{\rm EFT} = \mathcal{L}_{\rm SM} &+ \frac{\bar{c}_H}{2v^2}\partial^\mu(\phi^\dagger\phi)\partial_\mu(\phi^\dagger\phi) + \frac{\bar{c}_T}{2v^2}(\phi^\dagger \overleftrightarrow{D^\mu}\phi)(\phi^\dagger \overleftrightarrow{D_\mu}\phi) - \frac{\bar{c}_6\lambda}{v^2}(\phi^\dagger\phi)^3 + \frac{ig\bar{c}_W}{2m_W^2}(\phi^\dagger\sigma^k \overleftrightarrow{D^\mu}\phi)D^\nu W^k{}_{\mu\nu} \\ &+ \frac{ig'\bar{c}_B}{2m_W^2}(\phi^\dagger \overleftrightarrow{D^\mu}\phi)\partial^\nu B_{\mu\nu} + \frac{ig\bar{c}_{HW}}{m_W^2}(D^\mu\phi^\dagger)\sigma^k(D^\nu\phi)W^k_{\mu\nu} + \frac{ig'\bar{c}_{HB}}{m_W^2}(D^\mu\phi^\dagger)(D^\nu\phi)B_{\mu\nu} + \frac{g'^2\bar{c}_\gamma}{m_W^2}(\phi^\dagger\phi)B_{\mu\nu}B^{\mu\nu} \\ &+ \frac{g_s^2\bar{c}_g}{m_W^2}(\phi^\dagger\phi)G^A_{\mu\nu}G^{\mu\nu A} - \left[\frac{\bar{c}_u}{v^2}y_u(\phi^\dagger\phi)(\phi^\dagger\cdot\bar{Q}_L)u_R + \frac{\bar{c}_d}{v^2}y_d(\phi^\dagger\phi)(\phi\bar{Q}_L)d_R + \frac{\bar{c}_\ell}{v^2}y_\ell(\phi^\dagger\phi)(\phi\bar{L}_L)\ell_R + \text{H.c.}\right]. \quad (3)\end{aligned}$$

Here, $g = e/s_w$, $g' = e/c_w$, g_s stand for the SM gauge couplings and λ denotes the usual Higgs quartic coupling. The normalization of the dimension-6 Wilson coefficients $\bar{c}_i$ does not follow Eq. (2) but includes conventional prefactors which reflect a bias concerning their origin. We present further details on the EFT setup, the translation between the different bases, and the connection to Higgs observables in Appendix A 1.

B. Default versus v-improved matching

Matching the dimension-6 Lagrangian to a full model is a three-step procedure. Its starting point is the definition of a heavy mass scale Λ. Second, we integrate out the degrees of freedom above Λ, which leads to an infinite tower of higher-dimensional operators. Finally, this effective action is truncated so that only the dimension-6 terms, suppressed by $1/\Lambda^2$, remain. The matching is not unambiguous: on the one hand, Λ is usually not uniquely defined. Further ambiguities arise in the third step because a dimension-6 truncation does not tell us how $\mathcal{O}(\Lambda^{-4})$ contributions to the Wilson coefficients of the dimension-6 operators should be treated.

For the linear dimension-6 Lagrangian in terms of the doublet field ϕ the underlying assumption $\Lambda \gg v$ suggests to match the linear EFT to the full theory in the unbroken electroweak phase. An obvious choice for the matching scale is then the mass scale of new particles in the limit of $v \to 0$. We expand the effective action and drop all terms of $\mathcal{O}(\Lambda^{-4})$. This way, the truncation removes the parts of the Wilson coefficients of the dimension-6 operators that are suppressed by additional factors of $1/\Lambda$. This procedure is our default matching scheme.

In the absence of a clear hierarchy of scales, multiple heavy mass scales of the type $\Lambda \pm gv$ occur for instance through mixing effects in mass matrices, even if just one dimensionful parameter Λ governs the new physics. This raises the question if we can improve the agreement between full model and dimension-6 Lagrangian by incorporating effects of the nonzero electroweak VEV in the matching. In the first matching step, we can define Λ as the physical mass of the new particles in the broken phase, including contributions from v, rather than the mass scale in the unbroken phase. In addition, the third step gives us the choice to keep (part of) the $\mathcal{O}(\Lambda^{-4})$ terms of the Wilson coefficients. This is equivalent to expressing the coefficients in terms of phenomenologically relevant quantities such as mixing angles and physical masses, again defined in the broken phase. Both of these prescriptions effectively include effects from dimension-8 operators into the dimension-6 Lagrangian by once replacing $\phi^\dagger\phi \to v^2/2$. We will use the term *v-improved* matching for these alternative EFT definitions.

The truncation of the EFT Lagrangian is formally justified as long as $v \ll \Lambda$ and we only probe energies $E_{\rm phys} \ll \Lambda$. In this limit the dimension-8 operators as well as the Λ-suppressed terms in the Wilson coefficients are negligible; our two matching procedures then give identical

results. In the absence of a large enough scale separation, our bottom-up approach allows us to treat them independently. This way we can use the v-improved matching to enhance the validity of the dimension-6 Lagrangian.

The external energy scale depends on the specific process and observable, e.g. $E_{\rm phys} \sim m_h$ for on-shell Higgs coupling measurements, $E_{\rm phys} \sim m_{4\ell}$ for off-shell Higgs coupling measurements, $E_{\rm phys} \sim m_{hh}$ for Higgs pair production at threshold, or $E_{\rm phys} \sim p_{T,h}$ for boosted single or double Higgs production. In kinematic distributions the high-energy tails can probe significantly larger energy scales. This implies that the energy range where the EFT description is applicable is model dependent and observable dependent. Successively adding higher-dimensional operators should improve the situation, as long as the key scales $E_{\rm phys}, \Lambda$ are sufficiently separated. Of course, the EFT description fails spectacularly in the presence of new resonances in the relevant energy range, and we have to adjust the field content of the effective Lagrangian.

C. Self-consistency at the LHC

Interpreting LHC physics in terms of an effective theory involves a delicate balance between energy scales. On the one hand, new physics searches often rely on selection criteria which demand $E_{\rm phys} > m_h$ to separate a high-energy signal from the QCD background. On the other hand, a model-specific scale Λ limits the validity of the effective theory, as discussed above.

The extraction of Higgs properties during the LHC run I essentially relies on on-shell single Higgs production and decay. This allows us to roughly estimate the new physics scales they are able to probe. Assuming no loop suppression, a deviation from the total single Higgs production and decay rate lies within the experimental reach of the LHC if

$$\left| \frac{\sigma \times \mathrm{BR}}{(\sigma \times \mathrm{BR})_{\rm SM}} - 1 \right| = \frac{g^2 m_h^2}{\Lambda^2} \gtrsim 0.1 \Leftrightarrow \Lambda < \sqrt{10} g m_h \simeq 280\ \mathrm{GeV}, \tag{4}$$

where we assume a weakly interacting theory with $g^2 \sim 1/2$. Because of the limited precision of the available data, current Higgs results cannot test very high energy scales, at least for weakly coupled new physics [7]. For this simple power-counting argument we ignore that new physics might also change distributions and especially affect the high-energy tails. In this case the EFT expansion develops in two different directions: E/Λ and gv/Λ.

For loop-induced new physics effects, the corresponding loop suppression factor pulls Λ to even lower values:

$$\left| \frac{\sigma \times \mathrm{BR}}{(\sigma \times \mathrm{BR})_{\rm SM}} - 1 \right| = \frac{g^2 m_h^2}{16\pi^2 \Lambda^2} \gtrsim 0.1 \Leftrightarrow \Lambda < \frac{\sqrt{10} g m_h}{4\pi} \simeq 20\ \mathrm{GeV}. \tag{5}$$

This implies that the cutoff of the effective theory is below the electroweak scale. We can compensate for this by probing phase-space regions where m_h is not the relevant scale in the numerator. Only for moderately strongly coupled dynamics with $g = 1 \ldots \sqrt{4\pi}$ can one probe large enough energy scales for the EFT approach to be valid given the precision of the LHC Higgs program:

$$\left| \frac{\sigma \times \mathrm{BR}}{(\sigma \times \mathrm{BR})_{\rm SM}} - 1 \right| = \frac{g^2 m_h^2}{\Lambda^2} \gtrsim 0.1 \Leftrightarrow \Lambda < \sqrt{10} g m_h \simeq 400\ \mathrm{GeV} \ldots 1.4\ \mathrm{TeV}. \tag{6}$$

In fact, the EFT approach to Higgs observables has largely been motivated by the desire to describe models with strongly interacting electroweak symmetry breaking [32].

The increased statistics and Higgs production cross sections at run II will enable us to add a wide range of distributions and off-shell processes to the Higgs observables. They can probe higher energy scales $E_{\rm phys} \gg m_h$, which are more sensitive to differences between the dimension-6 and full model predictions. A well-known example is weak boson fusion, where the details of the ultraviolet completion can have a huge effect for example on the transverse momenta of the tagging jets [17–20].

III. MODELS VERSUS EFFECTIVE THEORY

The aim of this paper is to compare a comprehensive set of LHC predictions from specific new physics models with their corresponding effective field theory predictions. As discussed in Sec. II C, the applicability of the effective Lagrangian given in Eq. (3) is by no means guaranteed. We test it based on detailed comparisons of matched EFTs with the original, more or less UV-complete models, namely

(A) a scalar singlet extension with mixing effects and a second scalar resonance;
(B) two Higgs doublets, adding a variable Yukawa structure, a CP-odd, and a charged Higgs;
(C) scalar top partners, contributing to Higgs couplings at one loop; and
(D) a vector triplet with gauge boson mixing.

For each of these four models we introduce the setup and the main LHC features, discuss the decoupling in the Higgs sector, define the dimension-6 setup, and finally give a detailed account of the full and dimension-6 phenomenology at the LHC.

Our comparison covers the most relevant observables for LHC Higgs physics. We evaluate all amplitudes at tree level and take into account interference terms between Higgs and gauge amplitudes. Our acceptance and background rejections cuts are minimal, to be able to test the effective field theory approach over as much of the phase space as possible.

In the case of Higgs production through gluon fusion, we analyze the production process with a Higgs decay to four leptons or to photons:

$$pp \to h \to 4\ell, \qquad pp \to h \to \gamma\gamma. \tag{7}$$

For the photons we do not apply any cuts, while for $\ell = e$, μ we require

$$m_{4\ell} > 100\ \text{GeV} \quad \text{and} \quad m_{\ell^+\ell^-}^{\text{same flavor}} > 10\ \text{GeV} \tag{8}$$

to avoid too large contributions from the Z peak and bremsstrahlung.

For Higgs production in weak boson fusion (WBF), we evaluate the production process

$$ud \to hud \to W^+W^-ud \to (\ell^+\nu)(\ell^-\bar{\nu})ud. \tag{9}$$

We require the standard WBF cuts

$$\begin{aligned} &p_{T,j} > 20\ \text{GeV}, \qquad \Delta\eta_{jj} > 3.6, \qquad m_{jj} > 500\ \text{GeV}, \\ &p_{T,\ell} > 10\ \text{GeV}, \qquad \not{E}_T > 10\ \text{GeV}. \end{aligned} \tag{10}$$

Unlike for gluon fusion, the kinematics of the final state can now introduce new scales and a dependence on the UV structure of the model. The process is particularly interesting in the context of perturbative unitarity [34]. While the latter is satisfied in a UV-complete model by construction, deviations from the SM Higgs-gauge couplings in the EFT may lead to an increasing rate at very large energies [20,35], well outside the EFT validity range $E/\Lambda \ll 1$. To look for such signatures, we focus on the high-energy tail of the transverse mass distribution:

$$\begin{aligned} &m_T^2 = (E_{T,\ell\ell} + E_{T,\nu\nu})^2 - (\mathbf{p}_{T,\ell\ell} + \mathbf{p}_T^{\text{miss}})^2 \quad \text{with} \\ &E_{T,\ell\ell} = \sqrt{\mathbf{p}_{T,\ell\ell}^2 + m_{\ell\ell}^2}, \\ &E_{T,\nu\nu} = \sqrt{\not{E}_T + m_{\ell\ell}^2}. \end{aligned} \tag{11}$$

As the last single Higgs production process we evaluate Higgs-strahlung

$$qq \to Vh \tag{12}$$

with $V = W^\pm, Z$. We do not simulate the Higgs and gauge boson decays, assuming that we can always reconstruct for example the full $Zh \to \ell^+\ell^- b\bar{b}$ final state. No cuts are applied.

Finally, Higgs pair production is well known to be problematic when it comes to the effective theory description [36]:

$$gg \to hh. \tag{13}$$

Again, neither Higgs decays nor kinematic cuts are expected to affect our analysis, so we leave them out.

We test all these channels for the singlet and doublet Higgs sector extensions. For the top-partner and vector triplet models we focus on the WBF and Higgs-strahlung modes, which are the most sensitive. In the dimension-6 simulations we always include the square of the dimension-6 operator contributions. While these terms are technically of the same mass dimension as dimension-8 operators, which we neglect, we must keep them to avoid negative values of the squared matrix element in extreme phase-space regions. Notice that these situations do not necessarily imply a breakdown of the EFT expansion. On the contrary, they may appear in scenarios where new physics contributions dominate over the SM part, while the EFT expansion is fully valid (with $E/\Lambda \ll 1$). In such cases, the bulk effects stem from the squared dimension-6 terms instead of the interference with the SM, while the effects from dimension-8 operators are smaller and can be safely neglected.

Tree-level processes we generate with MadGraph5 [37], using publicly available model files [38] and our own implementations though FeynRules [39], which also provides the corresponding universal FeynRules output files [40]. For the dimension-6 predictions we resort to an in-house version of the HEL model file [41]. For all models we evaluate the Higgs-gluon and Higgs-photon couplings with the full one-loop form factors [42], including top, bottom and W loops as well as new particles present in the respective models. For Higgs pair production, we use a modified version of Ref. [43].

Other loop effects are analyzed using reweighting: we generate event samples using appropriate general couplings. Next, we compute the one-loop matrix element for each phase-space point and reweight the events with the ratio of the renormalized one-loop matrix element squared to the tree-level model. For the one-loop matrix elements we utilize FeynArts and FormCalc [44] with our own model files that include the necessary counterterms. The loop form factors are handled with dimensional regularization in the 't Hooft–Veltman scheme and written in terms of standard loop integrals. These are further reduced via Passarino-Veltman decomposition and evaluated with the help of LoopTools [45].

Generally we create event samples of at least 100 000 events per benchmark point and process for pp collisions at $\sqrt{s} = 13$ TeV. We use the CTEQ6L parton distribution function [46] and the default dynamical choices of the factorization and renormalization scale implemented in MadGraph. For the purpose of this project we limit ourselves to parton level and do not apply a detector simulation. The mass of the SM-like Higgs is fixed to $m_h = 125$ GeV [47]. For the top mass we take $m_t = 173.2$ GeV [48]. The Higgs width in each model is based on calculations with Hdecay [49], which we conveniently rescale and complement with additional decay channels if applicable.

A. Singlet extension

The simplest extension of the minimal Higgs sector of the Standard Model is by a real scalar singlet [50]. The extended scalar potential has the form

$$V(\phi,S) = \mu_1^2(\phi^\dagger\phi) + \lambda_1|\phi^\dagger\phi|^2 + \mu_2^2 S^2 + \lambda_2 S^4 + \lambda_3|\phi^\dagger\phi|S^2, \quad (14)$$

where the new scalar S can mix with the SM doublet ϕ provided the singlet develops a VEV, $\langle S\rangle = v_s/\sqrt{2}$. Details on the parametrization, Higgs mass spectrum and coupling patterns are given in Appendix A 2.

The additional scalar singlet affects Higgs physics in three ways: (i) mixing with the Higgs via the mixing angle α, which leads to a universal rescaling of all Higgs couplings to fermions and vectors; (ii) a modified Higgs self-coupling; and (iii) a new, heavy resonance H coupled to the Standard Model through mixing.

The key parameter is the portal interaction between the doublet and the singlet fields $\lambda_3(\phi^\dagger\phi)S^2$, which is responsible for the mixed mass eigenstates. The mixing reduces the coupling of the SM-like Higgs h to all Standard Model particles universally:

$$\Delta_x = \cos\alpha - 1 \quad \text{for } x = W, Z, t, b, \tau, g, \gamma, \ldots. \quad (15)$$

It also affects the self-coupling of the light Higgs, which takes on the form

$$g_{hhh} = 6\cos^3\alpha\lambda_1 v - 3\cos^2\alpha\sin\alpha\lambda_3 v_s + 3\cos\alpha\sin^2\alpha\lambda_3 v - 6\sin^3\alpha\lambda_2 v_s. \quad (16)$$

The parameter $\sin\alpha \simeq \alpha$ quantifies the departure from the SM limit $\alpha \to 0$. This limit can be attained in two ways: first, a small mixing angle can be caused by a weak portal interaction:

$$|\tan(2\alpha)| = \left|\frac{\lambda_3 v v_s}{\lambda_2 v_s^2 - \lambda_1 v^2}\right| \ll 1 \quad \text{if } \lambda_3 \ll 1. \quad (17)$$

The Higgs couplings to SM particles approach their SM values, but there is no large mass scale associated with this limit. In the extreme case of $\lambda_2, \lambda_3 \ll \lambda_1$ we find small $\alpha \approx -\lambda_3/\lambda_1 \times v_s/(2v)$ even for $v_s \lesssim v$. This situation is to some extent the singlet model counterpart of the *alignment without decoupling* scenario in the two-Higgs-doublet model (2HDM) [51,52] or the Minimal Supersymmetric Standard Model (MSSM) [53,54]. It relies nonetheless on a weak portal coupling and a small scale separation, which cannot be properly described by an effective field theory.

Second, the additional singlet can introduce a large mass scale $v_s \gg v$, giving us

$$\tan\alpha \approx \frac{\lambda_3}{2\lambda_2}\frac{v}{v_s} \ll 1 \quad \text{if } v \ll v_s, \quad (18)$$

where $\lambda_3/(2\lambda_2)$ is an effective coupling of up to order one. In this limit the heavy Higgs mass, which we identify as the heavy mass scale, is given by

$$m_H \approx \sqrt{2\lambda_2}\, v_s \equiv \Lambda. \quad (19)$$

In terms of the heavy scale Λ the Higgs couplings scale like

$$\Delta_x = -\frac{\alpha^2}{2} + \mathcal{O}(\alpha^3) \approx -\frac{\lambda_3^2}{4\lambda_2}\left(\frac{v}{\Lambda}\right)^2. \quad (20)$$

This is a dimension-6 effect. If we require $|\Delta_x| \gtrsim 10\%$ to keep our discussion relevant for the LHC, this implies

$$m_H \approx \Lambda < \frac{\sqrt{5}\lambda_3}{\sqrt{2\lambda_2}} v = 390\ \text{GeV} \times \frac{\lambda_3}{\sqrt{\lambda_2}}. \quad (21)$$

If we also assume that the ratio of quartic couplings is of the order of a perturbative coupling, $\lambda_3/\sqrt{\lambda_2} \lesssim 0.5$, the LHC reach in the Higgs coupling analysis translates into heavy Higgs masses below 200 GeV. For strongly coupled scenarios, $\lambda_3/\sqrt{\lambda_2} \lesssim 1\ldots\sqrt{4\pi}$, the heavy mass reach increases to $m_H \lesssim 0.4\ldots1.5$ TeV. This suggests that a weakly coupled Higgs portal will fail to produce a sizable separation of scales when looking at realistic Higgs coupling analyses. The question becomes if and where this lack of scale separation hampers our LHC analyses.

In the EFT approach the singlet model only generates $\mathcal{O}_H$ at dimension 6, with the Wilson coefficient

$$\bar{c}_H = \frac{\lambda_3^2}{2\lambda_2}\left(\frac{v}{\Lambda}\right)^2. \quad (22)$$

We give the details of the EFT description in Appendix A 2. As discussed in the previous section, the construction of the EFT is not unique. Instead of keeping only the leading term in the expansion in $1/\Lambda$, we can match the dimension-6 operators to the full, untruncated singlet model. In the broken phase the Higgs couplings are fully expressed through the mixing angle α, so the v-improved EFT truncated to dimension-6 operators gives the Wilson coefficient

$$\bar{c}_H = 2(1 - \cos\alpha). \quad (23)$$

We start our numerical analysis by defining five singlet benchmark points in Table I. The first three scenarios are in agreement with current experimental and theoretical constraints. This includes direct mass bounds from heavy Higgs searches at colliders, Higgs coupling measurements, electroweak precision observables, perturbative unitarity and vacuum stability [55]. We note that for S4 and S5 the combination of large heavy Higgs masses together with large mixing angles is incompatible with perturbative unitarity and electroweak precision constraints. We nevertheless keep such benchmarks for illustration purposes. Table I also includes the universal shift of the light Higgs couplings, both for the full singlet model and its dimension-6 EFT descriptions.

TABLE I. Benchmarks for the singlet extension. We show the model parameters and the universal coupling modification for the complete model, as well as the matching scale Λ, the Wilson coefficient $\bar{c}_H$, and the universal coupling modification in the EFT truncated to dimension 6. We also give these results for an alternative, v-improved construction. m_H and Λ are in GeV.

	Singlet				EFT			EFT (v-improved)	
Benchmark	m_H	$\sin\alpha$	v_s/v	$\Delta_x^{\text{singlet}}$	Λ	$\bar{c}_H$	Δ_x^{EFT}	$\bar{c}_H$	Δ_x^{EFT}
S1	500	0.2	10	−0.020	491	0.036	−0.018	0.040	−0.020
S2	350	0.3	10	−0.046	336	0.073	−0.037	0.092	−0.046
S3	200	0.4	10	−0.083	190	0.061	−0.031	0.167	−0.083
S4	1000	0.4	10	−0.083	918	0.183	−0.092	0.167	−0.092
S5	500	0.6	10	−0.200	407	0.461	−0.231	0.400	−0.200

In Table II we give the ratio of the total Higgs production cross sections in gluon fusion, WBF and Higgs-strahlung. They confirm what we expect from the coupling modification shown in Table I: qualitatively, the full singlet and the dimension-6 model predict similar shifts in the total rates. But there are differences in the coupling modifications $\Delta_x^{\text{singlet}}$ and Δ_x^{EFT} of up to 5%, translating into a rate deviation of up to 10%. In the v-improved EFT we find that the Higgs couplings and total rates agree exactly with the full model predictions. The dimension-6 operators are entirely sufficient to capture the coupling shifts, but a significant part of their coefficients are formally of $\mathcal{O}(v^4/\Lambda^4)$.

The most obvious source of discrepancy between the full model and the EFT is the heavy resonance H. It can for example be produced in gluon fusion and then observed as a peak in the $m_{4\ell}$ distribution. By construction, it will not be captured by the dimension-6 model. We illustrate this in the upper left panel of Fig. 1. For Higgs-strahlung production (Fig. 1, right panel), where the novel H resonance does not appear in an intermediate Born-level propagator and hence has no impact, we find instead excellent agreement between both descriptions over the entire phase space.

The second Higgs has a second, more subtle effect. In the full model, both Higgs exchange diagrams are needed to unitarize WW scattering. Correspondingly, the EFT description breaks perturbative unitarity roughly at the scale [35]

TABLE II. Cross section ratios of the matched dimension-6 EFT approximation to the full singlet model at the LHC. We show the leading Higgs production channels for all singlet benchmark points. The statistical uncertainties on these ratios are below 0.4%.

	$\sigma_{\text{EFT}}/\sigma_{\text{singlet}}$			$\sigma_{v\text{-improved EFT}}/\sigma_{\text{singlet}}$		
Benchmark	ggF	WBF	Vh	ggF	WBF	Vh
S1	1.006	1.006	1.004	1.001	1.001	1.000
S2	1.019	1.021	1.019	1.000	1.001	1.000
S3	1.119	1.118	1.118	1.000	0.999	1.000
S4	0.982	0.982	0.982	0.999	0.999	1.000
S5	0.925	0.925	0.925	0.999	0.999	1.000

$$m_{WW}^2 = \frac{16\pi v^2}{\bar{c}_H\left(1-\frac{\bar{c}_H}{4(1+\bar{c}_H)}\right)} \approx \left(\frac{1.7\ \text{TeV}}{\sin\alpha}\right)^2. \quad (24)$$

In our benchmark point S5, this is around 2.8 TeV. The incomplete cancellations between Higgs and gauge amplitudes means that the dimension-6 model tends to have a larger rate at energies already below this scale. For this specific benchmark choice, this can be seen in the lower left panel of Fig. 1, where we show the distribution of the transverse mass defined in Eq. (11) in the process $ud \to W^+W^-ud \to (\ell^+\nu)(\ell^-\bar{\nu})ud$, to which WBF production of both h and H contributes. We observe that the dimension-6 model predicts a slightly higher rate at large m_T than both the full singlet model and the SM. Given the very mild signal, which results from the fast decrease in the parton densities and the small mixing angle for realistic scenarios, such an effect is likely of no relevance for LHC physics.

A more interesting channel to study in the singlet model is Higgs pair production. The Higgs self-coupling is the only Higgs coupling which gains a momentum dependence in the matched EFT. In addition, there exists an approximate cancellation between the two leading amplitudes in the SM at threshold [56]. This induces a second relevant scale and with it a sensitivity to small deviations in the Higgs couplings. In Fig. 1 we give the m_{hh} distribution in the full and dimension-6 models. In addition, we show how the distributions would look in the full model without a H state and in the EFT without the momentum-dependent (derivative) terms given in Eq. (A31). Already at threshold and far away from the H resonance, the interference of the SM-like terms with the H diagrams makes up a significant part of the amplitude. In the EFT, the derivative terms are similarly relevant already at low energies. Close to threshold, the dimension-6 approximates the full model well. This agreement becomes worse towards the H pole [36]. The question of how the Wilson coefficients are expanded in v^2/Λ^2 does not play a role here.

If we limit ourselves to Higgs properties relevant for single Higgs production at the LHC, the modifications from a singlet extension are very simple: all Standard Model couplings acquire a common scaling factor, and no relevant

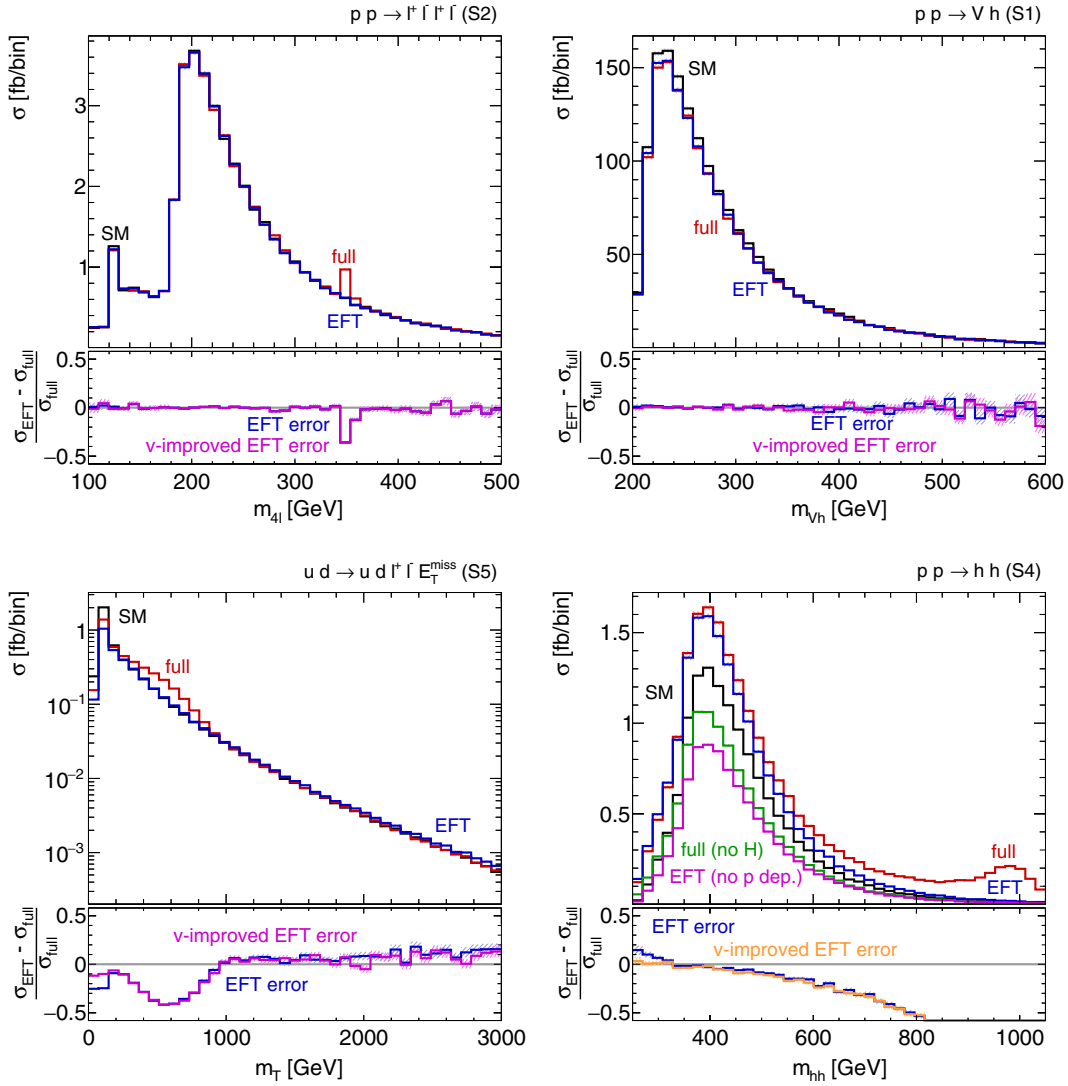

FIG. 1. Kinematic distributions in the singlet model. The different curves show the SM, full singlet model and singlet-matched dimension-6 predictions, respectively, as indicated in each panel. Top left: $m_{4\ell}$ distribution in the $gg \to h \to 4\ell$ channel after loose acceptance cuts for S2 in the full and effective models. Top right: m_{Vh} distribution in Vh production for S1. Bottom left: m_T distribution in the WBF $h \to \ell^+\ell^- E_T$ channel for S5. Bottom right: m_{hh} distribution in Higgs pair production for S4. For m_{hh} we show several contributions in the full theory and the dimension-6 approach. In all plots, the error bars give the statistical uncertainties.

new Lorentz structures appear at tree level. The dimension-6 setup reproduces this effect correctly: the reduced couplings to all SM fields alone do not require a large hierarchy of scales. An EFT construction in which the dimension-6 coefficients are not truncated at $\mathcal{O}(v^2/\Lambda^2)$ gives perfect agreement with the full theory, while expanding the coefficients to leading order in v^2/Λ^2 may lead to sizable deviations from the full model. Higgs pair production is different. There is a large contribution from off-shell H, while in the EFT the h self-coupling involves a derivative. These different structures lead to discrepancies between full and effective description that increase with momentum transfer. Finally, the effective theory by definition does not include the second resonance, so it fails whenever a heavy Higgs appears on shell in the full theory.

B. Two-Higgs-doublet model

The 2HDM [57] adds a second weak doublet with weak hypercharge $Y = +1$ to the SM Higgs sector. The combined potential reads

$$V(\phi_1,\phi_2) = m_{11}^2\phi_1^\dagger\phi_1 + m_{22}^2\phi_2^\dagger\phi_2 + \frac{\lambda_1}{2}(\phi_1^\dagger\phi_1)^2 + \frac{\lambda_2}{2}(\phi_2^\dagger\phi_2)^2 + \lambda_3(\phi_1^\dagger\phi_1)(\phi_2^\dagger\phi_2) + \lambda_4|\phi_1^\dagger\phi_2|^2 + \left[-m_{12}^2\phi_1^\dagger\phi_2 + \frac{\lambda_5}{2}(\phi_1^\dagger\phi_2)^2 + \text{H.c.}\right]. \quad (25)$$

The physical degrees of freedom are two neutral CP-even scalars h^0, H^0, one neutral CP-odd scalar A^0, and a set of

charged scalars $H^\pm$. The relevant model parameters are the mixing angle between the CP-even scalars α, the ratio of the VEVs $\tan\beta = v_2/v_1$, and the mixed mass term m_{12}. The latter induces a soft breaking of the discrete $\mathbb{Z}_2$ symmetry $\phi_i \to (-1)^i \phi_i$ (for $i = 1, 2$). The two-doublet structure allows for a rich variety of Higgs couplings to fermions. We refer the reader to Appendix A 3 for a detailed account of the model setup, Higgs spectrum, coupling patterns, and matched effective description.

Just as the singlet extension, the 2HDM predicts two types of LHC signatures: (i) scalar and VEV mixing lead to modified light Higgs couplings. Unlike for the singlet extension, these coupling modifications are not universal and reflect the more flexible flavor structure as well as the multiple scales of the model. (ii) There exist three heavy resonances $H^0, A^0, H^\pm$, which should have near-degenerate masses to avoid custodial symmetry breaking.

The light Higgs coupling to weak bosons $V = W, Z$ always scales like

$$\Delta_V = \sin(\beta-\alpha) - 1 = -\frac{\cos^2(\beta-\alpha)}{2} + \mathcal{O}(\cos^4(\beta-\alpha)). \tag{26}$$

We can insert the leading contribution of a mass-degenerate heavy Higgs sector and find

$$\Delta_V \approx \frac{\sin^2(2\beta)}{8}\left(\frac{v}{m_{A^0}}\right)^4. \tag{27}$$

While in the singlet model the light Higgs coupling to gauge bosons is shifted at $\mathcal{O}(v^2/\Lambda^2)$, Eq. (20), the same coupling is now affected at $\mathcal{O}(v^4/m_{A^0}^4)$, corresponding to a dimension-8 effect.

Two aspects turn the decoupling in the general 2HDM into a challenge: first, delayed decoupling effects appear after electroweak symmetry breaking [58]. For example, in type-II models we find [5]

$$\begin{aligned}\Delta_b &= -\tan\beta\sqrt{|2\Delta_V|} + \Delta_V + \mathcal{O}(\Delta_V^{3/2}) \\ &\approx -\tan\beta\frac{\sin(2\beta)}{2}\left(\frac{v}{m_{A^0}}\right)^2.\end{aligned} \tag{28}$$

This correction to the bottom Yukawa coupling corresponds to a dimension-6 effect, and already moderate values of $\tan\beta$ significantly delay the decoupling of the heavy 2HDM states in the Yukawa sector.

Second, unlike in the MSSM the Higgs self-couplings $\lambda_1 \ldots \lambda_5$ and m_{12} are not bounded from above. In combinations like $\lambda_j v^2$ they contribute to the interactions of the SM-like Higgs state, effectively inducing a new energy scale through terms of the kind $\sqrt{|2\Delta_V|}\sqrt{\lambda_j}v$ or proportional to m_{12}. They are significantly less suppressed than we would expect for the usual suppression $\sqrt{|2\Delta_V|}$—in particular if an additional factor $\tan\beta$ appears in this coupling deviation.

This additional, effectively lower mass scale driven by v leads to problems with any EFT derived from and matched to the full theory assuming only one new physics scale. While this should not be viewed as a problem of the EFT approach in general, it will require a v-improved matching procedure.

We first match the effective theory to the 2HDM in the unbroken phase. For this we define the new physics scale in terms of the mass terms in the potential of Eq. (25) and ratio of VEVs [16] as

$$\Lambda^2 = M^2 \equiv m_{11}^2\sin^2\beta + m_{22}^2\cos^2\beta + m_{12}^2\sin(2\beta). \tag{29}$$

The 2HDM generates a number of dimension-6 operators at tree level, for which the Wilson coefficients depend on the flavor structure. While the up-type Yukawa coupling is always modified the same way, the down-type and lepton couplings are different for type I and type II. We find

$$\begin{aligned}\bar{c}_u = \bar{c}_d^{\rm I} = \bar{c}_\ell^{\rm I} &= \frac{\sin(2\beta)\cot\beta}{2} \\ &\times \left[\frac{\lambda_1}{2} - \frac{\lambda_2}{2} + \left(\frac{\lambda_1}{2} + \frac{\lambda_2}{2} - \lambda_3 - \lambda_4 - \lambda_5\right)\cos(2\beta)\right]\left(\frac{v}{\Lambda}\right)^2, \\ \bar{c}_d^{\rm II} = \bar{c}_\ell^{\rm II} &= -\frac{\sin(2\beta)\tan\beta}{2} \\ &\times \left[\frac{\lambda_1}{2} - \frac{\lambda_2}{2} + \left(\frac{\lambda_1}{2} + \frac{\lambda_2}{2} - \lambda_3 - \lambda_4 - \lambda_5\right)\cos(2\beta)\right]\left(\frac{v}{\Lambda}\right)^2,\end{aligned} \tag{30}$$

where the superscripts I and II denote the type of the flavor structure.

Upon electroweak symmetry breaking, the physical heavy Higgs masses m_{H^0}, m_{A^0}, and $m_{H^\pm}$ acquire VEV-induced contributions $\sim\lambda_i v^2$ in addition to contributions from the heavy scale M. As in the singlet model, we therefore also consider a v-improved matching where the matching scale is $\Lambda = m_{A^0}$ and the Wilson coefficients are expressed in terms of mass eigenstates. In this setup, Eq. (30) remains unchanged, except that Λ is identified with m_{A^0}.

The two matching schemes exhibit significant differences in the 2HDM; for instance, the pseudoscalar mass is given by $m_{A^0}^2 = m_{12}^2/(\sin\beta\cos\beta) - \lambda_5 v^2$. This means that it does not coincide with M, unless we enforce a single mass scale $m_{11} \approx m_{22} \approx m_{12}$ and $\tan\beta \approx 1$.

The 2HDM benchmark points in Table III are in agreement with all current constraints, implemented with the help of 2HDMC [59], HiggsBounds [60], SuperIso [61], and HiggsSignals [62]. To better illustrate certain model features, in some scenarios we tolerate deviations between 1σ and 2σ in the Higgs couplings measurements. The key physics properties of the different 2HDM scenarios can be summarized as follows:

TABLE III. Benchmarks for the 2HDM extension. We show the model parameters and the heavy Higgs masses. All masses are in GeV.

	2HDM						
Benchmark	Type	$\tan\beta$	α/π	m_{12}	m_{H^0}	m_{A^0}	$m_{H^\pm}$
D1	I	1.5	−0.086	45	230	300	350
D2	II	15	−0.023	116	449	450	457
D3	II	10	0.032	157	500	500	500
D4	I	20	0	45	200	500	500

[D1] *Moderate decoupling.*—With Higgs couplings shifts of up to 2σ in terms of the LHC constraints. This generates $\Delta_{\tau,b,t} \approx \mathcal{O}(15\%)$ as well as a large $h^0H^+H^-$ coupling. Additional Higgs masses around 250…350 GeV can leave visible imprints.

[D2] *Supersymmetric.*—Reproducing the characteristic mass splittings and Higgs self-couplings of the MSSM with light top squarks [63].

[D3] *Sign-flipped bottom Yukawa.*—This is possible in type-II models at large $\tan\beta$, as shown in Eq. (28) [64]. This can be viewed as a manifestation of a delayed decoupling [58].

[D4] *Fermiophobic heavy Higgs.*—Possible only in type-I models for $\sin\alpha = 0$. The heavy Higgs H^0 is relatively light but essentially impossible to observe at the LHC [65,66].

In Table IV we show the heavy scales Λ and the Wilson coefficients for both the EFT matched in the unbroken phase and the v-improved EFT construction. In contrast to the singlet model, a significant v dependence of the heavy masses occurs even for parameter points in agreement with all relevant experimental and theoretical constraints. Only in one of our four benchmark scenarios does the heavy scale M approximate the physical mass m_{A^0}. The matching in the unbroken phase is particularly pathological in benchmark D1, where M^2 is negative and the signs of the Wilson coefficients are switched compared to the v-improved matching.

Table V confirms that matching in the unbroken phase does not reproduce the modified Higgs couplings, while the v-improved matching essentially captures the coupling shifts without a strong requirement on the hierarchy of scales. For our purpose we conclude that the expansion in powers of v/M is not well controlled, and we have to rely on v-improved matching for the 2HDM.

However, even in the v-improved EFT, the dimension-6 truncation can present an important source of deviations. According to Table V the operators $\mathcal{O}_u$, $\mathcal{O}_u$, and $\mathcal{O}_\ell$ modify the Higgs couplings similarly to the mixing, at least in the limit of small mixing angles. This is clearly visible e.g. in the MSSM-like scenario D2 as well as the fermiophobic scenario of benchmark D4, which are very well described by the dimension-6 Lagrangian, in spite of the lacking scale separation.

In Table VI we show LHC rate predictions by the dimension-6 approach and the full 2HDM. Depending on the benchmark, the dimension-6 truncation leads to up to 10% departures. A particularly interesting scenario is described by benchmark D3. In the full model, the bottom Yukawa is exactly sign flipped, a signature hardly visible at the LHC. Generating such a signature from higher-dimensional operators requires their contributions to be twice as large as the SM Yukawa coupling due to the enhancement of v/Λ by a large coupling. The EFT with default matching is certainly not valid anymore, and even the v-improved prescription fails to capture this coupling shift fully, leading to a significantly different coupling pattern.

TABLE IV. Matching scales and Wilson coefficients for the effective theory matched to the 2HDM. We give these results both for the EFT matching in the unbroken phase as well as for the v-improved matching with $\Lambda = m_{A^0}$.

	EFT			EFT (v-improved)			
Benchmark	$\lvert\Lambda\rvert$ [GeV]	$\bar{c}_u$	$\bar{c}_{d,\ell}$	Λ [GeV]	$\bar{c}_u$	$\bar{c}_{d,\ell}$	$\bar{c}_\gamma$
D1	100	−0.744	−0.744	300	0.082	0.082	1.61×10^{-4}
D2	448	0.000	0.065	450	0.000	0.065	4.16×10^{-6}
D3	99	0.465	−46.5	500	0.018	−1.835	1.05×10^{-4}
D4	142	0.003	0.003	500	0.000	0.000	1.48×10^{-4}

TABLE V. Normalized tree-level couplings of the light Higgs in our 2HDM benchmarks.

	Δ_V		Δ_t			$\Delta_b = \Delta_\tau$		
Benchmark	2HDM	EFT (both)	2HDM	EFT	EFT (v-improved)	2HDM	EFT	EFT (v-improved)
D1	−0.05	0.00	0.16	−0.74	0.08	0.16	−0.74	0.08
D2	0.00	0.00	0.00	0.00	0.00	0.07	0.07	0.07
D3	−0.02	0.00	0.00	0.46	0.02	−2.02	−46.5	−1.84
D4	0.00	0.00	0.00	0.00	0.00	0.00	0.00	0.00

TABLE VI. Cross section ratios of the matched dimension-6 EFT approximation to the full 2HDM at the LHC. We show the leading Higgs production channels for all 2HDM benchmark points. The statistical uncertainties on these ratios are below 0.4%.

	$\sigma_{v\text{-improved EFT}}/\sigma_{\text{2HDM}}$		
Benchmark	ggF	WBF	Vh
D1	0.872	1.109	1.108
D2	1.001	1.000	1.000
D3	1.022	1.042	1.042
D4	1.001	1.001	1.003

In the left panel of Fig. 2 we illustrate the coupling deviations in gluon fusion Higgs production with a decay $h \to \tau^+\tau^-$. The full 2HDM and the EFT give substantially different predictions for the size of the Higgs signal but do not affect the remaining distribution.

In addition, the charged Higgs contributes to the Higgs-photon coupling, an effect which is mapped onto the operator $\mathcal{O}_\gamma$. Within the v-improved EFT, one finds

$$c_\gamma = -\frac{g^2(\tan\beta+\cot\beta)}{12288\pi^2} \times \left[\left(\lambda_1+\lambda_2-2\lambda_3+6\lambda_4+6\lambda_5-8\frac{m_{h^0}^2}{v^2}\right)\sin(2\beta) + 2(\lambda_1-\lambda_2)\sin(4\beta) + (\lambda_1+\lambda_2-2\lambda_3-2\lambda_4-2\lambda_5) \times \sin(6\beta)\right]\left(\frac{v}{m_{A^0}}\right)^2. \quad (31)$$

There appears no nondecoupling term of $\mathcal{O}(\Lambda^0)$, because the charged Higgs loop decouples in the limit $m_{A^0} \to \infty$ with finite λ_i. If instead we keep m_{12} fixed and let one of the couplings λ_i grow with m_{A^0}, the charged Higgs does not decouple. Interestingly, Eqs. (30) and (31) show that in this model it is possible to realize *alignment without decoupling* scenarios [51–54], where the limit of SM-like couplings is achieved via very small prefactors of $(v/m_{A^0})^2$, while the additional Higgs states can remain moderately light—and hence potentially within LHC reach.

For all our benchmarks we find good agreement between the full 2HDM and the v-improved dimension-6 approach for on-shell Higgs decays to photons. In Table VII the rescaling of the Higgs-photon couplings shows slight discrepancies which can nearly entirely be traced back to the different couplings of the Higgs to the top and bottom in the loop due to the inaccurate truncation and are not related to the $H^\pm$ contribution.

This changes for off-shell Higgs production. At $m_{\gamma\gamma} \gtrsim 2m_{H^\pm}$, the $H^\pm$ in the loop can resolve the charged Higgs, enhancing the size of its contribution significantly. This effect is not captured by the effective operator and leads to a different behavior of the amplitude $gg \to h^0 \to \gamma\gamma$ between the full and effective model, as shown in the right panel of Fig. 2. However, the tiny rate and the large combinatorial background mean that this discrepancy will be irrelevant for LHC phenomenology. Similar threshold effects have been computed for the top-induced Higgs-gluon coupling and appear to be similarly irrelevant in practice [67].

The situation in Higgs pair production resembles the observations in the singlet model. The agreement can be worse already at threshold if the inaccurate truncation leads to differences in the Higgs-top couplings between the full and effective model.

Leaving the discussion of individual benchmarks behind, in Fig. 3 we demonstrate how deviations in the signal rates

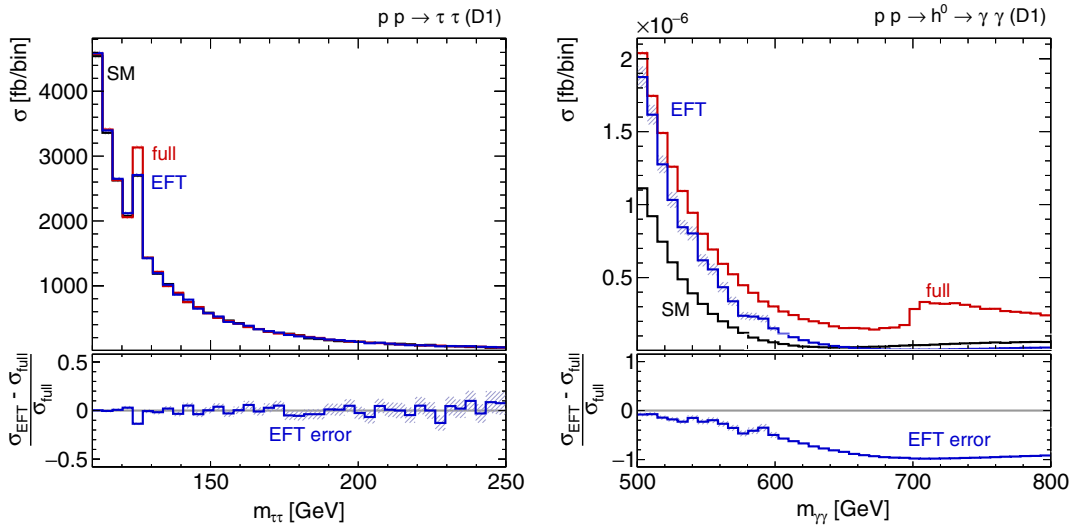

FIG. 2. Left: $m_{\tau\tau}$ distribution in the gluon fusion (ggF) $h^0 \to \tau^+\tau^-$ channel. Right: Off-shell behavior of the process $pp(gg) \to h^0 \to \gamma\gamma$ in 2HDM benchmark D1, only taking into account the Higgs diagrams. At $m_{\gamma\gamma} \gtrsim 2m_{H^\pm} = 700$ GeV, the charged Higgs threshold is visible.

TABLE VII. Normalized couplings of the light Higgs to gluons and photons in our 2HDM benchmarks. The bottom loop leads to small imaginary parts of Δ_g and Δ_γ. For the Higgs-photon coupling, these imaginary parts are always smaller than 1% of the real part of the amplitude and neglected here. The numbers in parentheses ignore the modification of the Higgs-fermion couplings, allowing us to separately analyze how well the $H^\pm$ loop is captured by $\mathcal{O}_\gamma$.

	Δ_g		Δ_γ			
Benchmark	2HDM	EFT (v-improved)	2HDM		EFT (v-improved)	
D1	$0.16 + 0.00i$	$0.08 + 0.00i$	−0.16	(−0.05)	−0.10	(−0.07)
D2	$0.00 + 0.00i$	$0.00 + 0.00i$	0.00	(0.00)	0.00	(0.00)
D3	$0.07 - 0.09i$	$0.02 + 0.00i$	−0.08	(−0.05)	−0.05	(−0.05)
D4	$0.00 + 0.00i$	$0.00 + 0.00i$	−0.05	(−0.05)	−0.05	(−0.05)

$\mu_{p,d}$ can be correlated; cf. Ref. [24]. The upper panels illustrate the dependence on the decoupling parameter $\sin(\beta-\alpha)$. In all cases we choose $\tan\beta = 1.5$, $m_{12} = 0$, degenerate heavy Higgs masses $m_{H^\pm,H^0,A^0} = 500$ GeV, and restrict ourselves to $\sin(\beta-\alpha) \geq 0.98$. All signal strength deviations are obtained by rescaling the SM production cross section, branching ratio and total width [68].

In the limit $\sin(\beta-\alpha) \to 1$ or $\Delta_V \to 0$ we find perfect agreement between the full model and the v-improved dimension-6 model. The latter also captures the nondecoupling part of the Higgs-photon coupling in the SM limit, $\mu_{\gamma\gamma} \neq 1$. Away from the SM-like limit the dimension-6 model slightly overestimates the signal strengths. This can for instance be attributed to Δ_V; it remains zero in the EFT while it decreases via $\mathcal{O}(v^4/\Lambda^4)$ corrections in the full

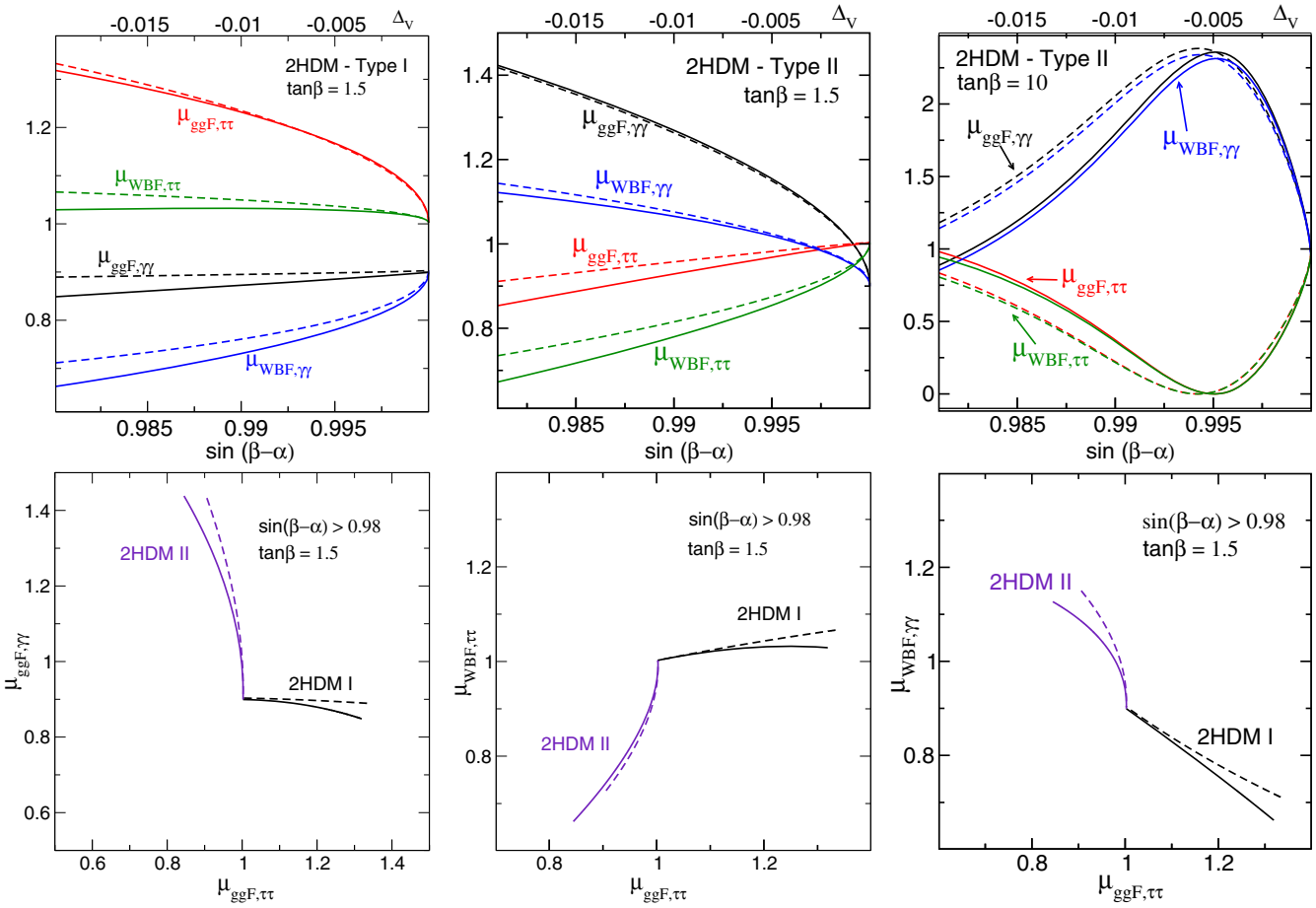

FIG. 3. Signal strength modifications in the 2HDM. The solid lines show the full model, while the dashed lines give the EFT predictions. Top: Signal strength $\mu_{p,d}$ for different Higgs production modes and decay channels in exemplary 2HDM setups, as a function of $\sin(\beta-\alpha)$. In the upper horizontal axis we track down the distance with respect to the SM-like limit through the coupling shift Δ_V (27). Bottom: Signal strength correlations μ_{p_1,d_1} versus μ_{p_2,d_2} between different channels for variable $\sin(\beta-\alpha)$.

model. Through the W loop this is also the main reason for the deviation in the $\gamma\gamma$ final states. Truncated negative $\mathcal{O}(v^4/\Lambda^4)$ corrections to Δ_τ are also in part responsible for the slight upward shift of $\mu_{\mathrm{ggF},\tau\tau}$ in the dimension-6 model. The behavior of the down-type Yukawas in type-II models, which are governed by $\Delta_{b,\tau} = -\cos(\beta-\alpha)\tan\beta + \mathcal{O}(v^4/\Lambda^4)$, leads to the strongly increased $\gamma\gamma$ rates at large $\tan\beta$, a feature which is well reproduced by the EFT.

Eventually, the 2HDM discussion leads us to the same conclusion as the singlet model: as long as the mixing is small, the new resonances do not contribute significantly; all the LHC probes in single Higgs production is a set of three coupling modifications Δ_x. New Lorentz structures do not play any role for the models considered. Barring the special case of Higgs pair production [65,69] the EFT captures most relevant aspects of Higgs phenomenology. A naive construction of the EFT by matching the effective dimension-6 Lagrangian to the 2HDM in the gauge symmetric phase fails to correctly describe the modified Higgs boson dynamics in typical 2HDM scenarios, since formally suppressed terms in v^2/Λ^2 as well as delayed decoupling or additional scales can become important for the phenomenologically relevant scenarios to be tested at the LHC.

C. Scalar top partners

New colored scalar particles are, strictly speaking, not an extension of the SM Higgs sector, but they can lead to interesting modifications of the LHC observables. We consider a scalar top-partner sector mimicking the top squark and sbottom sector of the MSSM. Its Lagrangian has the form

$$\begin{aligned}\mathcal{L} \supset\ & (D_\mu \tilde{Q})^\dagger (D^\mu \tilde{Q}) + (D_\mu \tilde{t}_R)^* (D^\mu \tilde{t}_R) - \tilde{Q}^\dagger M^2 \tilde{Q} - M^2 \tilde{t}_R^* \tilde{t}_R \\ & - \kappa_{LL} (\phi \cdot \tilde{Q})^\dagger (\phi \cdot \tilde{Q}) - \kappa_{RR} (\tilde{t}_R^* \tilde{t}_R)(\phi^\dagger \phi) \\ & - [\kappa_{LR} M \tilde{t}_R^* (\phi \cdot \tilde{Q}) + \text{H.c.}]. \end{aligned} \tag{32}$$

Here, $\tilde{Q}$ and $\tilde{t}_R$ are the additional isospin doublet and singlet, respectively, in the fundamental representation of $SU(3)_C$. Their mass terms can be different, but for the sake of simplicity we unify them to a single heavy mass scale M. The singlet state $\tilde{b}_R$ is assumed to be heavier and integrated out. This leaves us with three physical degrees of freedom, the scalars $\tilde{t}_1$, $\tilde{t}_2$ and $\tilde{b}_2 = \tilde{b}_L$. The eigenvalues of the top squark mass matrix

$$\begin{pmatrix} \kappa_{LL} \frac{v^2}{2} + M^2 & \kappa_{LR} \frac{vM}{\sqrt{2}} \\ \kappa_{LR} \frac{vM}{\sqrt{2}} & \kappa_{RR} \frac{v^2}{2} + M^2 \end{pmatrix} \tag{33}$$

define two masses $m_{\tilde{t}_1} < m_{\tilde{t}_2}$ and a mixing angle $\theta_{\tilde{t}}$. Again, we provide a detailed description of the model setup in Appendix A 4.

The main new physics effects in the Higgs sector are loop-induced modifications of the Higgs interactions, most significantly to Δ_g, Δ_γ, Δ_V, possibly including new Lorentz structures. The Yukawa couplings do not change at one loop, because we do not include gauge boson partners. As a side remark, the 2HDM described in Sec. III B combined with the scalar top partners given here corresponds to the effective description of the Minimal Supersymmetric Standard Model in the limit of infinitely heavy gauginos, sleptons, and light-flavor squarks.

Adding the top parters, the correction to the hVV coupling in the limit of small $\theta_{\tilde{t}}$ scales like

$$\Delta_V \approx \frac{\kappa_{LL}^2}{16\pi^2} \left(\frac{v}{m_{\tilde{t}_1}} \right)^2. \tag{34}$$

This shift can be sizable for relatively low top squark and sbottom masses but also for large couplings κ_{ij} to the Higgs sector.

As already noted for the 2HDM, the decoupling of the heavy scalars becomes nontrivial in the presence of a Higgs VEV. Following Eq. (33) the masses of the heavy scalar are not only controlled by M in the gauge symmetric phase, but they receive additional contributions of the type $\kappa_{LR} vM$, $\kappa_{LL} v^2$, or $\kappa_{RR} v^2$ after electroweak symmetry breaking. This leads to a mass splitting of order v between masses of order M. Large values of κ_{LR} increase this splitting. This means that in the full model the decoupling is best described in terms of $m_{\tilde{t}_1} < M$.

This motivates us to again define two different matching schemes. First, we stick to our default prescription and carry out the matching of the linear EFT Lagrangian to the full model in the unbroken phase. The matching scale Λ is then dictated by the intrinsic heavy field mass scale M and completely unrelated to v. The suppression scale of loop effects in the complete model and this matching scale in the EFT only agree in the limit $M - m_{\tilde{t}_1} \ll M$.

In this dimension-6 approach the top squark loops generate a number of operators:

$$\begin{aligned}
\bar{c}_g &= \frac{m_W^2}{24(4\pi)^2 M^2} [\kappa_{LL} + \kappa_{RR} - \kappa_{LR}^2], \\
\bar{c}_\gamma &= \frac{m_W^2}{9(4\pi)^2 M^2} [\kappa_{LL} + \kappa_{RR} - \kappa_{LR}^2], \\
\bar{c}_B &= -\frac{5 m_W^2}{12(4\pi)^2 M^2} \left[\kappa_{LL} - \frac{31}{50} \kappa_{LR}^2 \right], \\
\bar{c}_W &= \frac{m_W^2}{4(4\pi)^2 M^2} \left[\kappa_{LL} - \frac{3}{10} \kappa_{LR}^2 \right], \\
\bar{c}_{HB} &= \frac{5 m_W^2}{12(4\pi)^2 M^2} \left[\kappa_{LL} - \frac{14}{25} \kappa_{LR}^2 \right], \\
\bar{c}_{HW} &= -\frac{m_W^2}{4(4\pi)^2 M^2} \left[\kappa_{LL} - \frac{2}{5} \kappa_{LR}^2 \right], \\
\bar{c}_H &= \frac{v^2}{4(4\pi)^2 M^2} \left[2\kappa_{RR}^2 - \kappa_{LL}^2 - \left(\kappa_{RR} - \frac{1}{2} \kappa_{LL} \right) \kappa_{LR}^2 + \frac{\kappa_{LR}^4}{10} \right], \\
\bar{c}_T &= \frac{v^2}{4(4\pi)^2 M^2} \left[\kappa_{LL}^2 - \frac{\kappa_{LL} \kappa_{LR}^2}{2} + \frac{\kappa_{LR}^4}{10} \right].
\end{aligned} \tag{35}$$

TABLE VIII. Scalar top-partner Lagrangian parameters (left) and physical parameters (right) for representative model benchmarks. All masses are in GeV.

	Scalar top-partner model						
Benchmark	M	κ_{LL}	κ_{RR}	κ_{LR}	$m_{\tilde{t}_1}$	$m_{\tilde{t}_2}$	$\theta_{\tilde{t}}$
P1	500	−1.16	2.85	0.147	500	580	−0.15
P2	350	−3.16	−2.82	0.017	173	200	−0.10
P3	500	−7.51	−7.17	0.012	173	200	−0.10

In addition, we define a v-improved matching at the scale $\Lambda = m_{\tilde{t}_1}$ in the broken phase. The Wilson coefficients we obtain are the same as in Eq. (35), except that M is replaced by $m_{\tilde{t}_1}$.

Unlike in the previous two models, the top-partner loops not only induce modifications to the SM Higgs couplings but induce new Lorentz structures. In Table VIII we define a set of parameter space configurations, all with light and almost degenerate states and small mixing. The corresponding Wilson coefficients in our two matching schemes are given in Table IX. Unrealistic parameter choices with strong couplings are necessary to generate sizable loop corrections to the hVV couplings [70]. For fixed masses and mixing, the Higgs couplings to the top partners depend on the interplay between M^2 and the coupling constants κ. For small mixing and large M^2, light top-partner masses require large four-scalar couplings κ_{ii}. Conversely, if M^2 is close to the physical masses, the Yukawa couplings can be small. This illustrates the balance between the VEV-dependent (nondecoupling) and the explicit (decoupling) mass contributions.

Since the contributions from scalar top partners to the Higgs production in gluon fusion are well known [71], we focus on corrections to the hVV coupling in WBF and Higgs-strahlung, shown in Table X. In benchmark P1 the WBF cross section is reduced by about 0.6% compared to the Standard Model, with good agreement between effective and full descriptions. Such a scenario is not relevant for LHC measurements in the foreseeable future. In more extreme corners of the parameter space the loop effects in the full model grow, higher-dimensional terms in the EFT become larger, the validity of the latter worsens, and discrepancies between both increase. In benchmarks P2 and P3 the WBF rate is reduced by 9.1% and 43.5%, respectively, with respect to the Standard Model. In the left panel of Fig. 4 we show that this change in the total rate does not have dramatic effects in the kinematic distributions. By construction, the EFT based on the default matching captures only the formally leading term at $\mathcal{O}(v^2/\Lambda^2)$, only giving a reduction of 0.5% and 2.0%. The corresponding difference is again independent for example of the tagging jet's transverse momentum. With the v-improved matching, the cross section is reduced by 2.4% and 17.7%, still far from the result of the full model.

The results for Higgs-strahlung look similar: in the moderate benchmark P1 the predictions of the full model and the dimension-6 Lagrangian agree within 0.1%, but in this scenario the overall deviation from the Standard Model is negligible. In scenarios with larger loop effects, the dimension-6 predictions fails to capture most of the full top-partner loops. We demonstrate this in the right panel of Fig. 4. As for WBF, the agreement between EFT and full model becomes even worse in benchmark P3, with numerical results similar to those given for WBF Higgs production. Again the v-improved matching performs better than the default matching.

To summarize, the top-partner model for the first time generates a large set of dimension-6 operators through electroweak loops. However, in realistic scenarios with a large scale separation the loop corrections for example to the hVV vertex are tiny. Pushing for loop effects that are large enough to leave a visible imprint in WBF and Higgs-strahlung requires breaking the scale separation between the observed Higgs scalar and the top partners. In that case the EFT fails already for the total rates, and kinematic distributions hardly add to this discrepancy.

D. Vector triplet

Heavy vector bosons appear in many new physics scenarios and possibly also in data [72]. Their properties can be tested in Higgs measurements, provided they are connected to the gauge-Higgs sector of the Standard Model [14,73,74]. For these analyses the key property of new vector resonances are their SM charges. We analyze a massive vector field V_μ^a which is a triplet under $SU(2)$, couples to a scalar and fermion currents, and kinetically mixes with the weak gauge bosons of the Standard Model [14,74]. The Lagrangian includes the terms

TABLE IX. Matching scales (in GeV) and selected Wilson coefficient for the top-partner benchmarks, both for default and v-improved matching.

	EFT				EFT (v-improved)			
Benchmark	Λ	$\bar{c}_H$	$\bar{c}_W$	$\bar{c}_{HW}$	Λ	$\bar{c}_H$	$\bar{c}_W$	$\bar{c}_{HW}$
P1	500	0.0062	-3.11×10^{-7}	3.99×10^{-7}	500	0.0062	-3.11×10^{-7}	3.99×10^{-7}
P2	350	0.0043	-2.55×10^{-4}	2.55×10^{-4}	173	0.0176	-1.04×10^{-3}	1.04×10^{-3}
P3	500	0.0166	-2.97×10^{-4}	2.97×10^{-4}	173	0.1388	-2.48×10^{-3}	2.48×10^{-3}

TABLE X. Cross section ratios of the matched dimension-6 EFT approximation to the full scalar top-partner model at the LHC. We give the results both for the default matching scheme with matching scale $\Lambda = M$ as well as for the v-improved matching at $\Lambda = m_{\tilde{t}_1}$. The statistical uncertainties on these ratios are below 0.4%.

	$\sigma_{\text{EFT}}/\sigma_{\text{triplet}}$		σv-improved EFT$/\sigma_{\text{triplet}}$	
Benchmark	WBF	Vh	WBF	Vh
P1	1.000	0.999	1.000	0.999
P2	1.095	1.100	1.074	1.049
P3	2.081	1.904	1.749	1.363

$$\mathcal{L} \supset -\frac{1}{4}V^a_{\mu\nu}V^{\mu\nu a} + \frac{M_V^2}{2}V^a_\mu V^{\mu a} + i\frac{g_V}{2}c_H V^a_\mu [\phi^\dagger \sigma^a \overleftrightarrow{D}^\mu \phi] + \frac{g_w^2}{2g_V}V^a_\mu \sum_{\text{fermions}} c_F \bar{F}_L \gamma^\mu \sigma^a F_L + \frac{g_V}{2}c_{VVV}\epsilon_{abc}V^a_\mu V^b_\nu D^{[\mu}V^{\nu]c} + g_V^2 c_{VVHH} V^a_\mu V^{\mu a}\phi^\dagger\phi - \frac{g_w}{2}c_{VVW}\epsilon_{abc}W^{\mu\nu}V^b_\mu V^c_\nu. \quad (36)$$

The new field-strength tensor is $V^a_{\mu\nu} = D_\mu V^a_\nu - D_\nu V^a_\mu$ and the covariant derivative acts on the triplet as $D_\mu V^a_\nu = \partial_\mu V^a_\nu + g_V \epsilon^{abc} V^b_\mu V^c_\nu$. The coupling constant g_V is the characteristic strength of the heavy vector-mediated interactions, while g_w denotes the $SU(2)$ weak gauge coupling. It will turn out that c_{VVW} and c_{VVV} are irrelevant for Higgs phenomenology at the LHC. We give details of the model and the matching to the corresponding EFT in Appendix A 5.

The feature setting the vector triplet apart from the singlet, doublet, and top-partner models is that it directly affects the weak gauge bosons. The mixing of the new states with the W and Z bosons has two consequences: (i) a modification of the Higgs couplings to SM particles and (ii) new heavy states ξ^0, $\xi^\pm$.

The definition of mass eigenstates from the heavy vector and the SM-like gauge fields links the observable weak coupling g and the Lagrangian parameter g_w. For the coupling modifications this shift in the gauge coupling and the direct heavy vector coupling to the Higgs doublet combine to

$$\Delta_V \approx \frac{g^2 c_F c_H}{4}\left(\frac{v}{M_V}\right)^2 - \frac{3 g_V^2 c_H^2}{8}\left(\frac{v}{M_V}\right)^2,$$
$$\Delta_f \approx \frac{g^2 c_F c_H}{4}\left(\frac{v}{M_V}\right)^2 - \frac{g_V^2 c_H^2}{8}\left(\frac{v}{M_V}\right)^2. \quad (37)$$

The contribution from the shift in the weak coupling is identical for both coupling modifications. In addition, contributions from virtual heavy states ξ modify the phase-space behavior of Higgs signals in many ways.

Just as for the 2HDM and the top partners, the mass matrix for the massive vectors contains both the heavy scale M_V, which will eventually become the matching scale, and terms proportional to some power of v multiplied by potentially large couplings. The new vector states have roughly degenerate masses

$$\frac{m_\xi^2}{M_V^2} \approx 1 + g_V^2 c_{VVHH}\left(\frac{v}{M_V}\right)^2 + \frac{g_V^2 c_H^2}{4}\left(\frac{v}{M_V}\right)^2. \quad (38)$$

Even if there appears to be a clear scale separation $M_V \gg v$, large values of g_V, c_{VVHH}, or c_H can change m_ξ significantly and effectively induce a second mass scale. Just as for the top partners, a problem for the dimension-6 approach arises from virtual ξ diagrams contributing for example to WBF Higgs production. If $m_\xi < M_V \equiv \Lambda$, the lightest new particles appearing in Higgs production processes have masses below the matching scale of the linear representation. The way out of a poor agreement

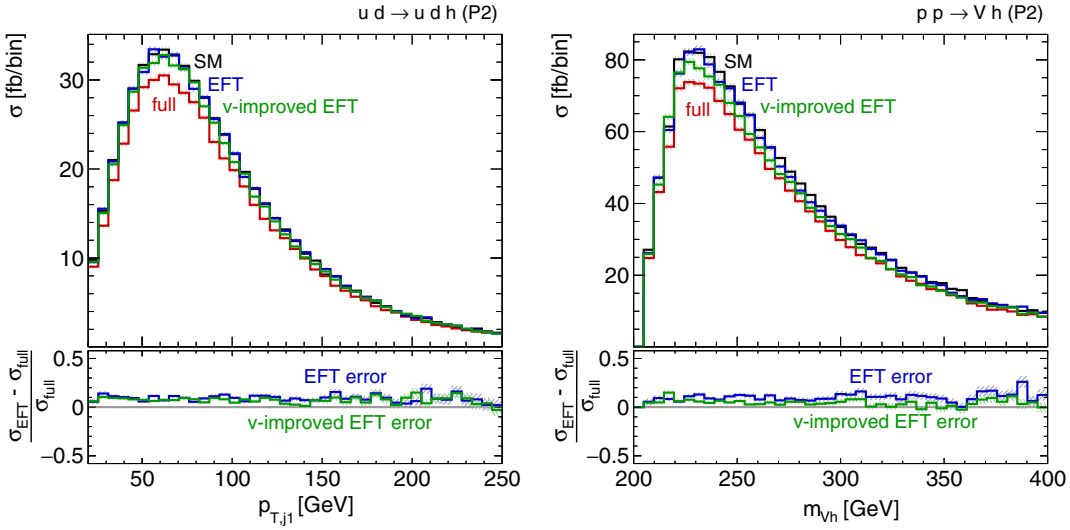

FIG. 4. Kinematic distributions for the top-partner model in benchmark P2. Left: Tagging jet properties in WBF Higgs production. Right: m_{Vh} distribution in Higgs-strahlung.

TABLE XI. Benchmark points for the vector triplet model.

	Triplet model					
Benchmark	M_V [GeV]	g_V	c_H	c_F	c_{VVHH}	m_ξ [GeV]
T1	591	3.0	−0.47	−5.0	2.0	1200
T2	946	3.0	−0.47	−5.0	1.0	1200
T3	941	3.0	−0.28	3.0	1.0	1200
T4	1246	3.0	−0.50	3.0	−0.2	1200
T5	846	1.0	−0.56	−1.32	0.08	849

between the full model and its dimension-6 description is again switching to a v-improved matching in the broken phase with matching scale $\Lambda = m_\xi$.

Integrating out the heavy vector triplet at tree level leaves us with dimension-6 Wilson coefficients

$$\bar{c}_H = \frac{3g^2v^2}{4M_V^2}\left[c_H^2\frac{g_V^2}{g^2} - 2c_F c_H\right], \quad \bar{c}_6 = \frac{g^2v^2}{M_V^2}\left[c_H^2\frac{g_V^2}{g^2} - 2c_F c_H\right],$$
$$\bar{c}_f = \frac{g^2v^2}{4M_V^2}\left[c_H^2\frac{g_V^2}{g^2} - 2c_F c_H\right], \quad \bar{c}_W = -\frac{m_W^2}{M_V^2}c_F c_H, \tag{39}$$

and four-fermion contributions that are irrelevant for Higgs physics. Additional loop-induced contributions will be further suppressed and do not add qualitatively new features, so we neglect them. As in the 2HDM, we compare this default matching to an alternative v-improved matching with matching scale $\Lambda = m_{\xi^0}$. The coefficients in Eq. (39) remain unchanged, except that M_V is replaced by m_{ξ^0}.

The main phenomenological features of this model reside in the Higgs-gauge interactions. In the dimension-6 description, these modifications are mapped (among others) onto $\mathcal{O}_W$, which induces momentum-dependent changes to the hWW and hZZ couplings. Therefore, our analysis focuses on WBF Higgs production and Higgs-strahlung, where the intermediate t-channel and s-channel gauge bosons can transfer large momenta.

As for the other models we study a set of benchmark points, defined in Tables XI and XII. Some of them are meant to emphasize the phenomenological possibilities of the vector triplet model. For those we ignore experimental constraints or parameter correlations from an underlying UV completion:

[T1–T2] All dimension-6 EFT operators except for $\mathcal{O}_W$ vanish along the line $c_H/c_F = 2g^2/g_V^2$. We aim for a large effect only in the hVV couplings. The large couplings induce different scales M_V and m_ξ.

[T3] The sign in front of $\mathcal{O}_W$ changes on another line in the (c_H, c_F) space. The remaining operators do not vanish.

[T4] The vector triplet couplings and masses satisfy the leading constraints from direct collider searches. For weak couplings ($g_V \leq 1$) resonances typically decaying to dilepton and neutrino final states have to stay above 3 TeV. For the strongly interacting case ($g_V > 1$) decays to dibosons tend to exclude masses below 1–1.5 TeV [74,75].

[T5] A weakly coupled UV completion can be based on the gauge group $SU(3) \times SU(2) \times SU(2) \times U(1)$ [76], arising for instance from deconstructed extra dimensions [77]. Its vector triplet phenomenology is effectively described by the parameter $\alpha = g_V/\sqrt{g_V^2 - g_w^2}$ together with the symmetry breaking scale f [74]:

$$M_V^2 = \alpha^2 g_V^2 f^2, \qquad c_H = -\alpha\frac{g_w^2}{g_V^2},$$
$$c_{VVHH} = \alpha^2\left[\frac{g_w^4}{4g_V^4}\right], \qquad c_F = -\alpha, \qquad c_{VVW} = 1,$$
$$c_{VVV} = -\frac{\alpha^3}{g_V}\left[1 - \frac{3g_w^2}{g_V^2} + \frac{2g_w^2}{g_V^4}\right]. \tag{40}$$

In Fig. 5 we show a set of kinematic distributions in WBF Higgs production. In addition to the predictions of the full vector triplet model and the matched EFT, we show distributions of the vector triplet model without contributions from ξ propagators. The corresponding production cross section ratios between full vector triplet model and EFT are given in Table XIII. For the full model we observe a significant modification of the rate relative to the Standard Model, especially towards large momentum transfers. They can be traced to the ξ fusion and mixed W-ξ fusion diagrams, which increase strongly with energy. In comparison, the modification of the hWW coupling only leads to a relatively mild rescaling. These contributions from ξ propagators can

TABLE XII. Matching scales and Wilson coefficients for the effective theory matched to the vector triplet model. We give these results both for the EFT matching in the unbroken phase as well as for the v-improved matching with $\Lambda = m_{\xi^0}$.

	EFT					EFT (v-improved)				
Benchmark	Λ [GeV]	$\bar{c}_W$	$\bar{c}_H$	$\bar{c}_6$	$\bar{c}_f$	Λ [GeV]	$\bar{c}_W$	$\bar{c}_H$	$\bar{c}_6$	$\bar{c}_f$
T1	591	−0.044	0.000	0.000	0.000	1200	−0.011	0.000	0.000	0.000
T2	946	−0.017	0.000	0.000	0.000	1200	−0.011	0.000	0.000	0.000
T3	941	0.006	0.075	0.100	0.025	1200	0.004	0.046	0.061	0.015
T4	1246	0.006	0.103	0.138	0.034	1200	0.007	0.111	0.149	0.037
T5	846	−0.007	−0.020	−0.027	−0.007	849	−0.007	−0.020	−0.027	−0.007

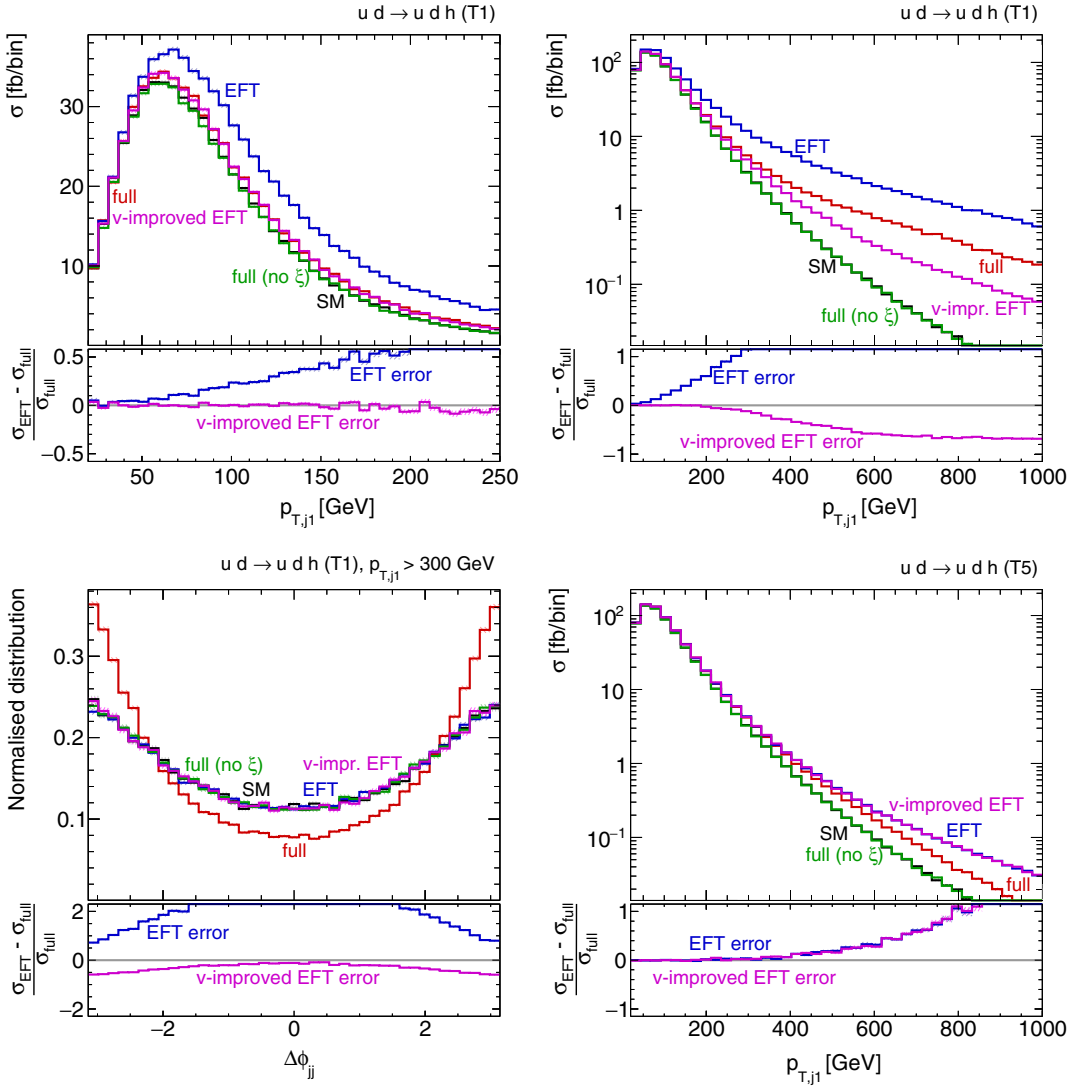

FIG. 5. Tagging jet distributions in WBF Higgs production in the vector triplet model. Top: $p_{T,j1}$ distribution in benchmark T1, focusing on the low (left) and high (right) transverse momentum regions. Bottom left: $\Delta\phi_{jj}$ distribution above a certain $p_{T,j1}$ threshold for T1. Bottom right: $p_{T,j1}$ distribution for scenario T5.

become relevant already at energy scales well below m_ξ. The weak boson virtualities inducing a momentum flow into the Higgs coupling are not the only source of deviation from the Standard Model; the azimuthal correlation between the tagging jets is well known to be sensitive to the modified Lorentz structure of the hWW vertex [19].

Qualitatively, the dimension-6 approach captures the features of the full model, driven by $\mathcal{O}_W$. In T1 and T2 a negative Wilson coefficient yields a nonlinear increase of the cross section with energy. Conversely, the positive coefficient in T3 reduces the rate with energy, eventually driving the combined amplitude through zero.

Comparing full and effective model for the more realistic benchmark points T4 and T5 we see good agreement in the bulk of the distribution. The deviations from the Standard Model are captured by the dimension-6 operators, including the momentum dependence coming from the ξ diagrams. Only at very large momentum transfer the validity of the EFT breaks down. For our realistic benchmark points the LHC is likely not sensitive to these subtle effects.

In the more strongly coupled benchmark points T1–T3, the full model predicts shifts in the jet distributions that are large enough to be relevant for the upcoming LHC run. We find good agreement between the full model and the default EFT only at low momentum transfer, where the effects of new physics are small. In particular in benchmark T1, this naive dimension-6 approach loses its validity already around $p_{T,j} \gtrsim 80$ GeV, a phase-space region highly relevant for constraints on new physics [7].[1] This does not

[1]Note, however, that these scenarios are already in tension with bounds from electroweak precision observables, but we nevertheless show them to illustrate the qualitative aspects of EFT breakdown.

TABLE XIII. Cross section ratios of the matched dimension-6 EFT approximation to the full vector triplet at the LHC. To avoid large contributions from the ξ resonance in the Vh channel, we only take into account the region $m_{Vh} < 600$ GeV. The statistical uncertainties on these ratios are below 0.4%.

	$\sigma_{\text{EFT}}/\sigma_{\text{triplet}}$		$\sigma_{v\text{-improved EFT}}/\sigma_{\text{triplet}}$	
Benchmark	WBF	Vh	WBF	Vh
T1	1.299	0.299	0.977	0.794
T2	1.045	0.737	0.992	0.907
T3	0.921	1.066	0.966	1.024
T4	1.026	0.970	1.012	0.978
T5	1.001	1.043	1.002	1.043

signal a breakdown of the E/Λ expansion, but a too large $c_i v^2/\Lambda^2$. It is linked to the difference between the scales m_ξ and M_V as given in Eq. (38), which the default matching procedure is blind to. Indeed, with the v-improved matching the agreement is significantly better, and the dimension-6 description departs from the full model only at high energies, $p_{T,j1} \gtrsim 300$ GeV.

The situation is similar in Higgs-strahlung, shown in Fig. 6. In the full model the ξ propagators again dominate over the modified hWW interaction. In addition, the interference with the ξ-mediated diagrams leads to a significant change of the rate and introduces a momentum dependence already far below the actual resonance. The relative sign of the interference between ξ amplitudes and SM-like diagrams is opposite to that in WBF.

In the EFT the operator $\mathcal{O}_W$ induces the corresponding strong energy dependence. A positive Wilson coefficient leads to a nonlinear increase of the cross section with the energy scale, probed by either m_{Vh} or the $p_{T,V}$. A negative coefficient leads to a decreasing amplitude with energy, including a sign flip. Like for the full model, these $\mathcal{O}_W$ terms have the opposite effect on the rate as in WBF.

The full and effective models agree relatively well in the more weakly coupled benchmarks at low energies. In the

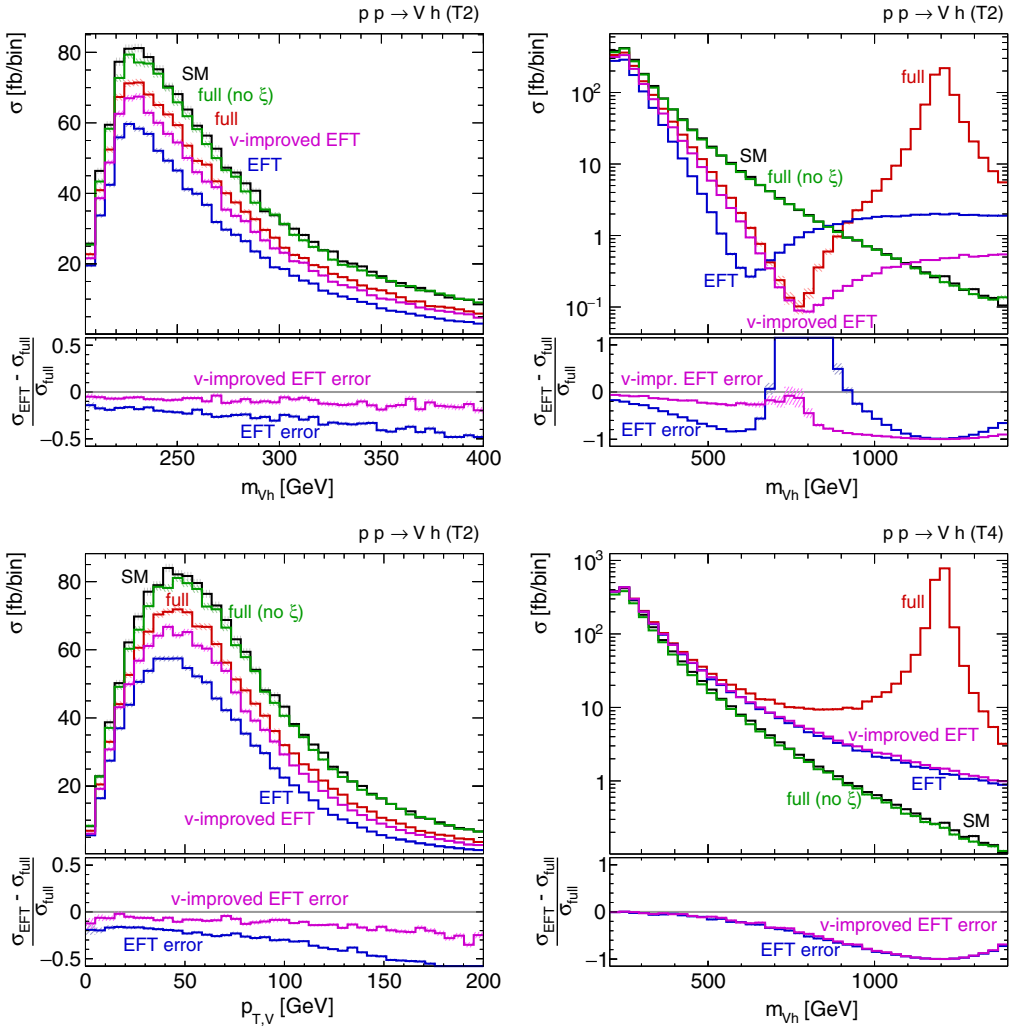

FIG. 6. Higgs-strahlung distributions in the vector triplet model. Top: m_{Vh} distribution for benchmark T2, focusing on the low (left) and high (right) invariant mass regions. Bottom left: $p_{T,V}$ distribution for the same benchmark. Bottom right: m_{Vh} distribution for T4.

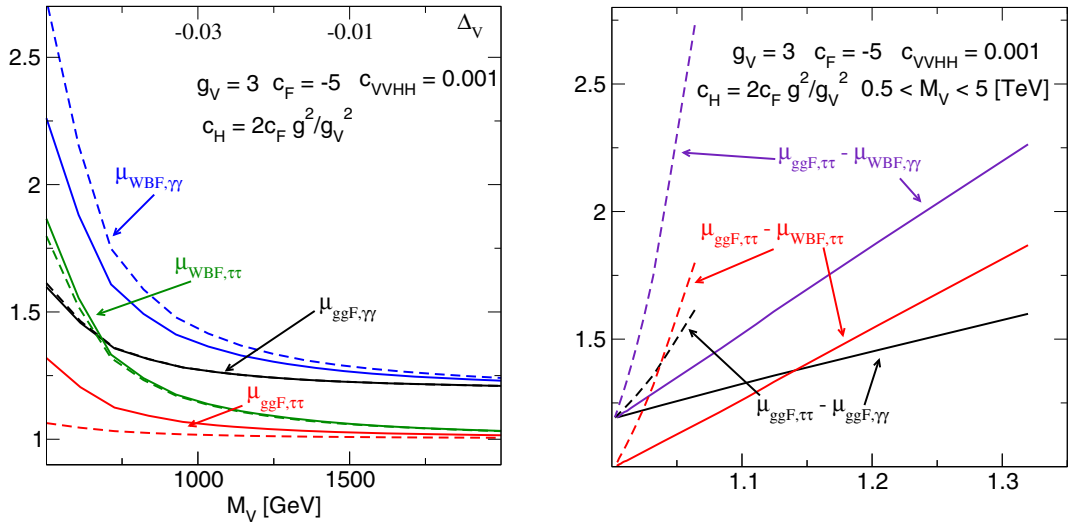

FIG. 7. Signal strength modifications in the vector triplet. The solid lines show the full model, while the dashed lines give the dimension-6 predictions for the default matching. Left: Signal strength $\mu_{p,d}$ for different Higgs production modes and decay channels for an exemplary vector triplet setup as a function of M_V. In the upper horizontal axis we show the deviation from the SM-like limit through the coupling shift Δ_V, Eq. (37). Right: Signal strength correlations μ_{p_1,d_1} versus μ_{p_2,d_2} between different channels for variable M_V.

realistic scenarios T4 and T5, this agreement extends over the most relevant part of the phase space, and the EFT successfully describes how the ξ propagators shift the Higgs-strahlung kinematics. With increasing energy, momentum-dependent effects in both the full model (due to the resonance) and the EFT (due to $\mathcal{O}_W$) become more relevant. While the sign of the effect is the same in full model and EFT, the size and energy dependence is different, and the EFT eventually fails to be a good approximation. At even higher energies, the "dips" at different energies in the full model and EFT as well as the ξ resonance in the full model mark the obvious failure of the effective theory.

For benchmarks T1–T3, where the effects are numerically much more relevant for the LHC, the range of validity of the default EFT is limited. The couplings are so large that in spite of a resonance mass $m_\xi \sim 1$ TeV the dimension-6 description already fails at $m_{Vh} \gtrsim 220$ GeV. Switching to the v-improved matching again ameliorates the dimension-6 approximation. Even then, this mismatch between full model and EFT is more pronounced in Higgs-strahlung than in WBF, because ξ contributions play a larger role in these s-channel diagrams than in the t-channel WBF amplitudes.

In Fig. 7 we again go beyond individual benchmark points and examine the agreement between full model and its dimension-6 description in terms of signal strengths, correlated for different Higgs production modes and decay channels. For definiteness, we assume vector triplet parameters in line with the benchmarks T1 and T2 and vary the heavy vector mass scale $M_V = 0.5\ldots5$ TeV. The dimension-6 coefficients are based on the default matching.

The huge deviations in the WBF signal strength are due to the sizable momentum-dependent effects in the fusion process. As discussed above, this behavior is poorly captured by the EFT for large vector couplings and fails dramatically for light mass scales. The same differences are visible from the different trajectories in the correlated signal strength plane, shown in the left panel. The mild offset from $\mu_{p,\gamma\gamma} = 1$ in the limit $M_V \gg v$ can be traced back to the nondecoupling $\xi^\pm$-mediated contribution to the $h\gamma\gamma$ loop. The $\mathcal{O}(c_F c_H v^4/m_V^4)$ contributions of dimension 8 and higher are responsible for the additional upward enhancement of the fermion Yukawas in the full model, which is in particular visible for $\mu_{gg,\tau\tau}$, where the full model predictions systematically surpass the EFT. Finally, we find that an enhanced top-W interference in Δ_γ pulls the full model $\gamma\gamma$ rates below the dimension-6-based predictions. The accidental counterbalance of the higher-dimension effects missing in the EFT explains the remarkable agreement with the full model for $\mu_{\mathrm{ggF},\gamma\gamma}$.

Like the additional scalar models discussed before, the vector triplet model offers regions in parameter space where the EFT works up to large momentum transfer for realistic scenarios. It successfully captures the virtual ξ contributions in the momentum-dependent contribution from $\mathcal{O}_W$, but these numerical effects are small. Relevant effects for the LHC occur if the separation of scales is spoiled by large couplings or light new particles. In this case we find substantial dimension-6 departures from the full model predictions for example in the bulk of the WBF distributions, which typically further increase with the energy scale. A modified dimension-6 description incorporating v-dependent effects improves the EFT accuracy such that large deviations only occur in the high-energy tails of distributions.

TABLE XIV. Possible sources of failure of dimension-6 Lagrangian at the LHC. We use parentheses where deviations in kinematic distributions appear but are unlikely to be observed in realistic scenarios.

		EFT failure		
Model	Process	Resonance	Kinematics	Matching
Singlet	On-shell $h \to 4\ell$, WBF, Vh, …			×
	Off-shell WBF, …		(×)	×
	hh	×	×	×
2HDM	On-shell $h \to 4\ell$, WBF, Vh, …			×
	Off-shell $h \to \gamma\gamma$, …		(×)	×
	hh	×	×	×
Top partner	WBF, Vh			×
Vector triplet	WBF		(×)	×
	Vh	×	(×)	×

IV. SUMMARY

An effective field theory for the Higgs sector offers a theoretically well-defined, efficient, and largely model-independent language to analyze extensions of the Standard Model in both rate measurements and kinematic distributions. A fit of dimension-6 operators to LHC Higgs measurements works fine [7] and constitutes the natural extension of the Higgs couplings analyses of run I. Most of the relevant higher-dimensional operators correspond to simple coupling modifications, supplemented by four operators describing new Lorentz structures in the Higgs coupling to weak bosons [7].

In this paper we have studied the validity of this approach from the theoretical side. We know that at the LHC a clear hierarchy of electroweak and new physics scales cannot be guaranteed; the question is whether dimension-6 operators nevertheless capture the phenomenology of specific UV-complete theories with sufficient accuracy. We have systematically compared a singlet Higgs portal model, a two-Higgs-doublet model, scalar top partners, and a heavy vector triplet to their dimension-6 EFT descriptions, based on the linear realization of electroweak symmetry breaking with a Higgs doublet. We have analyzed the main Higgs production and decay signatures, covering rates as well as kinematic distributions.

We have found that the dimension-6 operators provide an adequate description in almost all realistic weakly coupled scenarios. Shifts in the total rates are well described by effective operators. Kinematic distributions typically do not probe weakly interacting new physics with sufficient precision in the high-energy tails to challenge the effective operator ansatz. This is obvious for the extended scalar models, where new Lorentz structures and momentum-dependent couplings with dramatic effects in LHC distributions only appear at the loop level. A loop-suppressed effective scale suppression $E^2/(4\pi\Lambda)^2$ has to be compared with on-shell coupling modifications proportional to v^2/Λ^2. Only phase-space regions probing energies around $4\pi v \approx 3$ TeV significantly constrain loop contributions in the Higgs sector and eventually lead to breakdown of the effective field theory. In turn, a simple dimension-6 descriptions will capture all effects that are expected to be measurable with sufficient statistics at the LHC run II. On the other hand, the vector triplet model shows that modifications of the gauge sector can generate effects in LHC kinematics at tree level. However, we again find that for weakly interacting models and phenomenologically viable benchmark points they are described well by an appropriate set of dimension-6 operators.

Three sources for a possible breakdown of the dimension-6 description are illustrated in Table XIV[2]: First, the EFT cannot describe light new resonances. Such a signature at the LHC would be an obvious signal to stop using the EFT and switch to appropriate simplified models. Second, selected kinematic distributions fail to be described by the dimension-6 Lagrangian, in particular for Higgs pair production. Deviations in the high-energy tails of WBF and Higgs-strahlung distributions on the other hand are too small to be relevant in realistic weakly coupled scenarios. These two cases do not threaten LHC analyses in practice.

The third issue with the dimension-6 EFT description is linked to matching in the absence of a well-defined scale hierarchy. Even with only one heavy mass scale in the Lagrangian, the electroweak VEV together with large couplings can generate several new physics scales, defined by the masses of the new particles. A linear EFT description, which is justified by the SM-like properties of the newly discovered Higgs boson, should in principle be matched in the phase where the electroweak symmetry is unbroken. Such a procedure is blind to additional scales induced by the electroweak VEV, potentially leading to large errors in the dimension-6

[2]Forcing the EFT approach into a spectacular breakdown was the original aim of this paper, but to our surprise this did not happen.

approximation. Including v-dependent terms in the Wilson coefficients, which corresponds to matching in the broken phase, can significantly improve the EFT performance. We have explicitly demonstrated this for all the models considered in this paper.

Barring the detection of new light resonances, none of these complications with the dimension-6 description presents a major problem in using effective operators to fit LHC Higgs data. Most of them are purely theoretical issues that only need to be considered for the interpretation of the results.

ACKNOWLEDGMENTS

We would like to thank Juan Gonzalez-Fraile for fruitful discussions over many cups of coffee. T. P. would like to thank the HDays workshop in Santander for great discussions contributing to the presentation of this paper. J. B. is grateful to the DFG for his funding through the Graduiertenkolleg *Particle physics beyond the Standard Model* (GRK 1940). D. L.-V. is funded by the F.R.S.-FNRS *Fonds de la Recherche Scientifique* (Belgium). T. P. acknowledges support by the DFG Forschergruppe *New Physics at the LHC* (FOR 2239). The work of A. F. is funded in part by the U.S. National Science Foundation under Grants No. PHY-1212635 and No. PHY-1519175.

APPENDIX: MODELS AND MATCHING

1. Operator bases

As mentioned in Sec. II A, we here adopt the notation and conventions of Ref. [41], which is based on the SILH framework with the decomposition and normalization of the Wilson coefficients defined in Ref. [32]. For our purposes, it is enough to single out the subset that encodes all possible new physics contributions to the Higgs sector compatible with CP conservation and the flavor structure of the SM. These are given in Table XV and correspond to the Lagrangian in Eq. (3).

The conventions for how covariant derivatives act on the Higgs, fermion and gauge vector fields are fixed as follows:

$$\begin{aligned} D_\mu\phi &= \partial_\mu\phi - \frac{ig'}{2}B_\mu\phi - ig\frac{\sigma^a}{2}W^a_\mu\phi, \\ D_\mu F_L &= \partial_\mu F_L - ig'\frac{Y_{F_L}}{2}B_\mu F_L - ig\frac{\sigma^a}{2}W^a_\mu F_L, \\ D_\mu V^a_\nu &= \partial_\mu V^a_\nu + g\epsilon^{abc}W^b_\mu V^c_\nu, \\ D_\mu W^a_{\nu\rho} &= \partial_\mu W^a_{\nu\rho} + g\epsilon^{abc}W^b_\mu W^c_{\nu\rho}. \end{aligned} \tag{A1}$$

While the effective Lagrangian in Eq. (3) is written in terms of the fundamental SM gauge fields, the connection to physics observables is more easily seen in the mass-eigenstate basis, which we can write as

$$\begin{aligned} \mathcal{L} \supset & -\frac{m_H^2}{2v}g^{(1)}_{HHH}HHH + \frac{1}{2}g^{(2)}_{HHH}H(\partial_\mu H)(\partial^\mu H) - \frac{1}{4}g_{ggH}G^{\mu\nu A}G^A_{\mu\nu}H - \frac{1}{4}g_{\gamma\gamma H}F^{\mu\nu}F_{\mu\nu}H - \frac{1}{4}g^{(1)}_Z Z_{\mu\nu}Z^{\mu\nu}H - g^{(2)}_Z Z_\nu\partial_\mu Z^{\mu\nu}H \\ & + \frac{1}{2}g^{(3)}_Z Z_\mu Z^\mu H - \frac{1}{2}g^{(1)}_W W^{\mu\nu}W^\dagger_{\mu\nu}H - [g^{(2)}_W W^\nu\partial^\mu W^\dagger_{\mu\nu}H + \text{H.c.}] + g^{(3)}_W m_W W^\dagger_\mu W^\mu H \\ & - \left[g_u\frac{1}{\sqrt{2}}(\bar{u}P_R u)H + g_d\frac{1}{\sqrt{2}}(\bar{d}P_R d)H + g_\ell\frac{1}{\sqrt{2}}(\bar{\ell}P_R\ell)H + \text{H.c.}\right], \end{aligned} \tag{A2}$$

with the different effective couplings g_i quoted in Table XVI. More details on the notation and conventions can be found in Ref. [41].

Note that the Higgs-fermion coupling shift is given by $g_f \propto y_f(1-\bar{c}_H/2+3\bar{c}_f/2)$, but $\hat{\mathcal{O}}_f$ also shifts the fermion masses to $m_f = y_f v(1+\bar{c}_f/2)/\sqrt{2}$, yielding the result given above. Similarly, $\hat{\mathcal{O}}_H$ and $\hat{\mathcal{O}}_\gamma$ generate additional contributions to the Higgs-boson and gauge-boson kinetic terms, which are restored to their canonical form by the field redefinitions

$$\begin{aligned} H &\to H\left(1-\frac{1}{2}c_H\right), \\ Z_\mu &\to Z_\mu\left(1+\frac{4s_w^4}{c_w^2}c_\gamma\right), \\ A_\mu &\to A_\mu(1+4s_w^2c_\gamma) - Z_\mu\left(\frac{8s_w^3}{c_w}c_\gamma\right). \end{aligned} \tag{A3}$$

None of the operators considered in this basis affects the relations between g, m_W, v and G_F, so the SM relations

$$m_W = \frac{gv}{2}, \qquad G_F = \frac{\sqrt{2}g^2}{8m_W^2} = \frac{1}{\sqrt{2}v^2} \tag{A4}$$

can always be used to translate these coupling shifts from one scheme of input parameters to another.

Dimension-6 operators result in a modified pattern of Higgs interactions, leading to coupling shifts $g_{xxH} \equiv g^{\text{SM}}_{xxH}(1+\Delta_x)$ and also genuinely novel Lorentz structures. Interestingly, in general more than one of the effective operators in Table XV contributes to a given Higgs interaction in the mass basis, implying that it is in general not possible to establish a one-to-one mapping between Wilson coefficients and distorted Higgs couplings.

Note that the Wilson coefficients of the operators $\hat{\mathcal{O}}_T$ and $\hat{\mathcal{O}}_B + \hat{\mathcal{O}}_W$ are strongly constrained by electroweak

TABLE XV. Dimension-6 operators considered in our analysis. These correspond to a subset of the most general effective operator basis [32] describing new physics effects to the SM Higgs sector with CP-invariance and SM-like fermion structures.

Higgs fields
$\hat{\mathcal{O}}_H = \partial^\mu(\phi^\dagger\phi)\partial_\mu(\phi^\dagger\phi)$
$\hat{\mathcal{O}}_6 = (\phi^\dagger\phi)^3$
$\hat{\mathcal{O}}_T = (\phi^\dagger \overleftrightarrow{D}^\mu \phi)(\phi^\dagger \overleftrightarrow{D}_\mu \phi)$
Higgs and fermion fields
$\hat{\mathcal{O}}_u = (\phi^\dagger\phi)(\phi^\dagger \cdot \bar{Q}_L)u_R$
$\hat{\mathcal{O}}_d = (\phi^\dagger\phi)(\phi\bar{Q}_L)d_R$
$\hat{\mathcal{O}}_\ell = (\phi^\dagger\phi)(\phi\bar{L}_L)l_R$
Higgs and gauge boson fields
$\hat{\mathcal{O}}_{HB} = (D^\mu\phi^\dagger)(D^\nu\phi)B_{\mu\nu}$
$\hat{\mathcal{O}}_{HW} = (D^\mu\phi^\dagger)\sigma^k(D^\nu\phi)W^k_{\mu\nu}$
$\hat{\mathcal{O}}_g = (\phi^\dagger\phi)G^A_{\mu\nu}G^{\mu\nu A}$
$\hat{\mathcal{O}}_\gamma = (\phi^\dagger\phi)B_{\mu\nu}B^{\mu\nu}$
$\hat{\mathcal{O}}_B = (\phi^\dagger \overleftrightarrow{D}^\mu \phi)(\partial^\nu B_{\mu\nu})$
$\hat{\mathcal{O}}_W = (\phi^\dagger\sigma^k \overleftrightarrow{D}^\mu \phi)(D^\nu W^k_{\mu\nu})$

TABLE XVI. Subset of the dimension-6 operators which enter the different leading-order Higgs couplings which are relevant for LHC phenomenology, in the notation and conventions of Ref. [41] (see text). The different superscripts denote the various terms in the Lagrangian in Eq. (A2) and correspond to either a SM-like interaction with a rescaled coupling strength or to genuinely new Lorentz structures. The weak coupling constant is written as $g \equiv e/s_w$. The SM contribution to the loop-induced Higgs coupling to the gluons (photons) is denoted by g_H (a_H).

Coupling	Operators	Expression
$g_Z^{(1)}$	$\hat{\mathcal{O}}_{HB}, \hat{\mathcal{O}}_{HW}, \hat{\mathcal{O}}_\gamma$	$\frac{2g}{m_W c_w^2}[\bar{c}_{HB}s_w^2 - 4\bar{c}_\gamma s_w^4 + c_w^2\bar{c}_{HW}]$
$g_Z^{(2)}$	$\hat{\mathcal{O}}_{HW}, \hat{\mathcal{O}}_{HB}, \hat{\mathcal{O}}_W, \hat{\mathcal{O}}_B$	$\frac{g}{m_W c_w^2}[(\bar{c}_{HW} + \bar{c}_W)c_w^2 + (\bar{c}_B + \bar{c}_{HB})s_w^2]$
$g_Z^{(3)}$	$\hat{\mathcal{O}}_H, \hat{\mathcal{O}}_T, \hat{\mathcal{O}}_\gamma$	$\frac{gm_W}{c_w^2}[1 - \frac{1}{2}\bar{c}_H - 2\bar{c}_T + 8\bar{c}_\gamma\frac{s_w^4}{c_w^2}]$
$g_W^{(1)}$	$\hat{\mathcal{O}}_{HW}$	$\frac{2g}{m_W}\bar{c}_{HW}$
$g_W^{(2)}$	$\hat{\mathcal{O}}_{HW}, \hat{\mathcal{O}}_W$	$\frac{g}{m_W}[\bar{c}_W + \bar{c}_{HW}]$
$g_W^{(3)}$	$\hat{\mathcal{O}}_H$	$g(1 - \frac{1}{2}\bar{c}_H)$
g_f	$\hat{\mathcal{O}}_H, \hat{\mathcal{O}}_f (f = u,d,\ell)$	$\frac{\sqrt{2}m_f}{v}[1 - \frac{1}{2}\bar{c}_H + \bar{c}_f]$
g_g	$\hat{\mathcal{O}}_H, \hat{\mathcal{O}}_g$	$g_H - \frac{4\bar{c}_g g_s^2 v}{m_W^2}$
g_γ	$\hat{\mathcal{O}}_H, \hat{\mathcal{O}}_\gamma$	$a_H - \frac{8g\bar{c}_\gamma s_w^2}{m_W}$
$g_{HHH}^{(1)}$	$\hat{\mathcal{O}}_H, \hat{\mathcal{O}}_6$	$1 + \frac{5}{2}\bar{c}_6 - \frac{1}{2}\bar{c}_H$
$g_{HHH}^{(2)}$	$\hat{\mathcal{O}}_H$	$\frac{g}{m_W}\bar{c}_H$

precision data [32]. In this work, we allow ourselves, on occasion, to ignore these bounds to more distinctly illustrate the effects in the Higgs sector.

Translations between effective operator bases can be performed with the help of equations of motion, field redefinitions, integration by parts and Fierz identities. Here we quote a number of such relations which turn out to be particularly useful for the practitioner. For example, in addition to the effective operators in the SILH basis, we often find the operators

$$\hat{\mathcal{O}}_r = \phi^\dagger\phi(D_\mu\phi)^2, \qquad \hat{\mathcal{O}}'_{HF} = (\bar{f}_L\gamma^\mu\sigma^a f_L)(\phi^\dagger\sigma^a \overleftrightarrow{D}_\mu\phi),$$
$$\hat{\mathcal{O}}_D = (D^2\phi)^2, \qquad \hat{\mathcal{O}}'_{HH} = (\phi^\dagger\sigma^a \overleftrightarrow{D}_\mu\phi)(\phi^\dagger\sigma^a \overleftrightarrow{D}_\mu\phi). \tag{A5}$$

$\hat{\mathcal{O}}'_{HH}$ can be replaced by using the completeness relation of the Pauli matrices, which for arbitrary $SU(2)$ doublets ξ, χ, η, ψ leads to

$$\begin{aligned}(\xi^\dagger\sigma^a\chi)(\eta^\dagger\sigma^a\psi) &= \sum_{ijkl}\xi_i^*\sigma^a_{ij}\chi_j\eta_k^*\sigma^a_{kl}\psi_l \\ &= \sum_{ijkl}(2\delta_{il}\delta_{jk} - \delta_{ij}\delta_{kl})\xi_i^*\chi_j\eta_k^*\psi_l \\ &= 2(\xi^\dagger\psi)(\eta^\dagger\chi) - (\xi^\dagger\chi)(\eta^\dagger\psi). \end{aligned}\tag{A6}$$

Thus we find

$$\begin{aligned}\hat{\mathcal{O}}'_{HH} &= (\phi^\dagger\sigma^a D^\mu\phi)^2 + ((D^\mu\phi^\dagger)\sigma^a\phi)^2 - 2((D^\mu\phi^\dagger)\sigma^a\phi) \\ &\quad\times(\phi^\dagger\sigma^a D_\mu\phi) \\ &= (\phi^\dagger D^\mu\phi)^2 + ((D^\mu\phi^\dagger)\phi)^2 - 2[2((D^\mu\phi^\dagger)D^\mu\phi)(\phi^\dagger\phi) \\ &\quad - ((D^\mu\phi^\dagger)\phi)(\phi^\dagger D^\mu\phi)] \\ &= \hat{\mathcal{O}}_H - 4\hat{\mathcal{O}}_r. \end{aligned}\tag{A7}$$

The equation of motion for the W fields,

$$D^\nu W^a_{\mu\nu} = -ig\phi^\dagger\frac{\sigma^a}{2}\overleftrightarrow{D}_\mu\phi - g\sum_f \bar{f}_L\frac{\sigma^a}{2}\gamma_\mu f_L, \tag{A8}$$

gives rise to the identity

$$\sum_f \hat{\mathcal{O}}'_{HF} = \frac{2}{g}\hat{\mathcal{O}}_W - i\hat{\mathcal{O}}_H + 4i\hat{\mathcal{O}}_r. \tag{A9}$$

A global redefinition $\phi \to \phi + \alpha(\phi^\dagger\phi)\phi/v^2$ generates a shift in the Wilson coefficients

$$\begin{aligned} &c_H \to c_H + 2\alpha, \qquad c_r \to c_r + 2\alpha, \\ &c_6 \to c_6 + 4\alpha, \qquad c_f \to c_f + \alpha, \end{aligned}\tag{A10}$$

so that with the choice $\alpha = -c_r/2$ one can eliminate the operator $\mathcal{O}_r$ in favor of other operators:

$$\hat{\mathcal{O}}_r \leftrightarrow \left\{ -\frac{1}{2}\hat{\mathcal{O}}_H + 2\lambda\hat{\mathcal{O}}_6 + \sum_f \left[\frac{1}{2} y_f \hat{\mathcal{O}}_f + \text{H.c.} \right] \right\}. \quad \text{(A11)}$$

Finally, $\hat{\mathcal{O}}_D$ can be exchanged for others using the equation of motion for ϕ:

$$D^2\phi = -\mu^2\phi - 2\lambda\phi^\dagger\phi\phi - \sum_{\text{gen}} [y_u \bar{Q}_L^T u_R + y_d \bar{d}_R Q_L + y_\ell \bar{\ell}_R L_L]. \quad \text{(A12)}$$

This leads to

$$\hat{\mathcal{O}}_D = \mu^4\phi^\dagger\phi + 4\lambda\mu^2(\phi^\dagger\phi)^2 + \mu^2\sum_f y_f \bar{f}_L \phi f_R + 4\lambda^2(\phi^\dagger\phi)^3 + 2\lambda\sum_f y_f \phi^\dagger\phi(\bar{f}_L\phi f_R). \quad \text{(A13)}$$

The first three terms lead to a renormalization of the SM parameters μ, λ, y_f, without any impact on physical observables. The last two terms, however, mean that $\mathcal{O}_D$ is equivalent to the combination

$$\hat{\mathcal{O}}_D \leftrightarrow 4\lambda^2\hat{\mathcal{O}}_6 + 2\lambda\sum_f (y_f\hat{\mathcal{O}}_f + \text{H.c.}). \quad \text{(A14)}$$

a. HLM basis

Aside from the relatively simple case of the multi-Higgs sector extensions, we make use of the covariant derivative expansion [78,79] to analytically carry out the matching between the different UV completions to their corresponding EFT description. The method has been recently reappraised in Ref. [26] and employed in a number of studies [15,16,80,81]. By applying this method, the Wilson coefficients are readily obtained in a different operator basis (henceforth dubbed HLM):

$$\mathcal{L}_{\text{HLM}} = \sum_i \frac{k_i}{\Lambda^2}\mathcal{O}''_i. \quad \text{(A15)}$$

The HLM operators involving Higgs fields and their interaction with gauge bosons are listed in Table XVII. In addition, the HLM basis contains a subset of operators with no direct correspondence to the bosonic SILH operators, which must be rewritten with the help of equations of motion and field redefinitions, as we discuss below.

The operators in Table XVII translate to the SILH basis via

$$\begin{aligned}
&\mathcal{O}''_H = \frac{1}{2}\hat{\mathcal{O}}_H, \qquad \mathcal{O}''_6 = \mathcal{O}_6, \qquad \mathcal{O}''_T = \frac{1}{2}\hat{\mathcal{O}}_T,\\
&\mathcal{O}''_B = \frac{ig'}{2}\hat{\mathcal{O}}_B, \qquad \mathcal{O}''_W = \frac{ig}{2}\hat{\mathcal{O}}_W, \qquad \mathcal{O}''_{GG} = g_s^2\hat{\mathcal{O}}_g,\\
&\mathcal{O}''_{BB} = g'^2\hat{\mathcal{O}}_\gamma, \qquad \mathcal{O}''_{WB} = 2ig'\hat{\mathcal{O}}_B - 4ig'\hat{\mathcal{O}}_{HB} - g'^2\hat{\mathcal{O}}_\gamma,\\
&\mathcal{O}''_{WW} = -2ig'\hat{\mathcal{O}}_B + 2ig\hat{\mathcal{O}}_W + 4ig'\hat{\mathcal{O}}_{HB} - 4ig\hat{\mathcal{O}}_{HW} + g'^2\hat{\mathcal{O}}_\gamma.
\end{aligned} \quad \text{(A16)}$$

TABLE XVII. Bosonic CP-conserving Higgs operators in the HLM basis (left) and the HISZ basis (right). Here $\hat{B}_{\mu\nu} = ig'/2B_{\mu\nu}$ and $\hat{W}_{\mu\nu} = ig\sigma^k/2W^k_{\mu\nu}$.

HLM basis
$\mathcal{O}''_H = \frac{1}{2}\partial^\mu(\phi^\dagger\phi)\partial_\mu(\phi^\dagger\phi)$
$\mathcal{O}''_6 = (\phi^\dagger\phi)^3$
$\mathcal{O}''_T = \frac{1}{2}(\phi^\dagger \overleftrightarrow{D}^\mu \phi)(\phi^\dagger \overleftrightarrow{D}_\mu \phi)$
$\mathcal{O}''_B = \frac{ig'}{2}(\phi^\dagger \overleftrightarrow{D}^\mu \phi)\partial^\nu B_{\mu\nu}$
$\mathcal{O}''_W = \frac{ig}{2}(\phi^\dagger\sigma^k \overleftrightarrow{D}^\mu \phi)(D^\nu W^k_{\mu\nu})$
$\mathcal{O}''_{GG} = g_s^2(\phi^\dagger\phi)G^A_{\mu\nu}G^{\mu\nu A}$
$\mathcal{O}''_{BB} = g'^2(\phi^\dagger\phi)B_{\mu\nu}B^{\mu\nu}$
$\mathcal{O}''_{WW} = g^2(\phi^\dagger\phi)W^k_{\mu\nu}W^{\mu\nu k}$
$\mathcal{O}''_{WB} = gg'(\phi^\dagger\sigma^k\phi)B_{\mu\nu}W^{\mu\nu k}$
HISZ basis
$\mathcal{O}'_{\phi 1} = (D_\mu\phi)^\dagger\phi\phi^\dagger(D^\mu\phi)$
$\mathcal{O}'_{\phi 2} = \frac{1}{2}\partial^\mu(\phi^\dagger\phi)\partial_\mu(\phi^\dagger\phi)$
$\mathcal{O}'_{\phi 3} = \frac{1}{3}(\phi^\dagger\phi)^3$
$\mathcal{O}'_{GG} = (\phi^\dagger\phi)G^A_{\mu\nu}G^{\mu\nu A}$
$\mathcal{O}'_{BB} = \phi^\dagger\hat{B}_{\mu\nu}\hat{B}^{\mu\nu}\phi = -\frac{g'^2}{4}\phi^\dagger\phi B_{\mu\nu}B^{\mu\nu}$
$\mathcal{O}'_{WW} = \phi^\dagger\hat{W}_{\mu\nu}\hat{W}^{\mu\nu}\phi = -\frac{g^2}{4}\phi^\dagger\phi W^k_{\mu\nu}W^{\mu\nu k}$
$\mathcal{O}'_{BW} = \phi^\dagger\hat{B}_{\mu\nu}\hat{W}^{\mu\nu}\phi = -\frac{gg'}{4}(\phi^\dagger\sigma^k\phi)B_{\mu\nu}W^{\mu\nu k}$
$\mathcal{O}'_B = (D^\mu\phi)^\dagger\hat{B}_{\mu\nu}(D^\nu\phi) = i\frac{g}{2}(D^\mu\phi^\dagger)(D^\nu\phi)B_{\mu\nu}$
$\mathcal{O}'_W = (D^\mu\phi)^\dagger\hat{W}_{\mu\nu}(D^\nu\phi) = i\frac{g}{2}(D^\mu\phi^\dagger)\sigma^k(D^\nu\phi)W^k_{\mu\nu}$

In addition, the HLM basis contains extra operators with no SILH counterpart:

$$\mathcal{O}''_R = \phi^\dagger\phi(D_\mu\phi)^\dagger(D^\mu\phi), \qquad \mathcal{O}''_D = (D^2\phi)^2, \quad \text{(A17)}$$

which can be eliminated using Eqs. (A11) and (A14), respectively. The Wilson coefficients k_i of the HLM basis translate to the SILH coefficients $\bar{c}_i$ as follows:

$$\begin{aligned}
&\bar{c}_H = \frac{v^2}{\Lambda^2}(k_H - k_R), \quad \bar{c}_B = \frac{v^2}{\Lambda^2}\frac{g^2}{4}(k_B + 4k_{WB} - 4k_{WW}),\\
&\bar{c}_T = \frac{v^2}{\Lambda^2}k_T, \qquad \bar{c}_W = \frac{v^2}{\Lambda^2}\frac{g^2}{4}(k_W + 4k_{WW}),\\
&\bar{c}_6 = -\frac{v^2}{\Lambda^2}\left(\frac{k_6}{\lambda} + 2k_R + 4\lambda k_D\right),\\
&\bar{c}_{HB} = \frac{v^2}{\Lambda^2}g^2(k_{WW} - k_{WB}), \qquad \bar{c}_g = \frac{v^2}{\Lambda^2}\frac{g^2}{4}k_{GG},\\
&\bar{c}_{HW} = -\frac{v^2}{\Lambda^2}g^2 k_{WW}, \qquad \bar{c}_\gamma = \frac{v^2}{\Lambda^2}\frac{g^2}{4}(k_{BB} - k_{WB} + k_{WW}),\\
&\bar{c}_f = -\frac{v^2}{\Lambda^2}\left(\frac{1}{2}k_R + 2\lambda k_D\right),
\end{aligned} \quad \text{(A18)}$$

where for the sake of completeness we have included the coefficients of the redundant operators given in Eq. (A17).

b. HISZ basis

We also give the conversion to the popular HISZ basis [31] (see also Refs. [7,82] for recent studies in this framework)

$$\mathcal{L}_{\rm HISZ} = \sum_i \frac{f_i}{\Lambda^2}\mathcal{O}'_i, \tag{A19}$$

with Higgs-gauge operators given in Table XVII. We use the same conventions for the covariant derivative as above (note that this is not the case in some of the cited literature). The operators can then be translated via the relations

$$\begin{aligned}
&\hat{\mathcal{O}}_H = 2\mathcal{O}'_{\phi 2}, \qquad \hat{\mathcal{O}}_W = \frac{2i}{g}(\mathcal{O}'_{WW} + \mathcal{O}'_{BW} - 2\mathcal{O}'_W),\\
&\hat{\mathcal{O}}_{HW} = -\frac{2i}{g}\mathcal{O}'_W, \qquad \hat{\mathcal{O}}_T = 2\mathcal{O}'_{\phi 2} - 4\mathcal{O}'_{\phi 1},\\
&\hat{\mathcal{O}}_B = \frac{2i}{g'}(\mathcal{O}'_{BB} + \mathcal{O}'_{BW} - 2\mathcal{O}'_B), \qquad \hat{\mathcal{O}}_g = \mathcal{O}'_{GG},\\
&\hat{\mathcal{O}}_6 = 3\mathcal{O}'_{\phi 3}, \qquad \hat{\mathcal{O}}_{HB} = -\frac{2i}{g'}\mathcal{O}'_B, \qquad \hat{\mathcal{O}}_\gamma = -\frac{4}{g'^2}\mathcal{O}'_{BB}.
\end{aligned} \tag{A20}$$

The HISZ basis also includes the redundant operator $\mathcal{O}'_{\phi 4} = (D_\mu\phi)^\dagger(D^\mu\phi)\phi^\dagger\phi$, which can be removed using Eq. (A11). For the coefficients, we find

$$\begin{aligned}
&\bar{c}_H = \frac{v^2}{\Lambda^2}\left(\frac{1}{2}f_{\phi 1} + f_{\phi 2}\right), \qquad \bar{c}_W = -\frac{v^2}{\Lambda^2}\frac{g^2}{4}f_{WW},\\
&\bar{c}_T = -\frac{v^2}{\Lambda^2}\frac{1}{2}f_{\phi 1}, \qquad \bar{c}_B = \frac{v^2}{\Lambda^2}\frac{g^2}{4}(f_{WW} - f_{BW}),\\
&\bar{c}_6 = -\frac{v^2}{\Lambda^2}\frac{1}{3\lambda}f_{\phi 3}, \qquad \bar{c}_{HW} = \frac{v^2}{\Lambda^2}\frac{g^2}{8}(f_W + 2f_{WW}),\\
&\bar{c}_g = \frac{v^2}{\Lambda^2}\frac{g^2}{4g_s^2}f_{GG}, \qquad \bar{c}_{HB} = \frac{v^2}{\Lambda^2}\frac{g^2}{8}(f_B + 2f_{BW} - 2f_{WW}),\\
&\bar{c}_\gamma = \frac{v^2}{\Lambda^2}\frac{g^2}{16}(f_{BW} - f_{BB} - f_{WW}).
\end{aligned} \tag{A21}$$

2. Singlet extension

For the sake of simplicity we consider a minimal version of the singlet model, in which a discrete $\mathbb{Z}_2$ parity precludes additional (e.g. cubic) terms in the potential. The SM is then extended by including a real scalar singlet with the Lagrangian

$$\begin{aligned}
&\mathcal{L} = (D_\mu\phi)^\dagger(D^\mu\phi) + (\partial_\mu S)^2 - V(\phi, S),\\
&V(\phi, S) = \mu_1^2(\phi^\dagger\phi) + \lambda_1|\phi^\dagger\phi|^2 + \mu_2^2 S^2 + \lambda_2 S^4 + \lambda_3|\phi^\dagger\phi|S^2.
\end{aligned} \tag{A22}$$

The scalar doublet and singlets fields are expanded into components as

$$\phi = \begin{pmatrix} G^+ \\ \frac{1}{\sqrt{2}}(v + l^0 + iG^0) \end{pmatrix} \quad \text{and} \quad S = \frac{1}{\sqrt{2}}(v_s + s^0), \tag{A23}$$

where $v \equiv \sqrt{2}\langle\phi\rangle = 246$ GeV and $v_s \equiv \sqrt{2}\langle S\rangle$ denote their respective VEVs. The minimization condition for the potential of Eq. (A22) can be used to eliminate the parameters $\mu_{1,2}$ in favor of v and v_s. The CP-even components l^0 and s^0 mix to form a light (h) and a heavy (H) mass eigenstate:

$$\begin{aligned}
&h = l^0\cos\alpha - s^0\sin\alpha,\\
&H = l^0\sin\alpha + s^0\cos\alpha, \quad \text{where } \tan(2\alpha) = \frac{\lambda_3 v v_s}{\lambda_2 v_s^2 - \lambda_1 v^2}.
\end{aligned} \tag{A24}$$

Their masses are

$$m_{h,H}^2 = \lambda_1 v^2 + \lambda_2 v_s^2 \mp |\lambda_1 v^2 - \lambda_2 v_s^2|\sqrt{1 + \tan^2(2\alpha)} \tag{A25}$$

with $m_H^2 \approx 2\lambda_2 v_s^2 \gg m_h^2$ in the limit $v^2 \ll v_s^2$.

To perform the matching to the EFT, we identify the UV scale $\Lambda \equiv \sqrt{2\lambda_2}v_s \approx m_H$ for $v_s \gg v$. From the singlet-doublet mixing one then finds a universal coupling shift of the SM-like light Higgs to all other SM particles in Eq. (1), given by

$$\Delta \approx -\frac{\sin^2\alpha}{2} \approx -\frac{g_{\rm eff}^2}{2}\left(\frac{v}{\Lambda}\right)^2, \qquad g_{\rm eff} = \frac{\lambda_3}{\sqrt{2\lambda_2}}. \tag{A26}$$

Integrating out the heavy Higgs boson we find

$$\mathcal{L}_{\rm eff} \supset \frac{\sin^2\alpha}{2v^2}\partial^\mu(\phi^\dagger\phi)\partial_\mu(\phi^\dagger\phi) + \mathcal{O}(\Lambda^{-4}). \tag{A27}$$

We thus see that, up to dimension-6 operators the heavy-singlet-induced BSM effects in Higgs production and decay are completely captured by the operator $\hat{\mathcal{O}}_H$ (cf. Table XV) with coefficient

$$\bar{c}_H = \frac{\lambda_3^2}{2\lambda_2}\left(\frac{v}{\Lambda}\right)^2 + \mathcal{O}\left(\frac{v^4}{\Lambda^4}\right). \tag{A28}$$

The light Higgs couplings to fermions and gauge bosons in the singlet model are universally suppressed relative to the SM. In the full model and the EFT, respectively, they are given by

$$1+\Delta_x=\cos\alpha, \qquad 1+\Delta_x^{\rm EFT}=1-\frac{1}{2}\bar{c}_H. \tag{A29}$$

A more complex pattern emerges for the self-interactions involving at least one heavy Higgs field. We find

$$\begin{aligned} g_{hhH} &= -\frac{g_{\rm eff}(2m_h^2+m_H^2)}{v_s}\left[1+g_{\rm eff}\frac{v^2}{v_s^2}+\mathcal{O}\left(\frac{v^3}{v_s^3}\right)\right] \\ &\sim \lambda_3 v_s+\mathcal{O}(v), \\ g_{hHH} &= \frac{g_{\rm eff}v(m_h^2+2m_H^2)}{v_s^2}\left[1-g_{\rm eff}+\mathcal{O}\left(\frac{v}{v_s}\right)\right] \\ &\sim 2\lambda_3 v\left(1-\frac{\lambda_3}{2\lambda_2}\right)+\mathcal{O}\left(\frac{v^2}{v_s}\right), \end{aligned} \tag{A30}$$

in which we observe a characteristic nondecoupling behavior which manifests itself as a linear growth of g_{hhH} with the heavy Higgs mass. In the EFT, the leading self-interaction contribution enters via a dimension-8 operator, which is neglected in our dimension-6 analysis. Therefore, the sole Wilson coefficient $\bar{c}_H=\sin^2\alpha$ defines the singlet model EFT up to dimension 6.

On the other hand, let us emphasize a key structural difference between the $\hat{\mathcal{O}}_H$-induced and the UV-complete singlet model contributions to the Higgs self-coupling hhh. At variance with the latter, the effective operators also induces a new momentum structure into the self-coupling, namely adding derivatives in the Lagrangian or energy-dependent terms in the Feynman rules

$$\begin{aligned} \mathcal{L} &\supset -\frac{m_h^2}{2v}\left[\left(1-\frac{c_H v^2}{2\Lambda^2}\right)h^3-\frac{2c_H v^2}{\Lambda^2 m_h^2}h\partial_\mu h\partial^\mu h\right] \\ &= -\frac{m_h^2}{2v}\left(1-\frac{1}{2}\bar{c}_H\right)h^3+\frac{g}{2m_W}\bar{c}_H h\partial_\mu h\partial^\mu h, \end{aligned} \tag{A31}$$

which means that the SM-like h^3 term is not only rescaled but also endowed with new Lorentz structures involving derivatives. This kind of momentum dependence is encoded in the split into $g^{(1)}_{HHH}$ and $g^{(2)}_{HHH}$ in Eq. (A2). This effect does not correspond to the Higgs singlet mixing, where such a momentum dependence can only be generated via loop-induced heavy particle exchange with momentum-dependent couplings like a heavy fermion triangle.

3. Two-Higgs-doublet model

The most general gauge-invariant, CP-conserving potential with two scalar fields reads

$$\begin{aligned} V(\phi_1,\phi_2) &= m_{11}^2\phi_1^\dagger\phi_1+m_{22}^2\phi_2^\dagger\phi_2 \\ &\quad -[m_{12}^2\phi_1^\dagger\phi_2+\text{H.c.}]+\frac{\lambda_1}{2}(\phi_1^\dagger\phi_1)^2 \\ &\quad +\frac{\lambda_2}{2}(\phi_2^\dagger\phi_2)^2+\lambda_3(\phi_1^\dagger\phi_1)(\phi_2^\dagger\phi_2)+\lambda_4|\phi_1^\dagger\phi_2|^2 \\ &\quad +\left[\frac{\lambda_5}{2}(\phi_1^\dagger\phi_2)^2+\lambda_6(\phi_1^\dagger\phi_1)(\phi_1^\dagger\phi_2)\right. \\ &\quad \left.+\lambda_7(\phi_2^\dagger\phi_2)(\phi_1^\dagger\phi_2)+\text{H.c.}\right], \end{aligned} \tag{A32}$$

where the mass terms m_{ij}^2 and the dimensionless self-couplings λ_i are real parameters and $v_j=\sqrt{2}\langle\phi_j^0\rangle$. The ratio of VEVs is denoted as $\tan\beta=v_2/v_1$, whereas $v_1^2+v_2^2=v^2=(246\ \text{GeV})^2$ to reproduce the known gauge boson masses. For the Yukawa couplings, there are four possible scenarios that satisfy the SM flavor symmetry and preclude tree-level flavor-changing neutral currents [83]:

(i) type I, where all fermions couple to just one Higgs doublet ϕ_2;
(ii) type II, where up-type (down-type) fermions couple exclusively to ϕ_2 (ϕ_1);
(iii) lepton-specific, with a type-I quark sector and a type-II lepton sector; and
(iv) flipped, with a type-II quark sector and a type-I lepton sector.

In all four cases, the absence of tree-level flavor-changing neutral currents is protected by a global $\mathbb{Z}_2$ discrete symmetry $\phi_i\to(-1)^i\phi_i$ (for $i=1,\ 2$). The symmetry demands that $\lambda_{6,7}=0$ in Eq. (A32), but it can be softly broken by dimension-two terms in the Lagrangian, viz. $\mathcal{L}_{\rm soft}\supset m_{12}^2\phi_1^\dagger\phi_2+\text{H.c.}$

The Higgs mass-eigenstates follow from the set of rotations

$$\begin{aligned} \begin{pmatrix} H^0 \\ h^0 \end{pmatrix} &= R(\alpha)\begin{pmatrix} h_1^0 \\ h_2^0 \end{pmatrix}, \\ \begin{pmatrix} G^0 \\ A^0 \end{pmatrix} &= R(\beta)\begin{pmatrix} a_1^0 \\ a_2^0 \end{pmatrix}, \\ \begin{pmatrix} G^\pm \\ H^\pm \end{pmatrix} &= R(\beta)\begin{pmatrix} h_1^\pm \\ h_2^\pm \end{pmatrix}, \end{aligned} \tag{A33}$$

where

$$\begin{aligned} \phi_k &= \begin{pmatrix} h_k^+ \\ \frac{1}{\sqrt{2}}(v_k+h_k^0+ia_k) \end{pmatrix}, \\ R(\theta) &= \begin{pmatrix} \cos\theta & \sin\theta \\ -\sin\theta & \cos\theta \end{pmatrix}. \end{aligned} \tag{A34}$$

Since the two doublets contribute to giving masses to the weak gauge bosons, custodial symmetry will impose tight constraints on the viable mass spectrum of the model

[84,85]. Analytic relations linking the different Higgs masses and mixing angles with the Lagrangian parameters in Eq. (A32) can be found e.g. in Appendix A of [5]. The conventions $0 < \beta < \pi/2$ and $0 \leq \beta - \alpha < \pi$ guarantee that the Higgs coupling to vector bosons has the same sign in the 2HDM and in the SM. As we will next show, the decoupling limit implies that the light Higgs interactions approach the alignment limit, where $\cos\beta \sim |\sin\alpha|$ and the couplings become SM-like [51].

A 2HDM with large mass hierarchy between the light Higgs $m_{h^0} = \mathcal{O}(v)$ and its heavier companions $m_{H^0,H^\pm,A^0} \gg m_{h^0}$ can be readily mapped onto an EFT [16,51,86]. In the unbroken phase, we match by first rotating ϕ_1 and ϕ_2 into the so-called Higgs basis, where only one Higgs doublet obtains a vacuum expectation value, $\langle\phi_l\rangle = v/\sqrt{2}$, $\langle\phi_h\rangle = 0$ [16,87]. This doublet ϕ_l is then identified with the SM-like Higgs doublet, while the other doublet ϕ_h is integrated out. Its decoupling is described by the mass scale

$$\Lambda^2 = M^2 = m_{11}^2 \sin^2\beta + m_{22}^2 \cos^2\beta + m_{12}^2 \sin(2\beta) \tag{A35}$$

and the expansion parameter

$$x \equiv \frac{v^2 \sin 2\beta}{2M^2}\left[\frac{\lambda_1}{2} - \frac{\lambda_2}{2} + \left(\frac{\lambda_1}{2} + \frac{\lambda_2}{2} - \lambda_3 - \lambda_4 - \lambda_5\right)\cos 2\beta\right] + \mathcal{O}\left(\frac{v^4}{M^4}\right) \ll 1, \tag{A36}$$

where we assume perturbative couplings, $\lambda_i \lesssim \mathcal{O}(1)$.

As discussed in Sec. III B, the dimension-6 EFT defined this way does not provide a good approximation for scenarios where the LHC will have sensitivity to discover new physics. A more appropriate effective theory is obtained by matching at a physical mass instead of M. Specifically, this v-improved EFT is given by replacing $M \to m_{A^0}$ in Eqs. (A35) and (A36).

Similar to the singlet extension [see Eq. (A27)], mixing between the two CP-even Higgs boson at tree level causes the h^0 kinetic term to be rescaled, leading to

$$\bar{c}_H = x^2 = \mathcal{O}(\Lambda^{-4}). \tag{A37}$$

This corresponds to a dimension-8 term, which we neglect here. However, there exists a dimension-6 contribution to the triple light Higgs scalar interaction:

$$g^{(1)}_{h^0h^0h^0} = 1 + x^2\left[\frac{3}{2} - \frac{4m_{12}^2}{m_{h^0}^2 \sin 2\beta}\right] + \mathcal{O}(x^3) = 1 - x^2\frac{M^2}{\lambda v^2} + \mathcal{O}(M^{-3}). \tag{A38}$$

Nontrivial contributions to dimension-6 operators also arise in the Yukawa sector. For definiteness, we concentrate on 2HDM type I and II. At tree level and up to $\mathcal{O}(\Lambda^{-2})$, we find for the Wilson coefficients

$$\text{type I:}\quad \bar{c}_u = x\cot\beta, \qquad \bar{c}_d = x\cot\beta, \qquad \bar{c}_\ell = x\cot\beta, \tag{A39}$$

$$\text{type II:}\quad \bar{c}_u = x\cot\beta, \qquad \bar{c}_d = -x\tan\beta, \qquad \bar{c}_\ell = -x\tan\beta. \tag{A40}$$

The above expressions hold both in the standard EFT and the v-improved EFT, with the obvious replacement $M \to m_{A^0}$ for the latter. The operators $\hat{\mathcal{O}}_{HB}$, $\hat{\mathcal{O}}_{HW}$, $\hat{\mathcal{O}}_W$, $\hat{\mathcal{O}}_B$, $\hat{\mathcal{O}}_T$ and $\hat{\mathcal{O}}_\gamma$ receive contributions only at loop level, while $\hat{\mathcal{O}}_g = 0$ since there are no new colored particles in the 2HDM. The operator $\hat{\mathcal{O}}_\gamma$ receives a correction from the charged Higgs loop. Expanding this contribution, and using $m_{h^0}^2/m_{H^\pm}^2 = \mathcal{O}(x)$, we find

$$\Delta_\gamma = \frac{1}{g^{\rm SM}_{H\gamma\gamma}}\frac{e^2}{720\pi^2 v}\left[30\left(1 - [\cot\beta + \tan\beta]\frac{m_{12}^2}{m_{H^\pm}^2}\right) + \left(19 - 4[\cot\beta + \tan\beta]\frac{m_{12}^2}{m_{H^\pm}^2}\right)\frac{m_{h^0}^2}{m_{H^\pm}^2} - 30\cot(2\beta)[\cot\beta + \tan\beta]\frac{m_{12}^2}{m_{H^\pm}^2}x\right] + \mathcal{O}(x^2), \tag{A41}$$

where in the first row we identify characteristic nondecoupling terms contributing to $\mathcal{O}(x^0)$. On the other hand, the operator

$$\mathcal{L}_{\rm eff} \supset \frac{g'^2\bar{c}_\gamma}{m_W^2}(\phi^\dagger\phi)B_{\mu\nu}B^{\mu\nu} \tag{A42}$$

leads to

$$\Delta_\gamma^{\rm EFT} = \frac{1}{g^{\rm SM}_{H\gamma\gamma}}\frac{16 s_w^2 \bar{c}_\gamma}{v}. \tag{A43}$$

Identifying these expressions, we find within the v-improved EFT framework

$$\bar{c}_\gamma = \frac{g^2}{11520\pi^2}\left[30\left(1 - [\cot\beta + \tan\beta]\frac{m_{12}^2}{m_{H^\pm}^2}\right) + \left(19 - 4[\cot\beta + \tan\beta]\frac{m_{12}^2}{m_{H^\pm}^2}\right)\frac{m_{h^0}^2}{m_{H^\pm}^2} - 30\cot(2\beta)[\cot\beta + \tan\beta]\frac{m_{12}^2}{m_{H^\pm}^2}x\right]. \tag{A44}$$

In the full type-I 2HDM, the tree-level couplings shifts $g^{\rm 2HDM}_{h^0xx}/g^{\rm SM}_{hxx} = 1 + \Delta_x$ of the light Higgs are given by

$$1 + \Delta_V = \sin(\beta - \alpha), \qquad 1 + \Delta_t = \frac{\cos\alpha}{\sin\beta}, \qquad 1 + \Delta_b = \frac{\cos\alpha}{\sin\beta}, \qquad 1 + \Delta_\tau = \frac{\cos\alpha}{\sin\beta}, \tag{A45}$$

while in the type-II 2HDM they read

$$1+\Delta_V=\sin(\beta-\alpha),\qquad 1+\Delta_t=\frac{\cos\alpha}{\sin\beta},$$
$$1+\Delta_b=-\frac{\sin\alpha}{\cos\beta},\qquad 1+\Delta_\tau=-\frac{\sin\alpha}{\cos\beta}. \tag{A46}$$

The light Higgs coupling to a charged Higgs pair is given in all cases by

$$\frac{g_{h^0H^+H^-}}{g^{\rm SM}_{hhh}}=\frac{1}{3m^2_{h^0}}\left[\sin(\beta-\alpha)(2m^2_{H^\pm}-m^2_{h^0})+\frac{\cos(\alpha+\beta)}{\sin(2\beta)}\left(2m^2_{h^0}-\frac{2m^2_{12}}{\sin\beta\cos\beta}\right)\right], \tag{A47}$$

with $g^{\rm SM}_{hhh}=-3m^2_h/v$. Note that at tree level custodial symmetry ensures that both couplings to the weak gauge bosons $V=W,Z$ scale with the same factor $\sin(\beta-\alpha)$, a degeneracy that can be mildly broken by quantum effects [5].

In the effective model, we have[3]

$$\Delta^{\rm EFT}_V=0,\quad \Delta^{\rm EFT}_t=\bar c_u,\quad \Delta^{\rm EFT}_b=\bar c_d,\quad \Delta^{\rm EFT}_\tau=\bar c_\ell. \tag{A48}$$

The loop-induced couplings are more involved, giving

$$1+\Delta_g=\frac{1}{A^{\rm SM}_{gg}}\left[\sum_{f=t,b}(1+\Delta_f)A_f(\tau_f)\right], \tag{A49}$$

$$1+\Delta_\gamma=\frac{1}{A^{\rm SM}_{\gamma\gamma}}\left[\sum_{f=t,b}N_CQ_f^2(1+\Delta_f)A_f(\tau_f)+Q_\tau^2(1+\Delta_\tau)A_f(\tau_\tau)+(1+\Delta_W)A_v(\tau_W)-g_{h^0H^+H^-}\frac{m_Ws_w}{em^2_{H^\pm}}A_s(\tau_{H^\pm})\right], \tag{A50}$$

where $A^{\rm SM}_{xx}$ are the corresponding contributions in the SM. The conventional loop form factors read

$$A_s(\tau)=-\frac{\tau}{2}[1-\tau f(\tau)]=1/6+\mathcal{O}(\tau^{-1}),$$
$$A_f(\tau)=\tau[1+(1-\tau)f(\tau)]=2/3+\mathcal{O}(\tau^{-1}),$$
$$A_v(\tau)=-\frac{1}{2}[2+3\tau+3(2\tau-\tau^2)f(\tau)]=-7/2+\mathcal{O}(\tau^{-1}), \tag{A51}$$

$$f(\tau)=\begin{cases}-\frac{1}{4}\left[\log\frac{1+\sqrt{1-\tau}}{1-\sqrt{1-\tau}}-i\pi\right]^2 & \text{for } \tau<1\\ \left[\arcsin\frac{1}{\sqrt{\tau}}\right]^2 & \text{for } \tau\geq 1,\end{cases} \tag{A52}$$

and $\tau_x=4m_x^2/m^2_{h^0}$. In the effective model, we find

$$1+\Delta^{\rm EFT}_g=\frac{1}{A^{\rm SM}_{gg}}\left[\sum_{f=t,b}(1+\bar c_f)A_f(\tau_f)\right], \tag{A53}$$

$$1+\Delta^{\rm EFT}_\gamma=\frac{1}{A^{\rm SM}_{\gamma\gamma}}\left[\sum_{f=t,b}N_CQ_f^2(1+\bar c_f)A_f(\tau_f)+Q_\tau^2(1+\bar c_\ell)A_f(\tau_\tau)+A_v(\tau_W)+\frac{64\pi^2\bar c_\gamma}{g^2}\right]. \tag{A54}$$

The comparison of couplings in the full 2HDM and the EFT is summarized in Table XVIII.

4. Scalar top partners

The simplified scalar top-partner generation sector is described by the Lagrangian

$$\begin{aligned}\mathcal{L}\supset\ &(D_\mu\tilde Q)^\dagger(D^\mu\tilde Q)+(D_\mu\tilde t_R)^*(D^\mu\tilde t_R)\\ &-\underbrace{\tilde Q^\dagger M^2\tilde Q-M^2\tilde t_R^*\tilde t_R}_{\mathcal{L}_{\rm mass}}\\ &-\underbrace{\kappa_{LL}(\phi\cdot\tilde Q)^\dagger(\phi\cdot\tilde Q)-\kappa_{RR}(\tilde t_R^*\tilde t_R)(\phi^\dagger\phi)}_{\mathcal{L}_{\rm Higgs}}\\ &-\underbrace{[\kappa_{LR}M\tilde t_R^*(\phi\cdot\tilde Q)+\text{H.c.}]}_{\mathcal{L}_{\rm mixing}}.\end{aligned} \tag{A55}$$

TABLE XVIII. Tree-level Higgs coupling shifts Δ_x as a function of the 2HDM parameters. In the last column, the Wilson coefficients for the relevant dimension-6 operators in Table XV are matched to the 2HDM in the limit of decoupling heavy scalars $x\simeq v^2/M^2\ll 1$ [cf. Eq. (A36)].

Coupling	2HDM	EFT
$1+\Delta_t$	Type I: $x\cot\beta-\frac{x^2}{2}+\mathcal{O}(x^3)$	$\bar c_u=x\cot\beta$
	Type II: $x\cot\beta-\frac{x^2}{2}+\mathcal{O}(x^3)$	$\bar c_u=x\cot\beta$
$1+\Delta_b$	Type I: $x\cot\beta+\mathcal{O}(x^3)$	$\bar c_d=x\cot\beta$
	Type II: $-x\tan\beta+\mathcal{O}(x^3)$	$\bar c_d=-x\tan\beta$
$1+\Delta_\tau$	Type I: $x\cot\beta+\mathcal{O}(x^3)$	$\bar c_\ell=x\cot\beta$
	Type II: $-x\tan\beta+\mathcal{O}(x^3)$	$\bar c_\ell=-x\tan\beta$
$1+\Delta_V$	$1-\frac{x^2}{2}+\mathcal{O}(x^3)$	$\mathcal{O}^{d8}$
$1+\Delta_{h^0}$	$1-x^2(\frac{3}{2}-\frac{4m^2_{12}}{m^2_{h^0}\sin 2\beta})+\mathcal{O}(x^3)$	$\bar c_6=-x^2\frac{M^2}{\lambda v^2}$

[3]Note that the operator $\hat{\mathcal{O}}_\gamma$ introduces a new Lorentz structure for the h^0VV interaction, representing a charged Higgs loop. The results in Sec. III B reveal how large this effect turns out to be in practice.

We use the customary notation for the $SU(2)_L$ invariant product $\phi^a \cdot \tilde{Q}^b \equiv \epsilon_{ab}\phi^a\tilde{Q}^b$, with the help of the antisymmetric pseudotensor $\epsilon^{ab} \equiv (i\sigma^2)^{ab}$, so that $\epsilon^{12} = -\epsilon^{21} = 1$.

Notice that the term $\mathcal{L}_{\text{Higgs}}$ gives rise to scalar partner masses proportional to the Higgs VEV, mirroring the supersymmetric F-term contribution to the squark masses. By a similar token, the explicit mass terms $\mathcal{L}_{\text{mass}}$ are analogous to the squark soft-supersymmetry breaking mass terms; while $\mathcal{L}_{\text{mixing}}$ is responsible for the mixing between the gauge eigenstates, as a counterpart of the MSSM A terms. In the absence of an underlying supersymmetry, the Lagrangian in Eq. (A55) features no equivalent of the D-term contributions.

Collecting all bilinear terms from Eq. (A55) we get

$$\mathcal{L} \supset (\tilde{t}_L^* \tilde{t}_R^*) \begin{pmatrix} M_{LL}^2 & M_{LR}^2 \\ M_{RL}^2 & M_{RR}^2 \end{pmatrix} \begin{pmatrix} \tilde{t}_L \\ \tilde{t}_R \end{pmatrix}, \tag{A56}$$

where

$$\begin{aligned} M_{LL}^2 &= \kappa_{LL}\frac{v^2}{2} + M^2, \\ M_{LR}^2 &= M_{RL}^2 = \kappa_{LR} M \frac{v}{\sqrt{2}}, \\ M_{RR}^2 &= \kappa_{RR}\frac{v^2}{2} + M^2. \end{aligned} \tag{A57}$$

Assuming all parameters in Eq. (A55) to be real, the above mass matrix can be diagonalized through the usual orthogonal transformation $R(\theta_{\tilde{t}})$ which rotates the gauge eigenstates $(\tilde{t}_L, \tilde{t}_R)$ onto the mass basis $(\tilde{t}_1, \tilde{t}_2)$:

$$\begin{aligned} R(\theta_{\tilde{t}})\mathcal{M}_{\tilde{t}}^2 R^\dagger(\theta_{\tilde{t}}) &= \text{diag}(m_{\tilde{t}_1}^2, m_{\tilde{t}_2}^2), \\ \begin{pmatrix} \tilde{t}_1 \\ \tilde{t}_2 \end{pmatrix} = R(\theta_{\tilde{t}}) \begin{pmatrix} \tilde{t}_L \\ \tilde{t}_R \end{pmatrix} &= \begin{pmatrix} \cos\theta_{\tilde{t}} & \sin\theta_{\tilde{t}} \\ -\sin\theta_{\tilde{t}} & \cos\theta_{\tilde{t}} \end{pmatrix} \begin{pmatrix} \tilde{t}_L \\ \tilde{t}_R \end{pmatrix}. \end{aligned} \tag{A58}$$

The physical scalar partner masses and the mixing angle are then given by

$$\begin{aligned} m_{\tilde{t}_1}^2 &= M_{LL}^2\cos^2\theta_{\tilde{t}} + M_{RR}^2\sin^2\theta_{\tilde{t}} + 2M_{LR}^2\sin\theta_{\tilde{t}}\cos\theta_{\tilde{t}}, \\ m_{\tilde{t}_2}^2 &= M_{LL}^2\sin^2\theta_{\tilde{t}} + M_{RR}^2\cos^2\theta_{\tilde{t}} - 2M_{LR}^2\sin\theta_{\tilde{t}}\cos\theta_{\tilde{t}}, \end{aligned} \tag{A59}$$

$$\tan(2\theta_{\tilde{t}}) = \frac{2M_{LR}^2}{M_{LL}^2 - M_{RR}^2}. \tag{A60}$$

As we assume the right-handed partner $\tilde{b}_R$ to be heavy and thus decoupled, the sbottomlike scalar eigenstate $\tilde{b}_L$ undergoes no mixing and can be readily identified with the physical eigenstate.

To derive the effective theory, we compute the effective action at one loop with the help of the covariant derivative expansion [26,78,79], which is fully consistent with our mass degeneracy setup. Notice that, since the Lagrangian Eq. (A55) lacks any linear terms in the heavy scalar fields $\Psi \equiv (\tilde{Q}, \tilde{t}_R^*)$, the tree-level exchange of such heavy partners cannot generate any effective interaction at dimension 6.

Following our default matching prescription, we set the matching scale as $\Lambda = M$. The relevant Wilson coefficients in the SILH basis then read

$$\begin{aligned} \bar{c}_g &= \frac{m_W^2}{24(4\pi)^2M^2}[(\kappa_{LL}+\kappa_{RR}) - \kappa_{LR}^2], \\ \bar{c}_\gamma &= \frac{m_W^2}{9(4\pi)^2M^2}[(\kappa_{LL}+\kappa_{RR}) - \kappa_{LR}^2], \\ \bar{c}_B &= -\frac{5m_W^2}{12(4\pi)^2M^2}\left[\kappa_{LL} - \frac{31}{50}\kappa_{LR}^2\right], \\ \bar{c}_W &= \frac{m_W^2}{4(4\pi)^2M^2}\left[\kappa_{LL} - \frac{3}{10}\kappa_{LR}^2\right], \\ \bar{c}_{HB} &= \frac{5m_W^2}{12(4\pi)^2M^2}\left[\kappa_{LL} - \frac{14}{25}\kappa_{LR}^2\right], \\ \bar{c}_{HW} &= -\frac{m_W^2}{4(4\pi)^2M^2}\left[\kappa_{LL} - \frac{2}{5}\kappa_{LR}^2\right], \\ \bar{c}_H &= \frac{v^2}{4(4\pi)^2M^2}\left[(2\kappa_{RR}^2 - \kappa_{LL}^2) - \left(\kappa_{RR} - \frac{1}{2}\kappa_{LL}\right)\kappa_{LR}^2 + \frac{\kappa_{LR}^4}{10}\right], \\ \bar{c}_T &= \frac{v^2}{4(4\pi)^2M^2}\left[\kappa_{LL}^2 - \frac{\kappa_{LL}\kappa_{LR}^2}{2} + \frac{\kappa_{LR}^4}{10}\right]. \end{aligned} \tag{A61}$$

We also consider a v-improved matching. The only difference to the default matching is the choice of the matching scale $\Lambda = m_{\tilde{t}_1}$, which manifests itself as a rescaling of the Wilson coefficients in Eq. (A61) by a factor of $M^2/m_{\tilde{t}_1}^2$.

The scalar partner couplings to the Higgs boson can be written as

$$\begin{aligned} g_{h\tilde{t}_1\tilde{t}_1}/v &= \kappa_{LL}\cos^2\theta_{\tilde{t}} + \kappa_{RR}\sin^2\theta_{\tilde{t}} + \sin(2\theta_{\tilde{t}})\kappa_{LR}, \\ g_{h\tilde{t}_2\tilde{t}_2}/v &= \kappa_{LL}\sin^2\theta_{\tilde{t}} + \kappa_{RR}\cos^2\theta_{\tilde{t}} - \sin(2\theta_{\tilde{t}})\kappa_{LR}, \\ g_{h\tilde{b}_L\tilde{b}_L}/v &= \kappa_{LL}. \end{aligned} \tag{A62}$$

5. Vector triplet

We consider a real vector triplet field $V_\mu^{a=1,2,3}$ transforming under the SM gauge group as $(r_c, r_L, r_Y) = (\mathbf{1}, \mathbf{3}, 0)$. Its dynamics can be effectively described by means of the Lagrangian [74]

$$\mathcal{L} \supset -\frac{1}{4}V^a_{\mu\nu}V^{\mu\nu a} + \frac{M_V^2}{2}V^a_\mu V^{\mu a} + ig_V c_H V^a_\mu [\phi^\dagger \tau^a \overleftrightarrow{D}^\mu \phi] + \frac{g_w^2}{g_V} V^a_\mu c_F \sum_F \bar{F}_L \gamma^\mu \tau^a F_L + \frac{g_V}{2} c_{VVV} \epsilon_{abc} V^a_\mu V^b_\nu D^{[\mu} V^{\nu]c} + g_V^2 c_{VVHH} V^a_\mu V^{\mu a} \phi^\dagger \phi - \frac{g_w}{2} c_{VVW} \epsilon_{abc} W^{\mu\nu} V^b_\mu V^c_\nu, \tag{A63}$$

where the vector triplet field-strength tensor is $V^a_{\mu\nu} \equiv D_\mu V^a_\nu - D_\nu V^a_\mu$ and $\tau^a \equiv \sigma^a/2$ are the $SU(2)_L$ generators in the fundamental representation. The covariant derivative acts on the vector triplet field as $D_\mu V^a_\nu = \partial_\mu V^a_\nu + g\epsilon^{abc} V^b_\mu V^c_\nu$.

The coupling constant g_V stands for the characteristic strength of the heavy vector-mediated interactions, while g_w denotes the $SU(2)_L$ weak gauge coupling (which differs from the coupling strength g of the observable W boson due to W-V mixing; see below). The different dimensionless coefficients c_i quantify the relative strengths of the individual couplings. This parametrization weights the extra V and ϕ field insertions by one factor of g_V each, while gauge boson insertions are weighted by one power of the weak coupling. An exception is made for the couplings to fermions, where an extra weighting factor ${g_w}^2/{g_V}^2$ is introduced for a convenient power counting in certain UV embeddings [74]. For simplicity, it is assumed that the fermion current in Eq. (A63) is universal.

Equation (A63) is the most general Lagrangian compatible with the SM gauge group and CP invariance, provided that V^a_μ transforms as $V^a_\mu(\mathbf{x},t) \overset{CP}{\to} -(-1)^{\delta_{a2}} V^a_\mu(-\mathbf{x},t)$ as the SM vectors. Moreover, the Lagrangian obeys a global $SO(4) = SU(2)_L \times SU(2)_R$ symmetry, which is typical of strongly interacting dynamics.

Since V^a_μ is not manifestly gauged, this simplified vector triplet model in itself is not renormalizable. However, it can be easily linked to a gauge-invariant theory e.g. via the Higgs or the Stückelberg mechanisms [74].

An alternative model setup, which is particularly useful to construct the effective theory, introduces an explicit kinetic V-W mixing via the Lagrangian

$$\mathcal{L} \supset -\frac{1}{4}V^a_{\mu\nu}V^{\mu\nu a} + \frac{\tilde{M}_V^2}{2}V^a_\mu V^{\mu a} + g_V \tilde{c}_H V^a_\mu J^{\mu,a}_H + \frac{g_w^2}{2g_V} V^a_\mu \tilde{c}_F \sum_F J^{\mu,a}_F + \tilde{c}_{WV}\frac{g_w}{2g_V} D_{[\mu} V^a_{\nu]} W^{\mu\nu a} + \frac{g_V}{2}\tilde{c}_{VVV}\epsilon_{abc} V^a_\mu V^b_\nu D^{[\mu}V^{\nu]c} + g_V^2 \tilde{c}_{VVHH} V^a_\mu V^{\mu a}\phi^\dagger\phi - \frac{g_w}{2}\tilde{c}_{VVW}\epsilon_{abc} W^{\mu\nu} V^b_\mu V^c_\nu, \tag{A64}$$

where for convenience we have introduced the Higgs, fermion and vector current bilinears

$$J^{H,a}_\mu = \frac{i}{2}[\phi^\dagger \sigma^a \overleftrightarrow{D}_\mu \phi], \qquad J^{F,a}_\mu = \bar{F}_L \gamma_\mu \sigma^a F_L,$$
$$J^{W,a}_\mu = D^\nu W^a_{\mu\nu}. \tag{A65}$$

An appropriate field redefinition absorbs the kinetic mixing term $V^{\mu a}(D^\nu W_{\mu\nu})^a$ [88] and connects the parameters in the *tilded* basis of Eq. (A64) and *untilded* basis of Eq. (A63) through the relations

$$\begin{aligned}
M_V^2 &= \frac{g_V^2}{g_V^2 - \tilde{c}_{WV}^2 g_w^2}\tilde{M}_V^2,\\
c_H &= \frac{g_V}{\sqrt{g_V^2 - \tilde{c}_{WV}^2 g_w^2}}\left[\tilde{c}_H + \frac{g_w^2}{g_V^2}\tilde{c}_{WV}\right],\\
c_F &= \frac{g_V}{\sqrt{g_V^2 - \tilde{c}_{WV}^2 g_w^2}}[\tilde{c}_F + \tilde{c}_{WV}],\\
c_{VVHH} &= \frac{g_V^2}{g_V^2 - \tilde{c}_{WV}^2 g_w^2}\left[\tilde{c}_{VVHH} + \frac{g_w^2}{2g_V^2}\tilde{c}_{WV}\tilde{c}_H + \frac{g_w^4}{4g_V^4}\tilde{c}_{WV}^2\right],\\
c_{VVW} &= \frac{g_V^2}{g_V^2 - \tilde{c}_{WV}^2 g_w^2}\left[\tilde{c}_{VVW} - \frac{g_w^2}{g_V^2}\tilde{c}_{WV}^2\right],\\
c_{VVV} &= \frac{g_V^2}{(g_V^2 - \tilde{c}_{WV}^2 g_w^2)^{3/2}} \times \left[\tilde{c}_{VVV} - \frac{g_w^2}{g_V^2}\tilde{c}_{WV}(\tilde{c}_{VVW}+2) + 2\frac{g_w^2}{g_V^4}\tilde{c}_{WV}^3\right].
\end{aligned} \tag{A66}$$

a. Spectrum

The heavy vector sector in the gauge basis contains one neutral state $V^0_\mu \equiv V^3_\mu$ and two charged states $V^\pm_\mu \equiv (V^1_\mu \mp V^2_\mu)/\sqrt{2}$. Upon electroweak symmetry breaking only one vector state remains massless, which we readily identify with the standard photon field $A_\mu = c_w B_\mu + s_w W^3_\mu$. Here, the Weinberg angle is linked as usual to the electroweak gauge couplings $e = g_w s_w = g' c_w$, although at this stage we cannot yet relate it to electroweak observables before the mixing with the heavy vectors is included. The latter involves, for the neutral fields, the heavy vector component V^0 and the linear combination of B, W^3 orthogonal to the photon field. A similar mixing pattern appears in the charged sector, involving the field components $V^{1,2}_\mu, W^{1,2}_\mu$. The physical mass eigenstates can be written as

$$\begin{aligned}
Z_\mu &= \cos\theta_N(-s_w B_\mu + c_w W^3_\mu) + \sin\theta_N V^3_\mu,\\
\xi^0_\mu &= -\sin\theta_N(-s_w B_\mu + c_w W^3_\mu) + \cos\theta_N V^3_\mu,\\
W^\pm_\mu &= \cos\theta_C \frac{W^1_\mu \mp W^2_\mu}{\sqrt{2}} + \sin\theta_C \frac{V^1_\mu \mp V^2_\mu}{\sqrt{2}},\\
\xi^\pm_\mu &= -\sin\theta_C \frac{W^1_\mu \mp W^2_\mu}{\sqrt{2}} + \cos\theta_C \frac{V^1_\mu \mp V^2_\mu}{\sqrt{2}}.
\end{aligned} \tag{A67}$$

The mass eigenvalues are given by

$$m^2_{Z/\xi^0} = \frac{1}{2}\left[\hat{m}^2_V + \hat{m}^2_Z \mp \sqrt{(\hat{m}^2_Z - \hat{m}^2_V)^2 + c^2_H g^2_V \hat{m}^2_Z \hat{v}^2}\right] = \begin{cases} \hat{m}^2_Z\left(1 - \frac{c^2_H g^2_V}{4}\frac{\hat{v}^2}{\hat{m}^2_V} + \mathcal{O}(\hat{v}^4/\hat{m}^4_V)\right) \\ \hat{m}^2_V\left(1 + \frac{c^2_H g^2_V}{4}\frac{\hat{v}^2}{\hat{m}^2_V} + \mathcal{O}(\hat{v}^4/\hat{m}^4_V)\right), \end{cases} \tag{A68}$$

$$m^2_{W^\pm/\xi^\pm} = \frac{1}{2}\left[\hat{m}^2_V + \hat{m}^2_W \mp \sqrt{(\hat{m}^2_W - \hat{m}^2_V)^2 + c^2_H g^2_V \hat{m}^2_W \hat{v}^2}\right] = \begin{cases} \hat{m}^2_W\left(1 - \frac{c^2_H g^2_V}{4}\frac{\hat{v}^2}{\hat{m}^2_V} + \mathcal{O}(\hat{v}^4/\hat{m}^4_V)\right) \\ \hat{m}^2_V\left(1 + \frac{c^2_H g^2_V}{4}\frac{\hat{v}^2}{\hat{m}^2_V} + \mathcal{O}(\hat{v}^4/\hat{m}^4_V)\right). \end{cases} \tag{A69}$$

For the mixing angles, we find

$$\tan(2\theta_N) = \frac{c_H g_V \hat{v}\hat{m}_Z}{\hat{m}^2_V - \hat{m}^2_Z} = \frac{c_H g g_V}{2c_w}\frac{\hat{v}^2}{\hat{m}^2_V} + \mathcal{O}(\hat{v}^4/\hat{m}^4_V),$$
$$\tan(2\theta_C) = \frac{c_H g_V \hat{v}\hat{m}_W}{\hat{m}^2_V - \hat{m}^2_W} = \frac{c_H g g_V}{2}\frac{\hat{v}^2}{\hat{m}^2_V} + \mathcal{O}(\hat{v}^4/\hat{m}^4_V), \tag{A70}$$

or

$$\sin\theta_C = \frac{c_H g g_V}{4}\frac{v^2}{M^2_V} + \mathcal{O}(\hat{v}^4/\hat{m}^4_V). \tag{A71}$$

Here we define

$$\hat{m}_Z = \frac{g_w \hat{v}}{2c_w}, \qquad \hat{m}_W = \frac{g_w \hat{v}}{2}, \qquad \hat{m}^2_V = M^2_V + g^2_V c_{VVHH}\hat{v}^2, \tag{A72}$$

where $\hat{v}$ is the actual VEV of ϕ, which does not necessarily have the SM value of $v = 2m_W/g \approx 246$ GeV.

Notice that the V-W mixing also affects the weak current interactions, which are no longer governed by g_w. Instead, the physical Wff' coupling reads

$$g = \cos\theta_C g_w - \sin\theta_C c_F \frac{g^2_w}{g_V} = g_w\left(1 - \frac{c_F c_H g^2_w}{4}\frac{v^2}{M^2_V}\right) + \mathcal{O}(v^4/M^4_V). \tag{A73}$$

The relation between $\hat{v}$ and v can be read off from Eq. (A69), giving approximately

$$\frac{\hat{v}}{v} = 1 + \frac{c^2_H g^2_V}{8}\frac{v^2}{M^2_V} - \frac{c_F c_H g^2_w}{4}\frac{v^2}{M^2_V} + \mathcal{O}(v^4/M^4_V). \tag{A74}$$

The global $SU(2)_V$ custodial symmetry connects the charged and neutral current strengths through $m^2_W m^2_{\xi^\pm} = c^2_w m^2_Z m^2_{\xi^0}$, which generalizes the SM relation $m^2_W = c^2_w m^2_Z$. Compatibility with electroweak precision observables enforces nearly mass-degenerate states $m_{\xi^0} \simeq m_{\xi^\pm}$ for phenomenologically viable scenarios. In practice, we set up our model in the m_W-g scheme, i.e. taking as input parameters g, m_W, α, m_{h^0}, α_s; the model-specific parameters c_i; as well as the physical masses $m_{\xi^\pm}$. The mass spectrum and mixing angles we obtain by solving Eqs. (A68) and (A69) iteratively.

b. Effective theory

To construct the vector triplet EFT following the default matching, we identify the new physics scale $\Lambda = M_V$. Starting from the heavy triplet Lagrangian defined by Eq. (A64), we first integrate by parts the kinetic mixing term:

$$\tilde{c}_{WV}\frac{g_w}{2g_V} D_{[\mu} V^a_{\nu]} W^{\mu\nu a} = \tilde{c}_{WV}\frac{g_w}{g_V} V^{\mu,a}(D^\nu W^a_{\mu\nu}) = \tilde{c}_{WV}\frac{g_w}{g_V} V^{\mu,a} J^{Wa}_\mu, \tag{A75}$$

such that we can rewrite it in terms of the gauge current from Eq. (A65). Integrating out the heavy vector field V^a_μ one obtains the effective Lagrangian

$$\mathcal{L}_{\text{eff}} \supset \frac{\tilde{M}^2_V}{2} V^{\mu,a} V^a_\mu + V^a_\mu\left[g_V \tilde{c}_H J^{\mu,a}_H + \frac{g^2_w}{2g_V}\tilde{c}_F \sum_F J^{\mu,a}_F + \tilde{c}_{WV}\frac{g_w}{g_V} J^{Wa}_\mu\right] + \mathcal{O}(V^3), \tag{A76}$$

where we neglect those contributions involving higher powers in the heavy field, as they play no role in our analysis.

The Euler-Lagrange equation for V^a_μ,

$$[\partial^\mu\partial^\nu - g^{\mu\nu}\partial^2 - \tilde{M}^2_V]V^a_\nu = g_V \tilde{c}_H J^{\mu,a}_H + \frac{g^2_w}{2g_V}\tilde{c}_F\sum_F J^{\mu,a}_F + \tilde{c}_{WV}\frac{g_w}{g_V} J^{\mu,a}_W + \text{h.o. terms in } V^a_\mu,$$

leads to

$$V^{\mu,a} = -\frac{1}{\tilde{M}_V^2}\left[\tilde{c}_{WV}\frac{g_w}{g_V}J_W^{\mu,a} + g_V\tilde{c}_H J_H^{\mu,a} + \frac{g_w^2}{2g_V}\tilde{c}_F\sum_F J_F^{\mu,a}\right] + \mathcal{O}(p_V^2/\tilde{M}_V^4) + \mathcal{O}(V^2). \tag{A77}$$

Plugging Eq. (A77) into Eq. (A76), $\mathcal{L}_{\rm eff}$ can be expressed in terms of current products as

$$\begin{aligned}\mathcal{L}_{\rm eff} \supset & -\frac{g_w^4\tilde{c}_F^2}{8g_V^2\tilde{M}_V^2}J_F^{\mu,a}J_\mu^{Fa} - \frac{g_V^2\tilde{c}_H^2}{2\tilde{M}_V^2}J_H^{\mu,a}J_\mu^{Ha} - \frac{g_w^2\tilde{c}_F\tilde{c}_H}{2\tilde{M}_V^2}J_H^{\mu,a}J_\mu^{Fa} \\ & - \frac{g_w\tilde{c}_H\tilde{c}_{WV}}{\tilde{M}_V^2}J_H^{\mu,a}J_\mu^{Wa} - \frac{g_w^2\tilde{c}_{WV}^2}{2g_V^2\tilde{M}_V^2}J_W^{\mu,a}J_\mu^{Wa} \\ & - \frac{g_w^3\tilde{c}_F\tilde{c}_{WV}}{2g_V^2\tilde{M}_V^2}J_W^{\mu,a}J_\mu^{Fa}.\end{aligned} \tag{A78}$$

In the following, we disregard four-fermion operators since they are irrelevant for our analysis. The remaining five current products in Eq. (A78) can be expressed in terms of two independent ones by using Eq. (A8) (with the replacement $g \to g_w$), which corresponds to $J_W^{\mu,a} = g_w J_H^{\mu,a} + g_w J_F^{\mu,a}/2$:

$$\begin{aligned}\mathcal{L}_{\rm eff} \supset & -\frac{(g_V^2\tilde{c}_H + g_w^2\tilde{c}_{WV})^2}{2g_V^2\tilde{M}_V^2}J_H^{\mu,a}J_\mu^{Ha} \\ & - \frac{g_w^2(\tilde{c}_F + \tilde{c}_{WV})(g_V^2\tilde{c}_H + g_w^2\tilde{c}_{WV})}{2g_V^2\tilde{M}_V^2}J_H^{\mu,a}J_\mu^{Fa} \\ & + 4\text{-fermion}.\end{aligned} \tag{A79}$$

Using Eq. (A.4) in [74], it can be checked that this equation is invariant when changing between the tilded and untilded bases. With the help of Eqs. (A7), (A9), and (A11) (and again relabeling $g \to g_w$ in these relations) the two independent current products can be expressed in terms of dimension-6 operators as follows:

$$\begin{aligned}J_H^{\mu,a}J_\mu^{Ha} &= -\frac{1}{4}(\hat{\mathcal{O}}_H - 4\hat{\mathcal{O}}_r) \\ &= -\frac{1}{4}\left[3\hat{\mathcal{O}}_H - 8\lambda\hat{\mathcal{O}}_6 - 2\sum_f[y_f\hat{\mathcal{O}}_f + \text{H.c.}]\right], \\ J_F^{\mu,a}J_\mu^{Ha} &= \frac{i}{2}\hat{\mathcal{O}}'_{HF} \\ &= \frac{i\hat{\mathcal{O}}_W}{g_w} + \frac{1}{2}\left[3\hat{\mathcal{O}}_H - 8\lambda\hat{\mathcal{O}}_6 - 2\sum_f[y_f\hat{\mathcal{O}}_f + \text{H.c.}]\right],\end{aligned} \tag{A80}$$

where y_f denotes the bare Yukawa coupling $y_f \equiv \sqrt{2}m_f/v$. Plugging the above into Eq. (A79), one can easily read off the relevant Wilson coefficients of the EFT:

$$\begin{aligned}\bar{c}_H &= \frac{3g_w^2v^2}{4\tilde{M}_V^2}\left[\tilde{c}_H^2\frac{g_V^2}{g_w^2} - 2\tilde{c}_F\tilde{c}_{WV}\frac{g^2}{g_V^2} - 2\tilde{c}_F\tilde{c}_H - \tilde{c}_{WV}^2\frac{g^2}{g_V^2}\right], \\ \bar{c}_6 &= \frac{g_w^2v^2}{\tilde{M}_V^2}\left[\tilde{c}_H^2\frac{g_V^2}{g_w^2} - 2\tilde{c}_F\tilde{c}_{WV}\frac{g^2}{g_V^2} - 2\tilde{c}_F\tilde{c}_H - \tilde{c}_{WV}^2\frac{g^2}{g_V^2}\right], \\ \bar{c}_f &= \frac{g_w^2v^2}{4\tilde{M}_V^2}\left[\tilde{c}_H^2\frac{g_V^2}{g_w^2} - 2\tilde{c}_F\tilde{c}_{WV}\frac{g^2}{g_V^2} - 2\tilde{c}_F\tilde{c}_H - \tilde{c}_{WV}^2\frac{g^2}{g_V^2}\right], \\ \bar{c}_W &= \frac{m_W^2}{\tilde{M}_V^2}\left[-\tilde{c}_F\tilde{c}_H - \tilde{c}_H\tilde{c}_{WV} - \tilde{c}_F\tilde{c}_{WV}\frac{g_w^2}{g_V^2} - \tilde{c}_{WV}^2\frac{g^2}{g_V^2}\right].\end{aligned} \tag{A81}$$

In the untilded basis, these correspond to

$$\begin{aligned}\bar{c}_H &= \frac{3g_w^2v^2}{4M_V^2}\left[c_H^2\frac{g_V^2}{g_w^2} - 2c_Fc_H\right], \\ \bar{c}_6 &= \frac{g_w^2v^2}{M_V^2}\left[c_H^2\frac{g_V^2}{g_w^2} - 2c_Fc_H\right], \\ \bar{c}_f &= \frac{g_w^2v^2}{4M_V^2}\left[c_H^2\frac{g_V^2}{g_w^2} - 2c_Fc_H\right], \\ \bar{c}_W &= -\frac{m_W^2}{M_V^2}c_Fc_H\end{aligned} \tag{A82}$$

with $f = u, d, \ell$. Other than that, only four-fermion interactions are generated at tree level and at $\mathcal{O}(v^2/M_V^2)$; these are not relevant for our analysis and are not considered here.

As in the 2HDM and scalar partner models, we define an additional v-improved EFT by $\Lambda = m_{\xi^0}$, leading the same Wilson coefficients as above except that M_V is replaced by m_{ξ^0}.

c. Higgs couplings

On the EFT side, it is illustrative to discuss the origin of the Higgs coupling shifts within two different approaches. First we consider the EFT that keeps the fermionic operator $\hat{\mathcal{O}}'_{HF}$ [i.e. instead of using the conventional replacement in Eq. (A9) that maximizes the use of bosonic operators]. In this case, similar to Eq. (A73), a renormalization effect of the weak coupling occurs from V-W mixing:

$$g = g_w(1 - i\bar{c}'_{HF}), \tag{A83}$$

where g is the observable coupling between the W boson and SM fermions. In this EFT and using the untilded basis, the relevant Wilson coefficients are

$$\bar{c}_H = c_H^2\frac{3g_V^2v^2}{4M_V^2}, \qquad \bar{c}_f = \frac{1}{3}\bar{c}_H, \qquad \bar{c}'_{HF} = -ic_Fc_H\frac{g_w^2v^2}{4M_V^2}. \tag{A84}$$

Instead, if we now consider the EFT with the bosonic operator $\hat{\mathcal{O}}_W$, i.e. after applying the replacement in Eq. (A9), there is no additional renormalization of the weak coupling, so that $g = g_w$. The relevant Wilson coefficient are given in Eq. (A82).

Now we are in a position to determine the Higgs coupling shifts in the three models. For the Yukawa couplings we find

$$\begin{aligned}
\text{full model: } \Delta_f^{\text{full}} &= \frac{g_w}{g}\frac{v}{\hat{v}} - 1 = \frac{1}{c_{\theta_C} - c_F \frac{g_w}{g_V} s_{\theta_C}}\frac{v}{\hat{v}} - 1 = c_H^2 \frac{g_V^2 v^2}{8M_V^2} + c_F c_H \frac{g^2 v^2}{4M_V^2} + \mathcal{O}(M_V^{-4});\\
\text{EFT with } \hat{\mathcal{O}}'_{HF}\text{: } \Delta_f^{\hat{\mathcal{O}}'_{HF}} &= \frac{\bar{c}_H}{2} + \bar{c}_f = \frac{\bar{c}_H}{2} + \bar{c}_f + i\bar{c}'_{HF} = c_H^2 \frac{g_V^2 v^2}{8M_V^2} + c_F c_H \frac{g^2 v^2}{4M_V^2};\\
\text{EFT with } \hat{\mathcal{O}}_W\text{: } \Delta_f^{\hat{\mathcal{O}}_W} &= \frac{\bar{c}_H}{2} + \bar{c}_f = c_H^2 \frac{g_V^2 v^2}{8M_V^2} + c_F c_H \frac{g^2 v^2}{4M_V^2}.
\end{aligned} \tag{A85}$$

Similarly for the Higgs coupling to on-shell W bosons we get

$$\begin{aligned}
\text{full model: } \Delta_W^{\text{full}} &= \frac{1}{g m_W}\left(\frac{c_{\theta_C}^2 g^2 \hat{v}}{2(c_{\theta_C} - c_F \frac{g_w}{g_V} s_{\theta_C})^2} - c_H \frac{s_{\theta_C} c_{\theta_C} g g_V \hat{v}}{c_{\theta_C} - c_F \frac{g_w}{g_V} s_{\theta_C}} + 2 c_{VVHH} s_{\theta_C}^2 g_V^2 \hat{v}\right) - 1\\
&= c_H^2 \frac{3 g_V^2 v^2}{8M_V^2} + c_F c_H \frac{g^2 v^2}{4M_V^2} + \mathcal{O}(M_V^{-4});\\
\text{EFT with } \hat{\mathcal{O}}'_{HF}\text{: } \Delta_W^{\hat{\mathcal{O}}'_{HF}} &= \frac{g_w}{g}\left(1 - \frac{\bar{c}_H}{2}\right) - 1 = \frac{\bar{c}_H}{2} + i\bar{c}'_{HF} = c_H^2 \frac{3 g_V^2 v^2}{8M_V^2} + c_F c_H \frac{g^2 v^2}{4M_V^2};\\
\text{EFT with } \hat{\mathcal{O}}_W\text{: } \Delta_W^{\hat{\mathcal{O}}_W} &= \frac{\bar{c}_H}{2} + 2\bar{c}_W = c_H^2 \frac{3 g_V^2 v^2}{8M_V^2} + c_F c_H \frac{g^2 v^2}{4M_V^2}.
\end{aligned} \tag{A86}$$

[1] P. W. Higgs, Phys. Lett. **12**, 132 (1964); Phys. Rev. Lett. **13**, 508 (1964); F. Englert and R. Brout, Phys. Rev. Lett. **13**, 321 (1964).

[2] G. Aad *et al.* (ATLAS Collaboration), Phys. Lett. B **716**, 1 (2012); S. Chatrchyan *et al.* (CMS Collaboration), Phys. Lett. B **716**, 30 (2012).

[3] For pedagogical introductions see e.g. M. Spira and P. M. Zerwas, Lect. Notes Phys. **512**, 161 (1998); A. Djouadi, Phys. Rep. **457**, 1 (2008); T. Plehn, Lect. Notes Phys. **844**, 1 (2012).

[4] R. Lafaye, T. Plehn, M. Rauch, D. Zerwas, and M. Dührssen, J. High Energy Phys. 08 (2009) 009; M. Klute, R. Lafaye, T. Plehn, M. Rauch, and D. Zerwas, Phys. Rev. Lett. **109**, 101801 (2012); T. Plehn and M. Rauch, Europhys. Lett. **100**, 11002 (2012).

[5] D. López-Val, T. Plehn, and M. Rauch, J. High Energy Phys. 10 (2013) 134.

[6] For more or less constrained Higgs couplings analyses see e.g. J. Ellis and T. You, J. High Energy Phys. 06 (2013) 103; T. Corbett, O. J. P. Éboli, J. Gonzalez-Fraile, and M. C. Gonzalez-Garcia, Phys. Rev. D **87**, 015022 (2013); B. A. Dobrescu and J. D. Lykken, J. High Energy Phys. 02 (2013) 073; E. Massó and V. Sanz, Phys. Rev. D **87**, 033001 (2013); K. Cheung, J. S. Lee, and P.-Y. Tseng, J. High Energy Phys. 05 (2013) 134; P. P. Giardino, K. Kannike, I. Masina, M. Raidal, and A. Strumia, J. High Energy Phys. 05 (2014) 046; W.-F. Chang, W.-P. Pan, and F. Xu, Phys. Rev. D **88**, 033004 (2013); A. Djouadi and G. Moreau, Eur. Phys. J. C **73**, 2512 (2013); P. Bechtle, S. Heinemeyer, O. Stål, T. Stefaniak, and G. Weiglein, J. High Energy Phys. 11 (2014) 039; G. Bélanger, B. Dumont, U. Ellwanger, J. F. Gunion, and S. Kraml, Phys. Rev. D **88**, 075008 (2013); J. Bernon, B. Dumont, and S. Kraml, Phys. Rev. D **90**, 071301 (2014).

[7] T. Corbett, O. J. P. Éboli, D. Gonçalves, J. Gonzalez-Fraile, T. Plehn, and M. Rauch, J. High Energy Phys. 08 (2015) 156.

[8] C. Englert, A. Freitas, M. M. Mühlleitner, T. Plehn, M. Rauch, M. Spira, and K. Walz, J. Phys. G **41**, 113001 (2014).

[9] D. E. Morrissey, T. Plehn, and T. M. P. Tait, Phys. Rep. **515**, 1 (2012).

[10] S. Weinberg, Phys. Lett. **91B**, 51 (1980); S. R. Coleman, J. Wess, and B. Zumino, Phys. Rev. **177**, 2239 (1969); C. G. Callan, Jr., S. R. Coleman, J. Wess, and B. Zumino, Phys. Rev. **177**, 2247 (1969).

[11] C. J. C. Burges and H. J. Schnitzer, Nucl. Phys. **B228**, 464 (1983); C. N. Leung, S. T. Love, and S. Rao, Z. Phys. C **31**, 433 (1986); W. Buchmüller and D. Wyler, Nucl. Phys. **B268**, 621 (1986).

[12] For reviews see e.g. M. S. Bilenky and A. Santamaria, Nucl. Phys. **B420**, 47 (1994); G. Buchalla, A. J. Buras, and M. E. Lautenbacher, Rev. Mod. Phys. **68**, 1125 (1996);

[13] See e.g. I. M. Shoemaker and L. Vecchi, Phys. Rev. D **86**, 015023 (2012); G. Busoni, A. De Simone, E. Morgante, and A. Riotto, Phys. Lett. B **728**, 412 (2014); G. Busoni, A. De Simone, J. Gramling, E. Morgante, and A. Riotto, J. Cosmol. Astropart. Phys. 06 (2014) 060; O. Buchmueller, M. J. Dolan, and C. McCabe, J. High Energy Phys. 01 (2014) 025; D. Racco, A. Wulzer, and F. Zwirner, J. High Energy Phys. 05 (2015) 009.
[14] A. Biekoetter, A. Knochel, M. Krämer, D. Liu, and F. Riva, Phys. Rev. D **91**, 055029 (2015).
[15] C. Arnesen, I. Z. Rothstein, and J. Zupan, Phys. Rev. Lett. **103**, 151801 (2009); C. Englert and M. Spannowsky, Phys. Lett. B **740**, 8 (2015); M. de Vries, J. High Energy Phys. 03 (2015) 095; N. Craig, M. Farina, M. McCullough, and M. Perelstein, J. High Energy Phys. 03 (2015) 146; S. Dawson, I. M. Lewis, and M. Zeng, Phys. Rev. D **91**, 074012 (2015); A. Drozd, J. Ellis, J. Quevillon, and T. You, J. High Energy Phys. 06 (2015) 028; R. Edezhath, arXiv:1501.00992; L. Edelhäuser, A. Knochel, and T. Steeger, J. High Energy Phys. 11 (2015) 062.
[16] M. Gorbahn, J. M. No, and V. Sanz, J. High Energy Phys. 10 (2015) 036.
[17] J. Alwall, D. Rainwater, and T. Plehn, Phys. Rev. D **76**, 055006 (2007).
[18] C. Englert, D. Gonçalves-Netto, K. Mawatari, and T. Plehn, J. High Energy Phys. 01 (2013) 148.
[19] K. Hagiwara, Q. Li, and K. Mawatari, J. High Energy Phys. 07 (2009) 101; C. Englert, D. Gonçalves-Netto, K. Mawatari, and T. Plehn, J. High Energy Phys. 01 (2013) 148.
[20] J. Brehmer, J. Jaeckel, and T. Plehn, Phys. Rev. D **90**, 054023 (2014).
[21] A. Azatov, C. Grojean, A. Paul, and E. Salvioni, Zh. Eksp. Teor. Fiz. **147**, 410 (2015) [J. Exp. Theor. Phys. **120**, 354 (2015)].
[22] M. Buschmann, D. Gonçalves, S. Kuttimalai, M. Schonherr, F. Krauss, and T. Plehn, J. High Energy Phys. 02 (2015) 038.
[23] L. Berthier and M. Trott, J. High Energy Phys. 02 (2016) 069.
[24] K. Cranmer, S. Kreiss, D. López-Val, and T. Plehn, Phys. Rev. D **91**, 054032 (2015).
[25] S. Fichet and G. Moreau, arXiv:1509.00472.
[26] B. Henning, X. Lu, and H. Murayama, J. High Energy Phys. 01 (2016) 023.
[27] B. Grinstein and M. Trott, Phys. Rev. D **76**, 073002 (2007); R. Alonso, M. B. Gavela, L. Merlo, S. Rigolin, and J. Yepes, Phys. Lett. B **722**, 330 (2013); **726**, 926 (2013); G. Buchalla, O. Catà, and C. Krause, Nucl. Phys. **B880**, 552 (2014); I. Brivio, T. Corbett, O. J. P. Éboli, M. B. Gavela, J. Gonzalez-Fraile, M. C. Gonzalez-Garcia, L. Merlo, and S. Rigolin, J. High Energy Phys. 03 (2014) 024.
[28] G. Passarino, Nucl. Phys. **B868**, 416 (2013).
[29] C. Arzt, M. B. Einhorn, and J. Wudka, Nucl. Phys. **B433**, 41 (1995).
[30] B. Grzadkowski, M. Iskrzynski, M. Misiak, and J. Rosiek, J. High Energy Phys. 10 (2010) 085.
[31] K. Hagiwara, S. Ishihara, R. Szalapski, and D. Zeppenfeld, Phys. Rev. D **48**, 2182 (1993).
[32] G. F. Giudice, C. Grojean, A. Pomarol, and R. Rattazzi, J. High Energy Phys. 06 (2007) 045; R. Contino, M. Ghezzi, C. Grojean, M. Mühlleitner, and M. Spira, J. High Energy Phys. 07 (2013) 035.
[33] R. Alonso, E. E. Jenkins, and A. V. Manohar, Phys. Lett. B **739**, 95 (2014).
[34] J. M. Cornwall, D. N. Levin, and G. Tiktopoulos, Phys. Rev. Lett. **30**, 1268 (1973); **31**, 572(E) (1973); Phys. Rev. D **10**, 1145 (1974); **11**, 972(E) (1975); C. H. Llewellyn Smith, Phys. Lett. **46B**, 233 (1973); H. A. Weldon, Phys. Lett. **146B**, 59 (1984); Phys. Rev. D **30**, 1547 (1984); J. F. Gunion, H. E. Haber, and J. Wudka, Phys. Rev. D **43**, 904 (1991); T. Corbett, O. J. P. Éboli, and M. C. Gonzalez-Garcia, Phys. Rev. D **93**, 015005 (2016).
[35] T. Han, D. Krohn, L. T. Wang, and W. Zhu, J. High Energy Phys. 03 (2010) 082.
[36] U. Baur, T. Plehn, and D. L. Rainwater, Phys. Rev. Lett. **89**, 151801 (2002); M. Gillioz, R. Grober, C. Grojean, M. Mühlleitner, and E. Salvioni, J. High Energy Phys. 10 (2012) 004; S. Dawson, E. Furlan, and I. Lewis, Phys. Rev. D **87**, 014007 (2013).
[37] J. Alwall, R. Frederix, S. Frixione, V. Hirschi, F. Maltoni, O. Mattelaer, H.-S. Shao, T. Stelzer, P. Torrielli, and M. Zaro, J. High Energy Phys. 07 (2014) 079.
[38] Available from https://feynrules.irmp.ucl.ac.be/wiki/ModelDatabaseMainPage.
[39] A. Alloul, N. D. Christensen, C. Degrande, C. Duhr, and B. Fuks, Comput. Phys. Commun. **185**, 2250 (2014).
[40] C. Degrande, C. Duhr, B. Fuks, D. Grellscheid, O. Mattelaer, and T. Reiter, Comput. Phys. Commun. **183**, 1201 (2012).
[41] A. Alloul, B. Fuks, and V. Sanz, J. High Energy Phys. 04 (2014) 110.
[42] See e.g. A. Djouadi, Phys. Rep. **457**, 1 (2008), and references therein.
[43] Available from https://cp3.irmp.ucl.ac.be/projects/madgraph/wiki/HiggsPairProduction.
[44] T. Hahn, Comput. Phys. Commun. **140**, 418 (2001).
[45] T. Hahn and M. Pérez-Victoria, Comput. Phys. Commun. **118**, 153 (1999).
[46] J. Pumplin, D. R. Stump, J. Huston, H. L. Lai, P. M. Nadolsky, and W. K. Tung, J. High Energy Phys. 07 (2002) 012.
[47] ATLAS and CMS Collaborations, Phys. Rev. Lett. **114**, 191803 (2015).
[48] Tevatron Electroweak Working Group (CDF and D0 Collaborations), arXiv:1407.2682; ATLAS and CDF and CMS and D0 Collaborations, arXiv:1403.4427; K. Kröninger, A. B. Meyer, and P. Uwer, arXiv:1506.02800; Particle Data Group: http://pdg.lbl.gov/2014/reviews/rpp2014-rev-top-quark.pdf.
[49] A. Djouadi, J. Kalinowski, and M. Spira, Comput. Phys. Commun. **108**, 56 (1998).
[50] V. Silveira and A. Zee, Phys. Lett. **161B**, 136 (1985); R. Schabinger and J. D. Wells, Phys. Rev. D **72**, 093007 (2005); B. Patt and F. Wilczek, arXiv:hep-ph/0605188.
[51] J. F. Gunion and H. E. Haber, Phys. Rev. D **67**, 075019 (2003).
[52] N. Craig, J. Galloway, and S. Thomas, arXiv:1305.2424.
[53] M. Carena, I. Low, N. R. Shah, and C. E. M. Wagner, J. High Energy Phys. 04 (2014) 015.
[54] A. Delgado, G. Nardini, and M. Quirós, J. High Energy Phys. 07 (2013) 054.

[55] G. M. Pruna and T. Robens, Phys. Rev. D **88**, 115012 (2013); D. López-Val and T. Robens, Phys. Rev. D **90**, 114018 (2014); T. Robens and T. Stefaniak, Eur. Phys. J. C **75**, 104 (2015).
[56] T. Plehn, M. Spira, and P. M. Zerwas, Nucl. Phys. **B479**, 46 (1996); **531**, 655 (1998); X. Li and M. B. Voloshin, Phys. Rev. D **89**, 013012 (2014).
[57] J. F. Gunion, H. E. Haber, G. L. Kane, and S. Dawson, *The Higgs Hunter's Guide* (Addison-Wesley, Menlo Park, 1990); G. C. Branco, P. M. Ferreira, L. Lavoura, M. N. Rebelo, M. Sher, and J. P. Silva, Phys. Rep. **516**, 1 (2012).
[58] H. E. Haber, M. J. Herrero, H. E. Logan, S. Peñaranda, S. Rigolin, and D. Temes, Phys. Rev. D **63**, 055004 (2001).
[59] D. Eriksson, J. Rathsman, and O. Stål, Comput. Phys. Commun. **181**, 189 (2010).
[60] P. Bechtle, O. Brein, S. Heinemeyer, G. Weiglein, and K. E. Williams, Comput. Phys. Commun. **181**, 138 (2010); **182**, 2605 (2011).
[61] F. Mahmoudi, Comput. Phys. Commun. **180**, 1579 (2009).
[62] P. Bechtle, S. Heinemeyer, O. Stål, T. Stefaniak, and G. Weiglein, Eur. Phys. J. C **74**, 2711 (2014).
[63] M. Carena, S. Heinemeyer, O. Stål, C. E. M. Wagner, and G. Weiglein, Eur. Phys. J. C **73**, 2552 (2013).
[64] P. M. Ferreira, J. F. Gunion, H. E. Haber, and R. Santos, Phys. Rev. D **89**, 115003 (2014).
[65] B. Hespel, D. López-Val, and E. Vryonidou, J. High Energy Phys. 09 (2014) 124.
[66] LHC Higgs cross-section Working Group for BSM Higgs, https://twiki.cern.ch/twiki/bin/view/LHCPhysics/LHCHXSWG3Benchmarks2HDM.
[67] M. Buschmann, C. Englert, D. Gonçalves, T. Plehn, and M. Spannowsky, Phys. Rev. D **90**, 013010 (2014).
[68] S. Heinemeyer *et al.* (LHC Higgs Cross Section Working Group Collaboration), arXiv:1307.1347.
[69] U. Baur, T. Plehn, and D. L. Rainwater, Phys. Rev. D **69**, 053004 (2004); J. Baglio, O. Eberhardt, U. Nierste, and M. Wiebusch, Phys. Rev. D **90**, 015008 (2014).
[70] W. Hollik, T. Plehn, M. Rauch, and H. Rzehak, Phys. Rev. Lett. **102**, 091802 (2009).
[71] J. Berger, J. Hubisz, and M. Perelstein, J. High Energy Phys. 07 (2012) 016; S. Dawson and E. Furlan, Phys. Rev. D **86**, 015021 (2012); C. Y. Chen, S. Dawson, and I. M. Lewis, Phys. Rev. D **90**, 035016 (2014); S. Fajfer, A. Greljo, J. F. Kamenik, and I. Mustac, J. High Energy Phys. 07 (2013) 155; S. A. R. Ellis, R. M. Godbole, S. Gopalakrishna, and J. D. Wells, J. High Energy Phys. 09 (2014) 130.
[72] G. Aad *et al.* (ATLAS Collaboration), J. High Energy Phys. 12 (2015) 055; V. Khachatryan *et al.* (CMS Collaboration), Phys. Rev. D **91**, 052009 (2015); G. Aad *et al.* (ATLAS Collaboration), Phys. Rev. D **91**, 052007 (2015); CMS Collaboration, Report No. CMS-PAS-EXO-14-010;V. Khachatryan *et al.* (CMS Collaboration), J. High Energy Phys. 08 (2014) 174.
[73] I. Low, R. Rattazzi, and A. Vichi, J. High Energy Phys. 04 (2010) 126.
[74] D. Pappadopulo, A. Thamm, R. Torre, and A. Wulzer, J. High Energy Phys. 09 (2014) 060; a FeynRules implementation of the model is available from http://heidi.pd.infn.it/html/vector/index.html.
[75] A. Kaminska, arXiv:1505.04645.
[76] V. D. Barger, W. Y. Keung, and E. Ma, Phys. Rev. Lett. **44**, 1169 (1980).
[77] N. Arkani-Hamed, A. G. Cohen, and H. Georgi, Phys. Lett. B **513**, 232 (2001).
[78] M. K. Gaillard, Nucl. Phys. **B268**, 669 (1986).
[79] O. Cheyette, Nucl. Phys. **B297**, 183 (1988).
[80] C. W. Chiang and R. Huo, J. High Energy Phys. 09 (2015) 152.
[81] R. Huo, J. High Energy Phys. 09 (2015) 037.
[82] T. Corbett, O. J. P. Éboli, J. Gonzalez-Fraile, and M. C. Gonzalez-Garcia, Phys. Rev. D **87**, 015022 (2013).
[83] S. L. Glashow and S. Weinberg, Phys. Rev. D **15**, 1958 (1977).
[84] M. J. G. Veltman, Acta Phys. Pol. B **8**, 475 (1977).
[85] D. Toussaint, Phys. Rev. D **18**, 1626 (1978); J. M. Frère and J. A. M. Vermaseren, Z. Phys. C **19**, 63 (1983); S. Bertolini, Nucl. Phys. **B272**, 77 (1986); W. Grimus, L. Lavoura, O. M. Ogreid, and P. Osland, J. Phys. G **35**, 075001 (2008); W. Hollik, Z. Phys. C **32**, 291 (1986); **37**, 569 (1988); C. D. Froggatt, R. G. Moorhouse, and I. G. Knowles, Phys. Rev. D **45**, 2471 (1992); H.-J. He, N. Polonsky, and S.-f. Su, Phys. Rev. D **64**, 053004 (2001); W. Grimus, L. Lavoura, O. Ogreid, and P. Osland, Nucl. Phys. **B801**, 81 (2008).
[86] L. Randall, J. High Energy Phys. 02 (2008) 084; K. Blum and R. T. D'Agnolo, Phys. Lett. B **714**, 66 (2012).
[87] S. Davidson and H. E. Haber, Phys. Rev. D **72**, 035004 (2005); **72**, 099902 (2005).
[88] F. del Águila, J. de Blas, and M. Pérez-Victoria, J. High Energy Phys. 09 (2010) 033.